Strength grading of structural timber and EWP laminations of Norway spruce – Development potentials

Licentiate thesis

Jan Oscarsson

Linnæus University
School of Engineering
Report No. 15, 2012
ISBN: 978-91-86983-92-5

Thesis for the Degree of Licentiate of Engineering

Strength grading of structural timber and EWP laminations of Norway spruce

Development potentials

Jan Oscarsson

School of Engineering
Linnaeus University, 2012

Abstract

Strength grading of structural timber is a process by which value is added to sawn products. It is to the greater part carried out using machine grading based on statistical relationships between so called indicating properties and bending strength. The most frequently applied indicating property (IP) on the European market is the stiffness in terms of average modulus of elasticity (MOE) of a timber piece, although MOE is a material property that varies within timber.

A major limitation of today's grading methods is that the described relationships are relatively poor, which means that there is a potential for more accurate techniques. The main purpose of this research has been to initiate development of more accurate and efficient machine grading methods.

Strength of timber is dependent on the occurrence of knots. At the same time, knot measures applied as indicating properties until today have shown to be poor predictors of strength. However, results from this research, and from previous research, has shown that not only size and position of knots but also fibre deviations in surrounding clear wood are of great importance for local stiffness and development of fracture under loading. Thus, development of new indicating properties which take account of knots as well as properties of surrounding fibres, determined on a very local scale, was considered as a possible path towards better strength grading.

In the research, results from contact-free deformation measurements were utilized for analysis of structural behaviour of timber on both local and global level. Laser scanning was used for detection of local fibre directions projected on surfaces of pieces. Scanned information, combined with measures of density and average axial dynamic MOE, was applied for calculation of the variation of local MOE in the longitudinal board direction. By integration over cross-sections along a piece, a stiffness profile in edgewise bending was determined and a new IP was defined as the lowest bending MOE along the piece.

For a sample of Norway spruce planks, a coefficient of determination of 0.68 was achieved between the new IP and bending strength. For narrow side boards to be used as laminations in wet-glued glulam beams, the relationship between IP and tensile strength was as high as 0.77. Since the intended use of the narrow boards was as laminations in wet-glued beams, the possibility of grading them in a wet state was also investigated. Grading based on axial dynamic excitation and weighing gave just as good results in a wet state as when the same grading procedure was applied after drying.

It was also found that the relationship between the new IP and strength was dependent on what scale the IP was determined. Optimum was reached for moving average MOE calculated over lengths corresponding with approximately half the width of investigated pieces.

Implementation of the new IP will result in grading that is more accurate than what is achieved by the great majority of today's grading machines. The new method will probably also be particularly favourable for development of engineered wood products made of narrow laminations.

Keywords: bending strength, fibre angle, grain angle, knots, laser scanning, machine strength grading, modulus of elasticity, strain measurement, structural timber, tensile strength, wood

Sammanfattning

Hållfasthetssortering av konstruktionsvirke innebär att värdet på sågade produkter ökar. Sorteringen genomförs oftast med maskinella metoder baserade på statistiska samband mellan s.k. indikerande egenskaper och böjhållfasthet. Den indikerande egenskap (indicating property, IP) som är vanligast på den Europeiska marknaden är styvhet uttryckt som ett medelvärde för elasticitetsmodulen (modulus of elasticity, MOE) i ett virkesstycke, trots att MOE är en materialegenskap som varierar i virket.

En betydande begränsning med dagens sorteringsmetoder är att de beskrivna sambanden är förhållandevis svaga, vilket innebär att det finns en potential för metoder med högre noggrannhet. Det huvudsakliga syftet med detta doktorandprojekt har varit att initiera en utveckling mot sådana metoder.

Hållfasthet hos virke är beroende av förekomst av kvistar. Samtidigt har de kvistmått som fram till idag kommit till användning visat sig vara dåliga prediktorer av hållfasthet. Resultat från såväl denna som tidigare forskning har dock visat att inte bara kvistars storlek och läge, utan också variationen i fiberriktning i omgivande träfibrer, är av stor betydelse för lokal styvhet och brottförlopp under inverkan av last. Utveckling av nya IP som tar hänsyn till såväl kvistar som omgivande träfibrers egenskaper fastställda på mycket lokal nivå bedömdes vara en möjlig väg för att uppnå bättre hållfasthetssortering.

I detta doktorandprojekt användes beröringsfri deformationsmätning för analys av det strukturella beteendet hos virkesstycken på såväl lokal som global nivå. Laserskanning utnyttjades för detektering av lokala fiberriktningar projicerade på virkesstyckenas ytor. Med utgångspunkt från skannad information, virkesdensitet och medelvärde för axiell dynamisk elasticitetsmodul kunde variationen i lokal elasticitetsmodul i virkesstyckenas längdriktning bestämmas. Genom integration över tvärsektioner längs ett virkesstycke kunde en profil över hur böjstyvheten i styva riktningen varierade i virkesstyckets längdriktning beräknas. En ny IP definierades som den lägsta elasticitetsmodulen i böjning utmed virkesstyckets längd.

För ett urval av granplankor erhölls en förklaringsgrad på 0.68 mellan den nya indikerande egenskapen och böjhållfasthet. För smala sidobrädor avsedda att användas som lameller i våtlimmade limträbalkar var motsvarande förklaringsgrad mellan samma IP och draghållfasthet så hög som 0.77. Eftersom sidobrädorna var avsedda att användas som lameller i våtlimmade balkar genomfördes en studie avseende möjligheten att hållfasthetssortera i vått tillstånd med hjälp av axiell dynamisk excitering och vägning. Det visade sig att sådan sortering gav lika bra resultat som då samma metod användes efter torkning.

Sambandet mellan den nya indikerande egenskapen och hållfasthet visade sig också vara beroende av på vilken lokal nivå som egenskapen beräknades.

Optimum uppnåddes då den bestämdes som ett glidande medelvärde beräknat över en längd motsvarande ungefär halva virkesstyckets höjd.

Implementering av den nya sorteringsmetoden kommer att resultera i sortering som är noggrannare än vad som kan erhållas med det stora flertalet av de sorteringsmetoder som finns idag. Den nya indikerande egenskapen kommer sannolikt att bli särskilt gynnsam att använda för utveckling av ingenjörsmässiga träprodukter bestående av smala lameller.

Nyckelord: böjhållfasthet, draghållfasthet, elasticitetsmodul, fibervinkel, konstruktionsvirke, kvistar, laserskanning, maskinell hållfasthetssortering, trä, töjningsmätning

Acknowledgements

This licentiate thesis would not have been brought about without support and input from a number of people. The first one to be credited is Professor Hans Petersson who bears the main responsibility for me being registered as industrial doctoral candidate at the University in Växjö. HP has been a source of inspiration for more than 30 years, ever since he supervised my diploma work at Lund Institute of Technology in the beginning of the 1980s.

I owe many thanks to my tutor, Professor Anders Olsson. Working with him means that you never need to fear that you will run out of ideas about "what to do next". His thoroughness and exactitude is a great asset when, for example, scientific papers or thesis texts need to be scrutinized. A large number of mistakes and less well-reasoned accounts have been avoided thanks to his careful and competent examination of texts and formulations.

Together with research engineer Bertil Enquist, I have carried, scanned and broken many boards and planks. I have really enjoyed the long and sometimes late hours that we have spent together around various testing machines and measurement equipments in our joint quest for in-depth understanding of the behaviour of wood. Without Bertil, there would not have been any contact-free deformation measurements carried out within the scope of this project.

Contributions have also been made by Professors Marie Johansson, Bo Källsner, Erik Serrano, Thomas Thörnqvist and Charlotte Bengtsson, and Lic. Eng. Rune Ziethén. I am also grateful to my dear friend Senior Lecturer Hans Frisk who, in the course of my studies, has helped me out with some tricky integrals.

For an industry doctoral candidate, co-operation with the industry is important. In this case, I have had the benefit of fruitful collaboration with the Södra Timber AB, Växjö, and the Innovativ Vision AB, Linköping.

To carry out a doctoral candidate project in the research field of wood structural engineering you not only need time, commitment, advanced laboratory resources, industrial partners, and knowledgeable and experienced tutors and colleagues. You also need money. A lot of money. The financial support granted by The Knowledge Foundation, The Swedish Forest Industries Federation, FORMAS – The Swedish Research Council for Environment, Agricultural Science and Spatial Planning, CBBT – The Centre for Building and Living with Wood, The Kempe Foundations, The Bo Rydin Foundation, and my employer SP, is hereby gratefully acknowledged.

Finally, thoughts to my dear family with whom I share both joy and sorrow….

Växjö, October 2012
Jan Oscarsson

Appended papers

Paper I Jan Oscarsson, Anders Olsson and Bertil Enquist (2012) *Strain fields around knots in Norway spruce specimens exposed to tensile forces*. Wood Science and Technology, 46(4):593-610.

Paper II Jan Oscarsson, Anders Olsson, Marie Johansson, Bertil Enquist and Erik Serrano (2011) *Strength grading of narrow dimension Norway spruce side boards in the wet state using first axial resonance frequency*. International Wood Products Journal, 2(2):108-114.

Paper III Jan Oscarsson, Anders Olsson and Bertil Enquist (2012) *Determination of tensile strain fields in narrow Norway spruce side boards as a basis for verification of new machine strength grading methods.* Working paper, in preparation for submission.

Paper IV Anders Olsson, Jan Oscarsson, Erik Serrano, Bo Källsner, Marie Johansson and Bertil Enquist (2012) *Prediction of timber bending strength and in-member cross-sectional stiffness variation on basis of local wood fibre orientation.* Submitted to Wood Science and Technology.

Contents

1 Introduction

1.1 Structural timber – a product by nature

Wood is a material that is basically manufactured by nature itself. Whereas the mechanical properties of construction materials such as concrete, steel or aluminium could be varied by, for example, modifying concrete mix proportions, changing the reinforcement ratio in concrete elements, adjusting the quantity of different alloying materials in steel or aluminium mixtures or changing process parameters such as temperature or pressure, the possibility of influencing material properties in growing trees are, in comparison, rather limited. Säll (2002) claimed that wood properties of individual trees of Norway spruce (*Picea abies*) are mainly dependent on genetic heritage and growth conditions. Examples of the latter are stand density, social standing of a tree within a stand and site characteristics, including climate, topography of the terrain and also texture and nutritional status of the ground.

To improve structural wood properties of growing trees, various silvicultural measures are available. An increase of stand density will have a positive effect on several wood material parameters that, in turn, will improve the performance of timber for structural purposes. For example, a high stand density will as a rule lead to a decrease of both branch diameter in trees (*e.g.* Mäkinen and Hein 2006) and knot diameter in sawn timber. This will improve the timber quality with respect to strength and stiffness, since these properties are dependent on occurrence and size of knots (*e.g.* Johansson 2003). Figure 1

Figure 1. Typical fractures initiated at knots in structural timber subjected to bending load.

exhibits typical fractures of structural timber exposed to bending load. A low growth-rate, as obtained in stands with a high stand density, will also contribute to decreasing annual ring width (*e.g.* Herman *et al.* 1998), which will, in general, have a similar positive effect on strength and stiffness as a reduction of knot size (*e.g.* Hoffmeyer 1995; Kliger *et al.* 1995; Lundgren *et al.* 2007), however not as evident. Spiral grain, *i.e.* the inclination of the wood fibres in relation to the longitudinal direction of the log, is another characteristic that is important for the performance of sawn timber. According to Säll (2002), Norway spruce stands that are dense and free of gaps, will probably result in wood with relatively low risk of obtaining large grain angle and subsequent shape distortion in the form of twist in sawn timber. The fibre orientation in a board, *i.e.* the inclination of the fibres in relation to the longitudinal board direction, also affects strength and stiffness of a piece of timber, since the performance of these properties is much higher in the fibre direction than in directions perpendicular to the fibres (Dinwoodie 2000, after Baumann 1922).

Another silvicultural treatment that will contribute to a reduction of knot size in structural timber is pruning, *i.e.* removal of branches on standing trees. As a tree continues to grow after such a measure, knot-free clear wood with, in most cases, excellent structural properties will develop outside the removed branches. However, in Sweden this method is rarely applied on Norway spruce due to the risk for development of rot at the pruned branches (Thörnqvist 2011), whereas experiences from *e.g.* Germany are somewhat more positive (Metzler 1997).

Assessment of wood properties of standing trees has, according to Wang *et al.* (2007a), traditionally been carried out on the basis of simple physical measurements, *e.g.* height, diameter and taper, and visual inspection of stem surface characteristics such as size and distribution of knots and other defects. The spiral grain could be quantified on a trunk or log surface the bark of which has been peeled off (Säll 2002). A scribed line following the direction of the wood fibres is drawn on the debarked surface and the angle between this line and the longitudinal direction of the trunk could then be measured using a simple angle measurement device. However, it is also established that stiffness properties of standing trees can be estimated using acoustic measurement methods. For example, it has been found that there is a strong relationship between acoustic wave velocity measured between a transmitter probe and a receiver probe inserted into the sapwood of butt log parts of trees in stands of Radiata pine (*Pinus radiata*) and the modulus of elasticity (MOE) of core samples from the butt logs of the measured trees (Wang *et al.* 2007a; Wang *et al.* 2007b). The wave velocity was measured on the basis of acoustic energy introduced into the tree through a hammer impact on the transmitter probe, see Figure 2. However, acoustic measurements on lower parts of standing trees do not provide information about the stiffness variation over the entire length (or

height) of a tree. Such variation has been found by, for example, Kliger *et al.* (1995), who investigated the difference in, *inter alia*, bending stiffness between timber pieces cut from the cores of butt logs and top logs, respectively, of fast grown Norway spruce trees. They found that the stiffness was significantly higher in the top log pieces, which was, according to the authors, explained by smaller annual ring width and higher density in the core pieces cut from the top logs. Regarding application of acoustic measurements, Huang *et al.* (2003) claimed that such methods could be used to identify trees that, due to poor stiffness properties, are appropriate to be removed at thinning operations, *i.e.* at the selective removal of certain trees in a stand carried out to increase the growth-rate of the remaining trees and to enhance the profit of a future final cutting.

Figure 2. Stiffness property determination on standing trees using acoustic wave velocity measurement. Photos by courtesy of Fibre-gen, Inc., New Zealand.

After harvesting a stand that has been subjected to measurements and silvicultural treatments such as those described above, the knowledge about the structural wood properties of the harvested timber is, however, still limited. This is mainly due to the enormous variability of the material in general, both between and within logs. The property variation is explained by both the occurrence of local defects such as knots, cracks, top ruptures and compression wood, and the anisotropy of the material, *i.e.* the mechanical properties being different in longitudinal, radial and tangential directions, respectively, of the annual ring pattern of a log or a timber member. To be able to use wood as raw material for development and manufacturing of structural products intended for load bearing applications, the mentioned variability has to be managed and controlled in the sense that mechanical properties of manufactured products have to be predictable. This could be

achieved by means of two fundamentally different methods; either by non-destructive strength grading of logs and solid sawn timber, or by dismembering wood into *e.g.* chips, strands, veneers or sawn laminations and then glue or by other means join the disintegrated parts together, under influence of heat and pressure, into structural members such as beams, columns or panels.

Concerning the first method, logs are usually sorted according to diameter and species, but quality sorting with respect to outer log shape and wood characteristics such as density, spiral grain and knot volume is gradually becoming more frequent. Such log sorting is, in most cases, carried out using optical or X-ray scanners and it enables sawmills to classify logs according to specific material properties. The value yield of the sawn timber could then be increased by sawing each log into dimensions that optimize the utilization of the quality class of the log (Skog *et al.* 2010).

It has also been shown that strength and stiffness of sawn timber can be estimated already at log level, *i.e.* before the actual sawing operation, using techniques such as X-ray scanning (*e.g.* Källsner *et al.* 2002; Oja *et al.* 2005), resonance frequency techniques (*e.g.* Kliger *et al*. 2003), ultrasonic measurements (Sandoz 1996), or such acoustic methods as described above. However, the application of these measurement techniques on logs is surrounded by certain limitations. For example, Lycken *et al.* (2009) found that X-ray scanning of Norway spruce logs gives predictions with rather low accuracy and that resonance frequency measurement gives unreliable results when the technique is used on frozen logs. Furthermore, Brännström (2009) asserted that application of ultrasonic methods requires a reduction of the grading speed, since contact between sensors and the measured object is needed. Such contact is also required as regards measurement of acoustic wave velocity (see Figure 2). It is also likely that both ultrasonic and acoustic measurements are affected by logs being frozen. Thus, the described limitations of log grading imply that prediction of strength and stiffness of solid sawn structural timber, typically cut from the centre parts of a log, requires strength grading of individual timber members after sawing. Such grading is carried out on the basis of either visual inspection or application of certified grading machines. General requirements regarding both visual grading and machine grading are stated in the European Standard EN 14081-1. Visual grading is based upon visible defects being smaller than limits stipulated in a large number of visual grading standards listed in the European Standard EN 1912. Machine strength grading means that certain properties of a piece of timber are non-destructively measured as the piece passes through or by a grading machine. Statistical relationships between the measured properties and bending strength are subsequently applied for prediction of the latter. However, machine graded timber must also fulfill certain so called *visual override requirements* regarding defects that machines in general are unable to detect,

but the existence of which are reason for downgrading. According to EN 14081-1, this concerns fissures, warp, wane, rot, insect damage and abnormal defects such as compression wood and top ruptures. Thus, even if machine strength grading is applied, visual inspection is still required to a certain degree. Yet, it should be emphasized that the visual override could be carried out either manually or by machinery in the form of optical scanners.

As regards the second method of property control, *i.e.* gluing of disintegrated wood pieces into load bearing components such as beams or panels, a major benefit of the disintegration is that local defects in logs and timber pieces are also being dismembered. The subsequent joining together of the disintegrated parts means that the defects are disseminated, resulting in products with high shape stability and predictable and homogeneous mechanical properties with high performance and low variability. Structural wood products manufactured on the basis of disintegration and subsequent gluing are by definition called *Engineered Wood Products*, abbreviated *EWP*. An example of such a product is *Laminated Veneer Lumber* (*LVL*), see Figure 3 (left), which consists of several layers of veneer sheets about 3 mm thick, glued together and cut into prismatic structural members with the grains in all the veneers running parallel with the longitudinal axis of the product. Another typical EWP is *Parallel Strand Lumber* (*PSL*), manufactured from veneer strands with approximate dimensions 3×19×2400 mm (Lam and Prion 2003). Similar to LVL products, the grains in a PSL strand are oriented in the same direction as the PSL member's main axis. Examples of EWP panels are *plywood*, consisting of several layers of veneer sheets with orthogonally oriented grain directions in adjacent layers, and *Oriented Strand Board* (*OSB*), which are made of rectangular wooden flakes of approximate dimensions

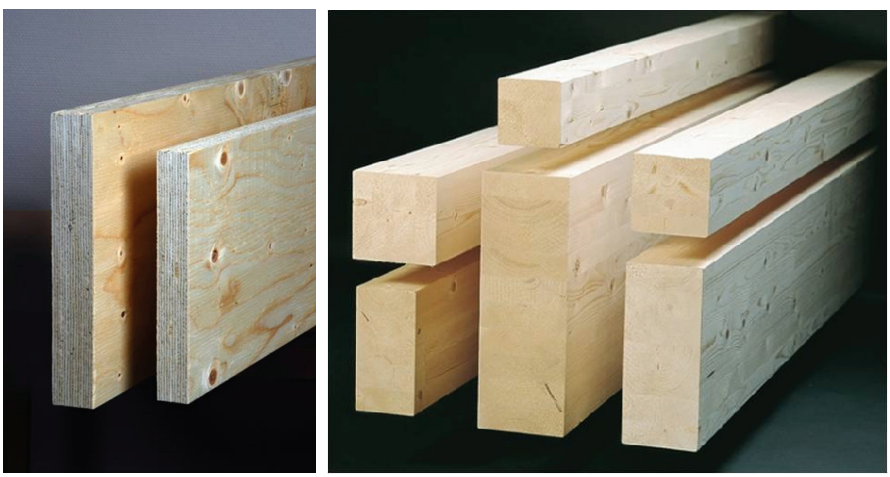

Figure 3. Engineered wood products: Laminated veneer lumber, LVL (left), and glulam beams (right). Photos by courtesy of Moelven Töreboda AB.

0.8×13×100 mm (Lam and Prion 2003) glued into sheets. A typical OSB includes three such sheets with different main orientation of the flakes in face and core layers, respectively (Lam and Prion 2003). A further and widely used EWP is *Glued-laminated timber*, or *glulam*, made up of strength graded laminations that are glued in the flatwise direction into structural elements with rectangular cross-section (Figure 3, right). Utilized laminations are typically strength graded structural timber with a thickness of 30-45 mm, *i.e.* the same kind of products that are used as solid load bearing studs and joists in timber framed structures. However, split centre cuts with thickness down to approximately 20 mm are also used, *e.g.* for use in service class 3 or in curved beams. Furthermore, it has recently been shown (Serrano *et al.* 2011) that glulam products with excellent structural properties can be achieved from wet glued laminations of strength graded Norway spruce side boards of narrow dimensions (thickness ≤ 25 mm). Thus, glulam products are composed of laminations that are graded using the same techniques as applied for strength grading of structural timber. In this respect, glulam could be considered as products that combine the concepts of EWP and strength grading of solid boards and planks. Such strength grading, *i.e.* grading of structural timber and EWP laminations, is what this thesis is about.

1.2 Research idea, objectives and realization

Strength grading of structural timber means that timber is sorted either by visual inspection or machine strength grading (see section 1.1) into strength classes, or strength grades, to which characteristic and mean values of structural properties are allocated. In the European Standard EN 338, a system of strength classes intended for use in structural codes is established. According to this standard, timber is allocated to a certain strength class on the basis of requirements regarding bending strength, stiffness in terms of mean MOE in bending, and density. According to EN 14081-2, these properties are defined as *grade determining properties*. The property values that are presented in EN 338 refer to timber having a moisture content that corresponds to a standard environment of 20 °C and 65 % relative humidity. For Norway spruce, this climate is consistent with an equilibrium moisture ratio of about 12 %.

For softwood species, the grades defined in EN 338 are indicated by the capital letter *C* followed by two digits that represent the characteristic bending strength of timber pieces graded into the class in question. The characteristic value corresponds to the 5-percentile bending strength value of all pieces graded into the class, which actually means that five percent of the pieces in a certain class may be weaker than the strength indicated by the class designation.

The Swedish market for strength grading of structural timber is dominated by machine grading methods. The quantity of machine graded timber has increased gradually during the last decade. In 2011, it had reached a volume of about 1.74 million m^3. The volume of timber graded on the basis of visual inspection has decreased correspondingly, amounting to about 0.1 million m^3 in 2011 (Stenman 2012).

Machine strength grading is, as described in section 1.1, in general based on statistical relationships between bending strength and measured timber properties, the latter also called *indicating properties*. According to the European Standard EN 14081-2, an *indicating property* is defined as a measurement or a combination of measurements that is a) made by a grading machine, and b) closely related to one or more of the grade determining properties.

Machine strength grading methods of today result, in general, in a maximum characteristic bending strength of 35-40 MPa, despite there are timber pieces being more than twice as strong. The reason why such high strength boards are not being graded is that the relationships between applied indicating properties and bending strength are rather weak. The consequence of this is that currently applied grading techniques are burdened with large safety margins. Thus, to be able to utilize the structural potential of timber with high strength, better grading methods are needed.

The primary purpose of this industry doctoral candidate project was to initiate development of new strength grading procedures for accurate and efficient grading of timber in terms of both stiffness and strength. Tools and theories identified to be of use in such a process were, for example, optical and laser surface scanning of timber members, finite element modeling and theories of fracture mechanics. From the outset of the research, it was well known that image analysis of pictures obtained from a WoodEye scanner available at Linnæus University, see Figure 4, could be applied for determination of wood properties such as spiral grain, local grain deviations and occurrence of knots and other defects on the surfaces of a board or a plank. On the basis of such information, finite element models of timber members, or parts of such members, could be established and applied for prediction of stiffness and strength. In the latter case, the possibility of using theories of fracture mechanics was considered as an option to be investigated.

The objectives that were formulated from the outset of the research were, first, to develop a method by which internal structural properties such as stiffness variation in a timber piece could be described and, second, that information about such variations should then be included in finite element models to be utilized for prediction of timber strength.

Figure 4. WoodEye scanner for optical and laser scanning of timber pieces.

Being employed at an industry research institute as the SP Technical Research Institute of Sweden, and at the same time being registered as a doctoral candidate at Linnæus University where the main part of the research concerning timber engineering is carried out in close co-operation with the industry, there is a danger, or a possibility, that the doctoral student becomes involved in time-consuming industry related research projects. The content of such projects will, to a considerable extent, reflect demands articulated by participating companies from which there is also an expectation that achieved results should be possible to implement within a rather short time. Doctoral candidate participation in projects of this type will, with pros and cons, influence the scope and the time frame of the research upon which licentiate and doctoral theses are based. The described course of events is, at least to some extent, what happened in this case. Paper I, dealing with local strain fields around knots in timber members exposed to tensile forces, Paper III, concerning evaluation of tensile strain fields along the entire length of side board surfaces, and Paper IV, describing a new strength grading method based upon scanned information about local fibre orientation along board surfaces, are fully in line with the original research plan. However, Paper II, dealing with strength grading of narrow side boards in the wet state, means that the scope of the doctoral project has been widened to comprise also issues regarding strength grading of EWP laminations and development of EWP products. Thus, the common denominator of the four papers is that they deal with development potentials for strength grading of structural timber and EWP laminations of Norway spruce. Papers II and III are results of a long-term research project initiated in co-operation with industrial partners and dealing

with wet-gluing of narrow Norway spruce side boards into glulam beams with first rate structural properties. One objective of both Paper I and III is to achieve a more thorough understanding of the development of strain fields around knots in timber members under load. Knowledge about such characteristics is of importance for development of more efficient grading methods, since strength and stiffness properties are, as mentioned in section 1.1, strongly dependent on the presence, location and size of knots in timber members. The strain field information is also valuable for comparison with and calibration of models, designed for prediction of stiffness and strength.

1.3 Theories, methods, materials and limitations

Machine strength grading of structural timber is based on application of theory of linear-elastic mechanics of materials, *i.e.* on the well known *Hooke's law* which states that the strain of a material is directly proportional to the load that is applied to it. Grading procedures are also dependent on statistical theories applied to express relationships between strength and different measureable timber properties. Such relationships are described in terms of *regression analyses*.

Methods applied in the research involved laboratory testing and post processing of measurement results using the finite element method, analytical calculations, optimization algorithms and regression analysis. The laboratory testing included optical contact-free deformations measurements based on white-light digital image correlation, determination of resonance frequencies corresponding to longitudinal modes of vibration induced into timber pieces by axial excitation, measurement of dimension and weight and subsequent determination of density of investigated pieces, measurement of fibre angle variation in the pieces using optical scanning of board surfaces illuminated by laser dots, determination of flatwise static bending stiffness utilizing a flatwise bending machine, and determination of strength and stiffness of pieces exposed to static edgewise bending test and static tension test, respectively. Principles for static edgewise bending test, axial resonance frequency determination, and flatwise static bending test are described in section 2.2.2.1. The contact-free deformations measurements are presented in section 4.2, and a description of the optical dot laser scanning is found in section 4.3. Also, further accounts of the experimental methods are found in the appended papers, respectively.

Regarding post processing of the measurement results, finite element and analytical calculations, respectively, and applied optimization principles are described in the papers in which each method is applied. Concerning regression analysis, the most frequently used type in connection with machine strength

grading of structural timber is *simple linear regression* which is described in more detail in section 2.1.

As regards materials, three different samples were used in the research. The first sample included only two test pieces, each one displaying a traversing knot. The second sample consisted of 116 narrow side boards of dimension 25×56×3000 mm, and the third one comprised 105 planks with as dimension (45×145×3600 mm) that is common for structural timber. The characteristics of the different samples are described in the papers in which they are utilized.

Limitations of this thesis are that all investigations and measurements have been performed on Norway spruce timber from sawmills located in the south of Sweden, and that the investigated development potentials only concern machine strength grading techniques.

2 Indicating properties – statistics and material characteristics

2.1 Basic statistics for machine strength grading

The fundamentals of machine strength grading of timber are the statistical relationships that exist between strength and various non-destructively measured wood properties. Statistical models that are utilized are based on the application of *regression analysis* by which the relationship between a *response variable Y*, *i.e.* the strength, and one or several *predictor variables* X_i, *i.e.* certain measurable wood properties, could be evaluated. In statistics textbooks, response variables are also denoted *dependent variables*, whereas predictor variables are also referred to as *independent variables* or *regressor variables*, see *e.g.* Montgomery (2009). A predictor variable is, as mentioned in section 1.2, denoted *indicating property* (IP) when regression analysis is applied in connection with strength grading of timber.

Linear regression analysis is most frequently used. It can be either *simple* och *multiple*. The former involves only one predictor variable / indicating property, whereas two or several of such properties are included in the latter. The description below is limited to simple linear regression, since strength class predictions of most grading machines of today are based upon only one single IP. However, it should be noted that there are also machines in which the prediction algorithms include more than one such property. An account of the basic concepts of multiple linear regression analysis is found in *e.g.* Montgomery (2009).

To carry out a simple linear regression analysis of structural timber, a sample of timber pieces is needed. For each piece in the sample, the response variable, *i.e.* the strength, and an IP, in most cases either a local or an average MOE value, are determined, often on the basis of measurement methods described in the European Standard EN 408. Applicable IP measures can also be determined using measurement techniques implemented in grading

machines. Strength and IP for each timber piece represent pair of observations which may be plotted in a scatter diagram, see example in Figure 5. The result of the regression analysis is a regression model that describes the linear relationship between strength and IP. The model is mathematically expressed as a regression line, see Figure 5, according to the equation

$$Y = \beta_0 + \beta_1 X \tag{1}$$

including the response variable Y (*i.e.* strength), the predictor variable X (*i.e.* the IP), and the parameters β_0 and β_1 representing, respectively, the interception between the regression line and the y-axis, and the inclination of the regression line. The line represents expected strength values (or long-run average strength values) as a function of IP values and it is determined on the basis of the method of least squares applied on errors ε, see Figure 5. The errors, or residuals, are equivalent with the difference between a particular strength observation and the strength value obtained from Equation (1) using the observed IP value that corresponds with the strength observation in question. Thus, the values of β_0 and β_1 are chosen in order to minimize the sum of the squares of the errors ε.

To evaluate to what extent a regression model could be used to predict the strength on the basis of a measured IP, the *coefficient of correlation*, denoted R, and the *coefficient of determination*, denoted R^2, are determined.

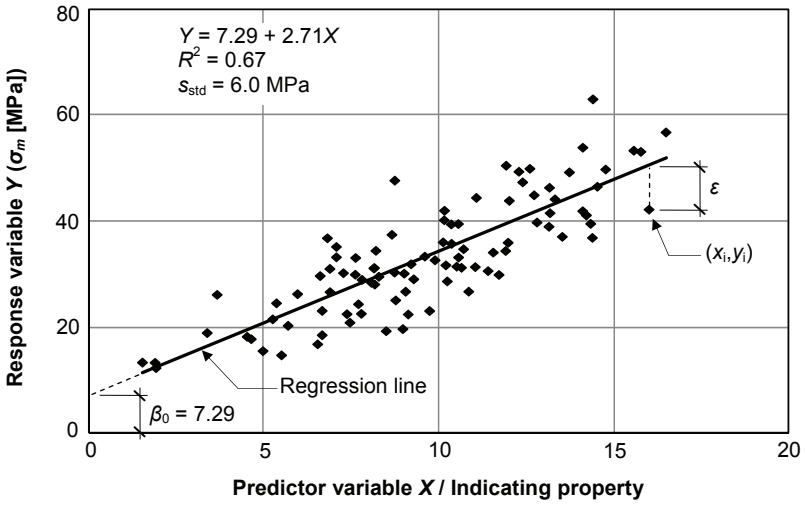

Figure 5. Scatter diagram showing the relationship between an IP and bending strength for a sample of structural timber pieces.

For a sample of n pair of observations of variables X and Y, the coefficient of correlation is calculated as

$$R = \frac{\mathrm{cov}(x,y)}{s_x \cdot s_y} = \frac{n\sum_{i=1}^{n} x_i y_i - \sum_{i=1}^{n} x_i \sum_{i=1}^{n} y_i}{\sqrt{n\sum_{i=1}^{n} x_i^2 - (\sum_{i=1}^{n} x_i)^2}\sqrt{n\sum_{i=1}^{n} y_i^2 - (\sum_{i=1}^{n} y_i)^2}} \quad (2)$$

where x_i and y_i are the values of each pair of observations (see Figure 5), cov(x,y) is the sample covariance and s_x and s_y are the sample standard deviations of the variables X and Y, respectively. For a sample of structural timber, R provides information about the degree of linearity in the relationship between IP and strength. The value of R is in the interval $-1 < R < 1$. Values close to zero means that there is no linear relationship, whereas values close to −1 or +1 means that there is a linear relationship that is either perfectly positive (R = +1, *i.e.* Y increases when X increases) or perfectly negative (R = −1, *i.e.* Y decreases when X increases).

Regarding the coefficient of determination, R^2, it is interpreted as the proportion of strength variation that is explained by the linearity between strength and IP. It could be determined either by squaring the R value calculated from Equation (2), or by application of

$$R^2 = \frac{\sum_{i=1}^{n} (y_i' - \bar{y})^2}{\sum_{i=1}^{n} (y_i - \bar{y})^2} \quad (3)$$

where y_i is an observed value of variable Y, y_i' is the predicted Y value calculated from Equation (1) using the observed value x_i that corresponds with y_i, and $\bar{y}$ is the mean of all the observations of Y in the sample.

Values of R^2 range between 0 and 1. For $R^2 = 1$, the entire variation of strength would be explained by variation of IP, whereas $R^2 = 0$ would mean that variation of strength is not influenced by variation of IP.

A further statistical quantity by which the accuracy of a simple linear regression model can be assessed is the *standard error of the estimate*, denoted s_{est} and given by

$$s_{est} = \sqrt{\frac{\sum_{i=1}^{n} (y_i - y_i')^2}{n-2}} \quad (4)$$

This measure is an estimator of the standard deviation of the errors, or residuals, $\varepsilon = y_i - y_i'$ (Blom 1970).

2.2 Wood material characteristics

2.2.1 Wood features

Development of methods for strength grading of structural timber requires a wide knowledge about the relationships between, on one hand, different wood material characteristics and, on the other hand, structural properties that are to be predicted. For clear wood, *i.e.* wood void of any defects, it is well known from research carried out by, for example, Foslie (1971) that both MOE and the bending strength in the direction of the grain are dependent on the clear wood density. Foslie's investigation was carried out on small pieces of Norway spruce, and by application of regression analysis he found an R^2 between MOE and density of 0.64. The corresponding relationships between density and strength were 0.66 in bending and 0.51 in tension, and an R^2 as strong as 0.76 was obtained between MOE and bending strength. For wood including defects such as knots, cracks, compression wood and top ruptures, the described relationships are weaker, see Table 1, but they are nevertheless utilized for strength predictions of structural timber.

An important feature of wood is that several characteristics which influence the structural properties vary considerably in the radial direction, *i.e.* from pith to bark. For example, the MOE of Norway spruce increases significantly, sometimes by a factor of two, from the pith and outwards (*e.g.* Wormuth 1993; Dahlblom *et al.* 1999) and similar observations, but less pronounced, have also been made for density (*e.g.* Steffen *et al.* 1997; Dahlblom *et al.* 1999). Another characteristic that vary in the same direction is the spiral grain. Close to the pith, fibres in Norway spruce trees are inclined slightly to the left, usually at its largest between annual rings number four to ten (Säll 2002). On the basis of measurements of 309 logs, Säll also found that the maximum grain angle was, on average, 3.1° with a standard deviation of 1.3°. Outwards, in the radial direction of a stem, the grain angles normally decreases linearly and the fibres close to the bark in trees older than 40-70 years are, according to Säll, in most cases inclined to the right. A further characteristic showing variation in the radial direction is the annual ring width. According to *e.g.* Perstorper *et.al.* (1995) and Herman *et al.* (1998), it is often larger in early years, but decreases towards the bark. It could be manipulated by silvicultural measures such as thinning, but after an increase of growth rate in the years following such a treatment, the ring width decreases again.

2.2.2 Strength and stiffness determining properties

2.2.2.1 Modulus of elasticity

As described in section 2.1, machine strength grading of structural timber is based upon statistical relationships between timber strength and various non-destructively measured wood properties. A number of such relationships are exhibited in Table 1 which is an extract from a table originally presented by Hoffmeyer (1995). That table is often referred to in publications regarding strength grading of structural timber.

Table 1. Statistical relationships, in terms of coefficient of determination (R^2), between strength of Norway spruce timber and various non-destructively measured wood properties (Hoffmeyer 1995). The investigations referred to are 1. Johansson et al. (1992), 2. Hoffmeyer (1984), 3. Hoffmeyer (1990), 4. Lackner and Foslie (1988), 5. Glos and Heimeshoff (1982), and 6. Johansson (1976).

Non-destructively measured wood properties	Coefficient of determination (R^2)						
	Bending strength				Tensile strength		
Source:	1	2	3	4	1	5	6
Knots	0.27	0.20	0.16	0.25	0.36	0.42	0.30
Annual ring width	0.21	0.27	0.20	0.44	0.36	0.33	0.28
Density	0.16	0.30	0.16	0.40	0.38	0.29	0.38
MOE	0.72	0.53	0.55	0.56	0.70	0.69	0.58
MOE, flatwise bending, short span	0.52				0.65		0.74
Knots + annual ring width	0.37	0.42	0.39		0.49		0.48
Knots + density	0.38		0.38		0.55	0.61	0.64
Knots + MOE	0.73	0.58	0.64		0.70	0.76	0.78

From the R^2 values presented in Table 1, it is evident that the best single predictor, or indicating property, of both bending and tensile strength is the stiffness expressed in terms of different MOEs. The values exhibited on row 4 refer to relationships between strength and more or less locally determined MOE in either edgewise bending or tension. However, regarding the values exhibited it is important to underline that R^2 values obtained from different investigations are *not* directly comparable, since different samples and different test set-ups were used.

As mentioned in section 1.2, a strength class intended for use in structural codes is, according to EN 338, indicated by the capital letter *C* followed by two digits representing the characteristic bending strength of the timber graded into the class. Structural timber is in general rectangular in shape, and the bending strength of a class is applicable for bending in both the edgewise and flatwise direction. However, even if structural timber is more or less exclusively exposed to bending in the edgewise direction when it is utilized as horizontally oriented load bearing components, the bulk of grading machines and grading

methods that are available on the market are based upon MOE measures being determined on the basis of either dynamic excitation in the axial direction or static bending over a certain width of span in the flatwise direction. Thus, even if MOE is a material property that varies in both longitudinal and lateral directions of a timber piece, the MOEs that are determined by grading techniques of today actually reflect MOE variation over a certain length. Different values will be obtained depending on which type of load case or MOE measurement technique that is applied. Table 2 exhibits mean value, standard deviation and relationship with bending strength (σ_m) in terms of coefficient of determination (R^2) for five different MOE measures determined for a sample of 105 Norway spruce planks of dimensions 45×145×3600 mm. The first three of these measures were utilized in the research presented in the attached Paper IV and the first four were applied in an investigation in which timber bending strength was predicted on the basis of resonance frequencies corresponding to edgewise bending modes of vibration (Olsson *et al.* 2012). The last one was based upon actual dimensions, measured for each individual plank, whereas the others were determined on the basis of nominal dimensions.

Table 2. Mean value, standard deviation and relationship with bending strength (σ_m) in terms of coefficient of determination (R^2) for five different MOE measures obtained from investigating 105 planks of Norway spruce (see Paper IV and Olsson et al. 2012).

Method for assessment of MOE	Symbol	Mean value [GPa]	Standard deviation [GPa]	R^2 between MOE and σ_m
Locally, static edgewise bending	E_m	11.0	2.8	0.74
Globally, static edgewise bending	$E_{m,g}$	10.6	2.3	0.72
Axial dynamic excitation[1]	$E_{a,1}$	12.4	2.6	0.59
Edgewise dynamic excitation[2]	$E_{b,1}$	12.7	2.7	0.65
Locally, static flatwise bending	E_{cook}	9.7	1.9	0.62

1. First axial mode of vibration.
2. First transversal (edgewise) mode of vibration.

For the planks referred to in Table 2, both local and global static MOE in the edgewise direction were determined on the basis of bending tests carried out in accordance with EN 408. The test set-up is shown in Figure 6. The critical section at which failure was expected to occur was selected in each piece by means of visual inspection. As stipulated in the European Standard EN 384 (clause 5.2), this section was positioned between the two point loads and the tension edge of each piece was chosen at random after the critical section had been decided upon. Two different deformations, denoted *v* and *w* in Figure 6, were measured. The local deformation, *v*, includes deformation due to bending only, since there are no shear forces in the mid span between the two loads. The global deformation, *w*, includes shear but also local effects, such as indentation perpendicular to the grain at the supports.

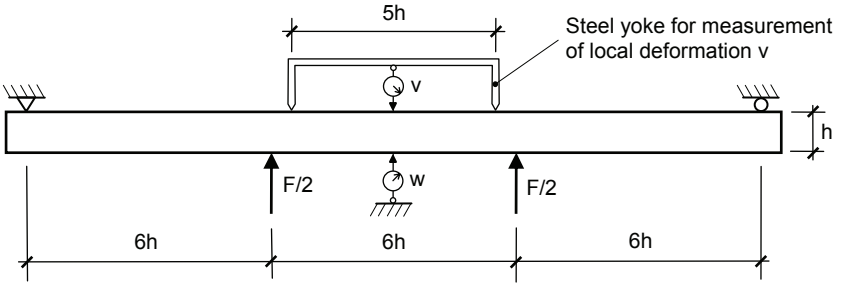

Figure 6. Test set-up according to EN 408 for determination of static edgewise bending stiffness, locally (E_m) as well as globally ($E_{m,g}$), and bending strength (σ_m).

The local static edgewise MOE was calculated as

$$E_m = \frac{al^2(F_2 - F_1)}{16I(v_2 - v_1)} \tag{5}$$

in which a is the distance between one of the point loads and the nearest support, l is the length (equal to $5h$) of the steel yoke over which the local deformation v is measured (see Figure 6), I is the second moment of inertia, F_2-F_1 is the increment of load (*i.e.* the increment of the sum of the two point loads) measured between two points on the straight portion of the load-deformation graph, and v_2-v_1 is the increment of deformation corresponding to F_2-F_1.

The global static edgewise MOE was calculated from the expression

$$E_{m,g} = \frac{L^3(F_2 - F_1)}{bh^3(w_2 - w_1)}\left[\left(\frac{3a}{4L}\right) - \left(\frac{a}{L}\right)^3\right] \tag{6}$$

where a and F_2-F_1 are the same as in Equation (5), h is the depth of the board, and L is the total span in bending, *i.e.* $L=18h$ according to Figure 6.

Axial dynamic MOEs were calculated as (*e.g.* Ohlsson and Perstorper 1992)

$$E_{a,n} = 4\rho\left(\frac{f_{a,n} \cdot L_{tot}}{n}\right)^2 \tag{7}$$

where $f_{a,n}$ is the axial resonance frequency that corresponds with the n^{th} axial mode, ρ is the board density at the time of measurement of axial resonance frequency, and L_{tot} is the total length of the board. The axial dynamic MOE value that is presented in Table 2, and there denoted $E_{a,1}$, was calculated on the basis of the first axial resonance frequency. The vibrations were excited from a blow of an impulse hammer at one end of the board and measured by an accelerometer that was fastened using wax at the other end.

The determination of MOE using resonance frequencies for edgewise bending modes of vibration is more complicated in comparison with MOE determination using axial resonance frequencies, since transversal vibrations include shear, which means that the shear modulus, G, also has to be regarded. In the investigation presented by Olsson *et al*. (2012), the six lowest resonance frequencies of edgewise bending modes were measured for the 105 boards in a similar way as for the axial modes, apart from the fact that the vibrations were excited from a hammer blow at the narrow edge at one end of the board, and that the accelerometer at the other board end was fastened on the same edge. The bending resonance frequencies were denoted $f_{b,n}$ where n refers to the n^{th} resonance frequency. Corresponding MOEs, represented as $E_{b,n}$, were calculated for each board on the basis of an assumed shear modulus G=700 MPa, a measured board density, Timoshenko beam theory by which shear deformations are taken into account, and a finite element board model for modeling the stiffness of the board. In Table 2, the mean value and the standard deviation for $E_{b,1}$, *i.e.* the MOE corresponding with the resonance frequency for the first edgewise bending mode, is exhibited. For clarity, it should be noted that G has very little influence on resonance frequencies of lower bending modes. According to the Bernoulli-Euler beam theory, in which shear deformations are neglected, the edgewise MOE for free-free boundary conditions, meaning that the beam is floating, is determined as

$$E_{b,n} = \frac{4mL_{tot}^4 f_{b,n}^2}{\gamma_n^2 \pi^2 I} \tag{8}$$

where

$$\gamma_n = \left[n + \left(\frac{1}{2} \right) \right]^2 \tag{9}$$

and n is the number of the mode of vibration, m is the mass per length unit, ρ is the board density, L_{tot} is the total board length, I is the second moment of inertia in the edgewise direction and h is the depth of the board, see Figure 6. Thus, application of Equation (8) means that $E_{b,1}$ can be approximated from

$$E_{b,1} = \frac{4mL_{tot}^4 f_{b,1}^2}{\gamma_1^2 \pi^2 I} \approx 0.96 \frac{\rho L_{tot}^4 f_{b,1}^2}{h^2} \tag{10}$$

The local static MOE in flatwise bending, denoted E_{cook}, was determined using a three-point bending machine of make Cook-Bolinder, see Figure 7 (left). The boards were fed through the machine at a feed speed of 40 m.p.s., which was the lowest speed possible to set. A low feed speed reduces the board vibrations, which, in turn, contributes to more stable and reliable measurements. As a board is passed through the machine, it is exposed to a

flatwise three-point bending at which the board is supported by two fixed rollers located at a distance of 900 mm, see Figure 7. A pre-determined deflection δ of 5.6 mm is applied and the corresponding load needed to achieve this deflection is registered by a load cell at a measurement interval of one (1) cm between measurement points along the board's length. To account for possible initial bow, the boards are fed through the machine twice with different bending directions and the average load at every measurement point is calculated. The corresponding $E_{cook,local}$ values are calculated as

$$E_{cook,local} = \frac{P_{average} \cdot L^3}{48 I \delta} \tag{11}$$

where $P_{average}$ is the average load at every measurement point, L is the distance between the fixed rollers and I is the second moment of inertia in the flatwise direction. Moving average MOE values for intervals of ten cm along the length of the board were then calculated and the lowest of these average values was chosen as the board's E_{cook} value, *i.e.* the local static MOE in flatwise bending. Regarding the Cook-Bolinder measurements, it might be considered as somewhat misleading to characterize E_{cook} as a *static* MOE, due to the vibrations that occur in a board on its way through the machine. The MOE value is *static* in comparison with $E_{a,n}$ and $E_{b,n}$, but as a consequence of the board vibrations, *quasi-static* might be a more appropriate term.

The results presented in Table 2 show that MOE values determined using dynamic excitation ($E_{a,1}$ and $E_{b,1}$) are higher than corresponding values obtained from static bending in both edgewise (E_m and $E_{m,g}$) and flatwise (E_{cook}) directions. It is also shown that E_{cook} is the MOE measure that gives the

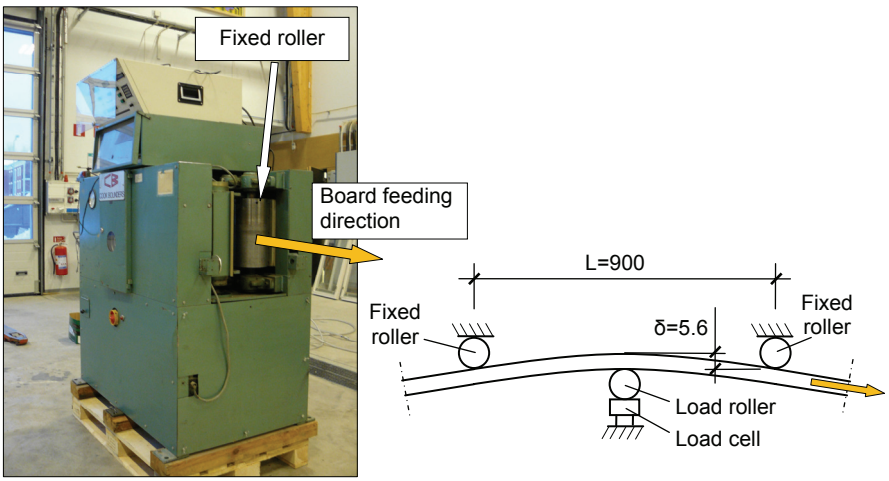

Figure 7. Measurment principle (right) for Cook-Bolinder strength grading machine (left).

lowest MOE value. The described differences between the MOE measures could be explained by various combinations of interacting factors.

There are at least two reasons why $E_{a,1}$ and $E_{b,1}$ are higher than E_m. Firstly, the two dynamically determined MOEs both reflect average MOE values for entire boards, whereas the E_m is measured locally over the assumed weakest section. Secondly, the two "dynamic" MOEs are determined on the basis of resonance frequencies that are measured instantaneously, whereas the local static edgewise MOE is based upon deformations that are measured over a certain period of time and, thus, allowing for creep deformations to develop (see *e.g.* Larsson *et al.* 1998).

The global static MOE, $E_{m,g}$, is also affected by creep since it is measured over the same period of time as E_m, see Figure 6, but unlike E_m, it represents, just as the two dynamically determined MOEs, an average MOE for the entire board. Nonetheless, the achieved $E_{m,g}$ exhibited in Table 2 was even somewhat lower than E_m, a relationship that also could be found in other investigations, *e.g.* Källsner and Ormarsson (1999). According to their research, one reason why $E_{m,g}$ determined in agreement with EN 408 results in low MOE values is that vertical compression perpendicular to the grain occurs at the supports when load is applied. Consequently, an increase of the global deformation, *i.e.* the deformation denoted w in Figure 6, is measured. A further enlargement of this deformation is, according to Källsner and Ormarsson (1999), observed for tested planks that are initially twisted. At the start of a bending test, such shape distortion results in lack of full contact between the supports and the edge surface of the planks. When load is gradually applied, the area of contact is increased due to rotation of the plank ends, but this rotation also results in an increase of the measured mid span deformation. Another factor that contributes to an underrating of $E_{m,g}$ in relation to E_m is that the former includes shear deformations (Boström 1999). Thus, of the two edgewise bending MOEs that are determined statically, the one that is measured locally is the one that is most appropriate as indicating property for determination of strength class.

Finally, the E_{cook} value, which was the lowest MOE value achieved for the 105 planks, was, just as the E_m value, determined locally at a critical board section, but on the basis of a somewhat different span and load case (900 mm, see Figure 7). However, the creep that is assumed to affect E_m is not reflected in E_{cook}, since the measurement of applied load in the flatwise bending machine is done instantly and continuously along a board as it is fed through the machine. Still, the E_{cook} value was 12 % lower than E_m, which actually indicates that the creep effect on deformations used for determination of E_m and $E_{m,g}$ is probably rather limited. The relationship between E_{cook} and E_m has previously been investigated by, for example, Steffen *et al.* (1997) who found that the local flatwise MOE, determined using a Cook-Bolinder strength grading machine, was considerably lower than the local edgewise static MOE determined from bending test according to EN 408. This was explained by two

main factors. Firstly, E_{cook}, being determined on the basis of three-point bending tests, includes shear deformations which accounts for about half the difference between E_{cook} and E_m. Secondly, the natural variation of MOE over the cross section of a piece of structural timber cut from the centre of a log contributes to an increase of E_m. This can be explained by reference to Figure 8, which shows an example of a sawing pattern, a so called 2X-log pattern, which is frequently used in sawmilling operations. As described in section 2.2.1, MOE increases in the radial direction of a tree, *i.e.* from the pith and outwards. The ratio between MOE measured for mature wood close to the bark and MOE measured for juvenile wood close to the pith could be as high as two, see Figure 8 (right). When boards such as those shown in Figure 8 are bended in the edgewise direction, the MOE distribution over the cross section is favourable, since the fibres with the highest MOE values are located in the parts of the cross section where the largest strains occur. This will, in turn, contribute to a higher E_m value. On the other hand, when the boards are bended in the flatwise direction, parts of the largest strains will be obtained in the juvenile wood which will result in a comparatively low E_{cook}.

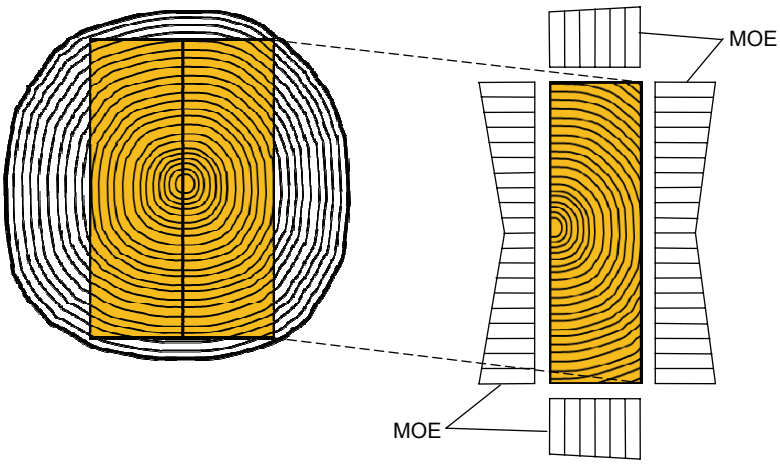

Figure 8. 2X-log sawing pattern (left) and variation of MOE along the edges of a board sawn from such a sawing pattern (right).

2.2.2.2 Knots

It is well known that strength of structural timber is reduced when knot size is increased, but from simple linear regression analysis, using strength as response variable and different measures reflecting the occurrence of knots as a single predictor variable, limited relationships in terms of coefficient of determination are actually found. The R^2 values reported in Table 1 between tensile strength and applied knot measures varied between 0.30 and 0.42, and

R^2 between knots and bending strength was even lower; between 0.16 and 0.27. Once again, and as mentioned in the first paragraph after Table 1 in section 2.2.2.1, it should be stressed that results from different investigations in Table 1 are *not* directly comparable, since different samples and different test set-ups were used.

The knot measures that were included in the six investigations referred to in Table 1 were determined on the basis of visual inspection. In total, more than ten different knot measures were applied. A common denominator of the investigations was that various so called *knot area ratios* (KAR) were applied in all of them. Two such ratios widely used also in other research (*e.g.* Lam *et al.* 2004) are *total knot area ratio* (TKAR) and *margin knot area ratio* (MKAR). Both are defined in the British Standard BS 4978, the former as *ratio of the sum of the total projected cross-sectional areas of all knots intersected by any cross-section to the total cross-sectional area of the piece* and the latter as *ratio of the sum of the projected cross-sectional areas of all knots or portions of knots in a margin intersected at any cross-section, to the cross-sectional area of margin*. These definitions are visualized in Figure 9. According to BS 4978, different knots shall be included as part of the same cross-section if any part of the knots or the grain disturbances around them overlap along the length of the timber piece. In that way, the effect of knot clusters could be regarded. The *margin* is understood as one of the outer quarters of the width of the piece. Thus, application of MKAR means that the position of the knots within a cross-section is taken into consideration. It should be noted that there are other definitions of both TKAR and MKAR than the ones presented in BS 4978. For example, Isaksson (1999) calculated MKAR as the sum of the projected cross-sectional knot areas in *both* outer quarters of the cross-section of a timber piece, divided by half the cross-sectional area. He also determined TKAR and MKAR on the basis of the sum of the projected knot areas of knots located within a longitudinal "window" of 150 mm length, see Figure 9. Similar "windows" were also applied in two of the investigations (no. 1 and no. 5) referred to in Table 1.

The results of the investigations in Table 1 showed that the relationship between strength and occurrence of knots could be improved if knot positions within a cross-section were regarded, but the relationship was still poor. Similar weak correlations between bending strength and position related knot measures were also found by Isaksson (1999) and Ziethén (2006).

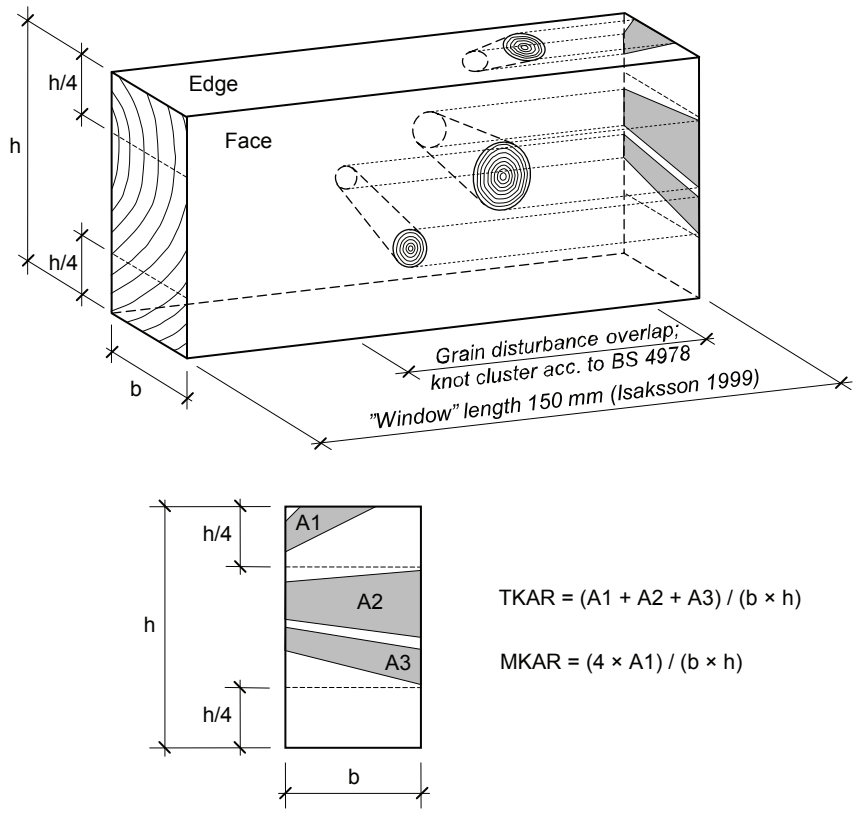

Figure 9. Definition of knot area ratios TKAR and MKAR. Top: Knot projection on a cross-sectional plane according to BS 4978, and "window" length defined by Isaksson (1999) for calculation of KAR values of knot clusters. Bottom: Projected cross-sectional areas of knots, and equations for determination of TKAR and MKAR, respectively, according to BS 4978.

The results presented in Table 1 show that the relationship between knots and board strength could be improved using *multiple linear regression analysis*. When MOE measures and knots measures were applied together as indicating properties, the multiple linear regression resulted in R^2 values as high as 0.73 with respect to bending strength, and 0.78 with respect to tensile strength. However, these high R^2 were mainly due to strong relationship between strength and MOE.

When knot measures were combined with density or annual ring width, a considerable increase of R^2 between such combinations of indicating properties and bending strength were achieved, see Table 1, in comparison with what was obtained when a knot measure was used as indicating property alone.

From the results presented in this section, it could be concluded that knot measures as suggested and defined in the research referred to above do not

alone provide a firm ground for strength grading. At the same time it is well known that the presence of knots has a large influence on the initiation of fractures in structural timber (see for example Figure 1). Attention should also be called to the fact that the design of visual strength grading rules, such as those stated in the Inter-Nordic standard INSTA 142, in general implies that the occurrence, location and size of knots are crucial for the grading. In an investigation concerning visual strength grading carried out by Johansson *et al.* (1998) it was found that about 65 % of the boards graded in the investigation were downgraded due to the presence of knots or knot clusters. Further evaluation of the results showed that the presence of knots was the cause of fracture for 91 % of the tested boards (Johansson 2003).

As a consequence of what has been related above, two somewhat contradictory conclusion that can be drawn regarding knots are that they, on one hand, have a very strong influence on the load bearing capacity of a board, but the usefulness of various knot measures as regards prediction of bending strength is, on the other hand, rather poor when knots are used as single indicating properties. However, when a knot measure and an MOE measure are used together as IPs in multiple linear regression, the knot measure may contribute to stronger relationships between strength and IPs (see investigations 2, 3, 5 and 6 in Table 1). Nevertheless, establishment of theories and models that could provide more reliable descriptions of the relationship between knots and bending strength would offer opportunities for development of more accurate strength grading methods.

2.2.2.3 Spiral grain and other fibre angle deviations

Spiral grain is a further wood characteristic that is important not only, as mentioned in section 1.1, for shape stability of structural timber, but also for the strength and stiffness. Since these latter properties are far better in the longitudinal direction of the grain than in the perpendicular direction, an increase of the grain angle in relation to the longitudinal direction of a timber member implies a decrease of the member's structural performance. This also holds for local grain disturbances occurring, for example, close to knots, at top ruptures and in areas where cross-grained wood is found.

Research concerning the relationship between grain angle and strength of timber was carried out already in the early 1920s. Relationships between grain direction and strength in tension, compression and bending, respectively, were presented, see Figure 10 (Dinwoodie 2000, after Baumann 1922), and an empirical formula for the relationship between varying grain angle and compression strength of spruce was introduced (Hankinson 1921). In the latter research it was also found that the formula was valid when applied to other wood species as well. On the basis of further research (see Kollman and Côté 1968), the original formula was modified to include both compression and tensile strength. In this developed form, it can be written as

$$f_\theta = \frac{f_0 \cdot f_{90}}{f_0 \sin^n \theta + f_{90} \cos^n \theta} \tag{12}$$

where f_θ is the strength at angle θ from the grain direction, f_0 is the strength parallel to the grain, f_{90} is the strength perpendicular to the grain, and n is an empirically determined constant that is dependent on the load being applied in either tension or compression.

Hatayama (1984), investigating four different wood species, found that the grain angle distribution in the vicinity of traversing wide-face knots could be described by an empirical function expressed as

$$\theta = \frac{15 \cdot \sqrt{N^\phi \cdot \phi}}{\sqrt{x}} - \frac{\phi}{2} - 5 \tag{13}$$

in which θ is the three-dimensional grain inclination (degrees), $\varnothing$ is the diameter of the knot (cm) defined as the average of the knot diameters measured on opposite wide-faces, x is a horizontal distance (cm) from the knot (see Figure 11), and N is an empirically determined constant the variation of which ($0.9 \leq N \leq 1.3$) is dependent on the species and whether the knot is dead or intergrown. Grain angle functions established for various combinations of loading, species and type of knots were used by Hatayama for determination of the corresponding constants n in Hankinson's formula. For this purpose, strength in tension and compression were experimentally determined for different strips cut from boards containing single wide-face knots (see Figure 11). The n values for the different combinations of load, species and knots were achieved on the basis of finding a good fit between the experimentally obtained strength of the strips and corresponding strength calculated using Hankinson's formula. Finally, tensile, compression and bending strength were experimentally determined for three samples of knotted boards (one sample for each testing mode) with cross section dimensions varying from 15×95 mm to 40×235 mm. Each sample included pieces of all four species and the total numbers of investigated boards calculated as the sum of all four species were 55 in tension, 121 in compression and 57 in bending. The strength of the boards was also predicted using the described expressions of Hankinson's formula, including the fitted n values. The relationships between experimentally measured and calculated (predicted) strengths were *not* presented in terms of correlation (R) or coefficient of determination (R^2), but such value could be calculated using the results presented in Hatayama's paper. The R^2 values, here calculated as average of the investigated species, were found to be as strong as 0.88 for tension, 0.80 for compression and 0.78 for bending.

Hatayama also showed that Hankinson's formula could be used for prediction of MOE in tension and that this MOE value decreases rapidly with

increasing grain angle. The latter has also been established in research carried out by Ormarsson (1999).

Even if the applicability of Hatayama's grain angle function according to Equation (13) is limited since it is developed only for traversing wide-face knots, it shows that knowledge about grain disturbances around knots could be utilized for the purpose of obtaining accurate predictions of strength properties of timber. For a more detailed discussion concerning the findings of Hatayama (1984), see Foley (2003).

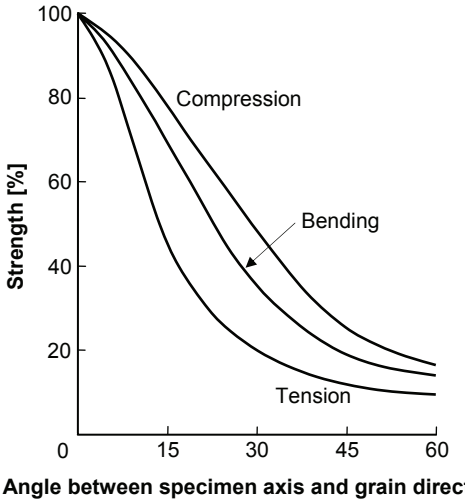

Figure 10. Effect of grain angle on tensile, bending and compression strength of timber (Dinwoodie 2000, after Baumann 1922).

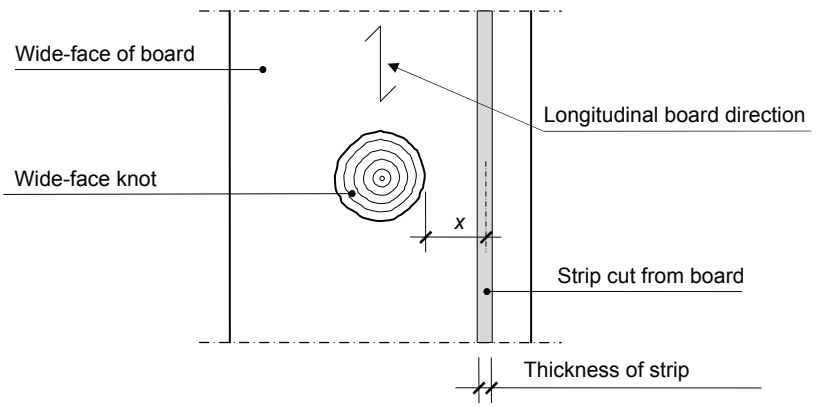

Figure 11. Strips cut at different distances x from wide-face knots for determination of the relationship between three-dimensional grain angle and strength in tension and compression, respectively (Hatayama 1984).

The variation of grain angle on the surface of a timber piece can be determined on the basis of tracheid effect scanning (*e.g.* Petersson 2010). This effect means that a beam of laser light that strikes a wood surface will be scattered within the wood and that the scattering is larger in the fibre direction than in the direction perpendicular to the fibres. This implies that a laser dot that illuminates a wood surface will take the shape of an ellipse oriented in parallel with the fibre direction. The grain angle can also be determined by *e.g.* application of microwaves (Schajer and Bahar Orhan 2006) or by dielectric scanning (Bechtel and Allen 1987).

2.2.2.4 Density

As mentioned in the first paragraph of section 2.2.1, the correlation between clear wood density and strength is rather strong in both tension and bending, whereas these relationships are weaker when determined for timber, *i.e.* for boards and planks of full size.

Timber density is one of the three wood characteristics that are referred to as *grade determining properties* for structural timber assigned to strength classes of EN 338. As mentioned in the first paragraph of section 1.2, the characteristic and mean densities given in EN 338 refer to timber with a moisture ratio of about 12 %.

Results from investigations concerning the relationship between timber density and strength in bending as well as in tension are shown in Table 1. In bending, the R^2 values vary between 0.16 and 0.40, and in tension they are, on average, somewhat higher ($0.29 \leq R^2 \leq 0.38$). However, and as asserted in the paragraph immediately after Table 1, this difference may to some extent be explained by the fact that different samples and different test set-ups were used in the investigations referred to in Table 1. It is also important to note that oven-dry density (0 % moisture ratio) was applied in investigations no. 1 and no. 3-6. As regards the remaining investigation (no. 2), it is not quite clear what density measure that was applied.

For the sample of 105 planks (with dimension 45×145×3600 mm) that was used in the investigation described in Paper IV and discussed in section 2.2.2.1 (see Table 2), the coefficient of determination between bending strength and density at 12 % moisture ratio (ρ_{12}) was 0.27, which is similar to the corresponding values presented in Table 1. However, the research presented in Paper II concerned 116 boards with dimension 25×56×3000 mm tested in tension, and the relationship between tension strength and density (ρ_{12}) was for this sample as low as R^2=0.12, *i.e.* a much lower value than what was found in the tension tests exhibited in Table 1. The reason for this is most likely related to the very narrow dimensions of the boards described in Paper II, which make both strength and stiffness very sensitive to occurrence of large knots, and, as a consequence, less dependent on properties such as density.

From the R^2 values presented in the two last paragraphs, it is evident that the relationship between density and strength of a timber piece is moderate, in spite of the fact that density is a *grade determining property*. At the same time the relationship between density and MOE is often rather strong (*e.g.* Olsson *et al.* 2012). This implies that the benefit of applying density as a second indicating property, *i.e.* to be used in combination with MOE for prediction of strength, is limited.

The main reason why density is elevated to the status of *grade determining property* can be referred to the relationship between density and the load-bearing capacity of fasteners such as nails, bolts and dowels installed in connections of timber structures. The characteristic strength of such fasteners are calculated according to formulas in Eurocode 5 (EN 1995) and these strengths, and formulas, are most often dependent on the characteristic timber density as defined in EN 338. Accurate information about the density is also crucial for accurate determination of axial dynamic MOE of a piece of timber, see Equation (7).

2.2.2.5 Annual ring width

When strength grading is carried out on the basis of visual rules such as BS 4978 or the Nordic visual strength grading rules INSTA 142, both referred to in EN 1912, it is not possible to predict the board density *directly*. Instead, visual grading standards include limits concerning maximum annual ring width. By such requirements, density is *indirectly* regarded (Hoffmeyer 1984), which is explained by the fact that the density in late wood is much higher than in early wood. When the annual ring width decreases, the part of the board cross section that is covered by the heavier late wood increases, which also creates an increase of the board density. However, the correlation between annual ring width and density that has been found in previous research is modest. In investigations presented by Hoffmeyer (1990), Johansson *et al.* (1992) and Johansson *et al.* (1998), the R^2 values varied from 0.18 to 0.38. Consequently, to use annual ring width as a substitute for density in visual grading can be questioned. Concerning the relationship between strength and annual ring width, it is on a similar level as R^2 between strength and density, see Table 1.

Regarding the machine strength grading techniques of today, measures of annual ring width are actually not applied as grading parameters. As mentioned in section 1.1, general requirements regarding both visual and machine grading are included in the European Standard EN 14081-1, and the parts that are applicable for machine grading are void of limitations concerning annual ring width.

2.2.2.6 Top ruptures

This kind of defect is caused by the top of a tree being broken off by *e.g.* browsing game or load of heavy snow or wind. When such damage occurs, one of the branches just below the rupture of the stem bends upwards and takes the place as leading shoot. As the tree continues to grow, the grain disturbances caused by the top rupture are overgrown and the damage could later in the life time of the tree be observed as a crook on the stem. On boards cut from logs that contain top ruptures, the grain disturbances appear in different ways depending on the orientation of the saw cuts. When the plane of these cuts are parallel with the plane of the crook in the stem, as shown in Figure 12, the grains are oriented in a pattern that corresponds with the crook. However, when the saw cut plane is perpendicular to the plane of the stem crook, the damage is more difficult to observe since the top rupture produces a so called *diving angle*, also denoted *out-of-plane angle*, between the fibre direction and the observed face of the board.

Top rupture occurs rather seldom but when it does it has a serious effect on the strength and stiffness of boards and planks. In an investigation of about 500 timber pieces of Norway spruce (Johansson *et al.* 1992), *i.e.* investigation no. 1 in Table 1), the point with the lowest flatwise bending stiffness was located in each piece. In almost all of them it coincided with either knots or top ruptures.

To the knowledge of the author of this thesis, none of the strength grading machines that are available on the market today include detection of top ruptures. This also holds for optical scanners that are utilized for visual override, but occasionally, when such scanning is applied, grain deviations caused by top ruptures are identified as cross-grained wood (Svensson 2012). However, to be able to identify actual top ruptures in the process of strength grading, manual inspection still has to be relied upon. Implementation of top rupture detection algorithms in grading machines or scanners is a challenge to be addressed in the future.

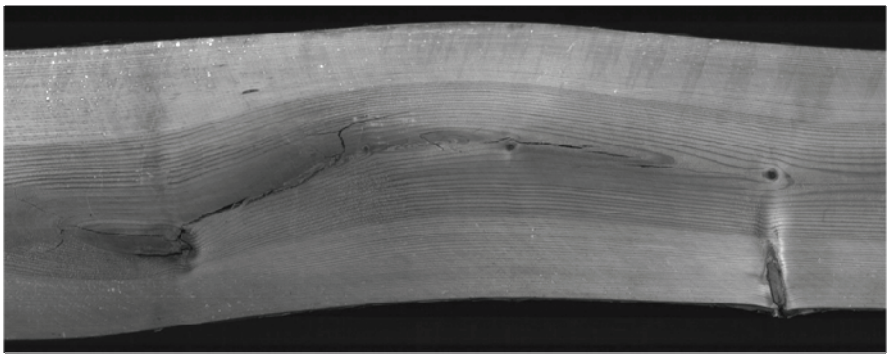

Figure 12. Top rupture in sawlog of Scots pine (Skog et al. 2011).

Regarding identification of top ruptures on logs, Skog *et al.* (2011) investigated the possibility of using the sharpness of the crook of sawlogs as indicator. Outer shape and heartwood shape of logs of Scots pine (*Pinus sylvestris*) was determined on the basis of data from an optical three-dimensional log scanner and an X-ray scanner, respectively. The research showed that both shapes can be applied for detection of top ruptures.

2.2.2.7 Compression wood

When a tree is exposed to eccentric load caused by *e.g.* snow load, wind load or stem inclination induced by the tree growing on sloping ground, so called *reaction wood* is formed as a means for the stem to re-erect itself and to retain vertical growth (Säll 2002). In softwoods, this kind of wood is called *compression wood* since it is formed on the compression side of the stem. In hardwoods, the formation takes place on the opposite side and the wood is, consequently, called *tension wood*.

Compression wood is characterized by a higher late wood proportion in the annual rings (Isaksson 1999). This is, in turn, due to the walls of late wood fibres being thicker in compression wood than in normal wood (Johansson 2003), which also implies a higher density in the former type of wood (Isaksson 1999). The thickness of early wood fibres in compression wood is, however, about the same as in normal wood (Ormarsson 1999).

Another difference between compression wood and normal wood is found within the cell wall. In compression wood, the so called S_3 layer of the cell wall is missing and the microfibril angle in the S_2 layer is much larger than the corresponding angle in normal wood. This results in a considerable reduction of the longitudinal MOE (Johansson 2003) and an increased shrinkage in compression wood (Dinwoodie 2000).

As regards load bearing capacity of compression wood, it is found that tensile strength is lower and compression strength is higher than that of normal wood (Dinwoodie 2000). Thus, due to high density, low tensile strength and low longitudinal MOE, density is a very poor indicating property for strength of compression wood (Foley 2003). It is also well known that tensile failure in compression wood often is brittle, see Figure 13.

In visual inspection of timber, compression wood is identified as areas with darker brownish colour. According to the visual override requirements in EN 14081-1, it is characterized as an abnormal defect (Brundin 2011), which could be accepted as long as the reduction in strength that is caused by it is obviously less than what is caused by other defects to which visual override requirements are applicable. Rules that are somewhat more adapted to practical use are found in *e.g.* INSTA 142 in which the occurrence of compression wood is, *inter alia*, limited to 10 % of the cross sectional area of timber pieces graded to strength classes C18, C24 and C30.

Figure 13. Brittle tensile fractures in compression wood. Left: Lamination fracture in wet glued beam (dim. 50×300×5400 mm) with laminations of Norway spruce side boards. Right: Structural timber (dim. 45×145×3600 mm) included in the tests presented in Paper IV.

Most grading machines on the European market utilize average board MOEs as indicating property. Consequently, it can be presumed that such measures include the effect of low MOE in compression wood. When it comes to visual override requirements, compression wood can be identified and evaluated manually, but it may be difficult to discern, particularly on flatwise surfaces of timber pieces, since its colour may resemble the colour of both rot and pith. The possibility of detecting compression wood using different scanning techniques has been investigated by Nyström (2002), who found that a combination of colour detection and tracheid effect scanning was the most promising method for industrial implementation. The tracheid effect is dependent on the wood density, implying that conduction of light in the fibre direction of compression wood is reduced in comparison with clear wood, due to the larger cell wall thickness in compression wood.

2.2.2.8 Rot

Rot is a serious defect that is caused by different kinds of rot fungi that attack and degrade the walls in wood fibres. The growth of such funguses is dependent on temperature. They can, according to Nylinder and Fryk (2011), grow at a temperature in the range of 0-40 °C with an optimum between 25 to 32 °C. They also need access to free water in the wood cells, *i.e.* a moisture content (MC) that exceeds the fibre saturation point, which for Norway spruce normally occurs at about 30 % MC. The growth is at its largest at 40-80 % MC (Nylinder and Fryk 2011).

Root rot is a defect that is caused by funguses attacking root systems, primarily via stumps from recently felled trees. Also root damages caused by forestry machines applied at thinning operations imply a risk for root rot infestation (Nylinder and Fryk 2011).

Saw logs may also be attacked by rot. Immediately after the cutting of a stand, the MC in the saw logs is in most cases far too high for the funguses to develop. However, in the summer the MC could quickly decrease to levels at which growth conditions are favourable. Accordingly, the development of rot in saw logs could be avoided by retaining a high MC. This could be achieved by wet storing, which means that water is sprinkled over log piles (Nylinder and Fryk 2011).

Due to the deterioration of the cell wall, a rot fungi attack results in a fast reduction of the strength. Limitations regarding occurrence of rot is included in the visual override requirements in EN 14081-1. *Soft rot*, *i.e.* rot that has reached an advanced stage of development at which the strength of the wood cells is strongly reduced, is not permitted in timber members graded to *any* strength class. *Dote*, also called *firm rot*, is, on the other hand, accepted in strength classes C18 and below, since this concept refers to rot at an early stage at which strength has not changed to any appreciable extent.

Following an attack of most of the existing rot fungi, the colour of the wood turns brownish, which means that this kind of defect might be detected by use of optical colour scanners. However, and as mentioned in section 2.2.2.7, the colour of the attacked wood cells is sometimes similar to that of pith or compression wood, implying a certain degree of limitation as regards optical rot detection. Rot may also be identified on the basis of either ultrasonic measurements (Beall 2002) or acoustic methods (Råberg *et al.* 2005), but application of these techniques require, as mentioned in section 1.1, contact between sensors and measured logs or timber pieces. Consequently, it can be concluded that manual visual inspection is, as yet, the most common method for identification of rot.

3 Strength grading – machines, techniques and standards

3.1 Strength grading in the past

Ever since man in a far distant past began to use wood as material for building of shelters and making of tools, it is most likely that knowledge about the difference in properties between both various kinds of species and different wood pieces has been available and utilized. Tradition and craftsmanship was the basis for timber sorting until some 150 years ago. In Sweden, the first actual rules for quality sorting of sawn timber were introduced in the second half of the 19th century. They concerned *appearance grading* based on visual inspection and they were implemented on a local basis in various districts along the coast of northern Sweden (Eliasson 2005). The concept of *appearance grading* refers to grading of sawn timber intended for other purposes than load-bearing structures. Such grading is still applied and on the European market of today it follows the rules laid down in the European Standard EN 1611-1.

The first detailed rules concerning visual strength grading of structural timber were introduced in the USA in the beginning of the 1920s (Glos 1995) and an American standard laying down principles for such grading was published in 1927 (Madsen 1992). During the following decades, similar rules were implemented in European countries. For example, strength grading based on visual inspection was standardized in Germany in 1939 (Glos and Heimeshoff 1982) and in Sweden the first edition of the so called *T-rules* for visual grading and marking of *T-timber* were published in 1951 (Anon 1981).

The shortcomings of visual grading is rather obvious since only visible defects such as knots, cross-grained wood and compression wood can be regarded, whereas intrinsic timber properties such as density and various measures of MOE could not. As shown in Table 1, the MOE is the timber property that is by far the one that is best correlated with strength. According to Madsen (1992), the idea of applying this relationship as a basis for strength grading of timber was presented in both the USA and in Australia in the late 1950s, but according to Hoffmeyer (1984) it was not until some years later that thorough documentation of strength properties of structural timber was begun.

Non-destructive flatwise bending machines for MOE measurements were introduced in Australia, the USA and the UK in the 1960s (Glos 1995) and the first grading machine in Sweden was approved in 1974 (Johansson *et al.* 1992).

3.2 Strength grading of today

Many visual strength grading rules implemented in Europe more than half a century ago are still in practice, most often in slightly developed editions. As an example, the Swedish *T-rules* are today embodied in the previously mentioned Inter-Nordic standard INSTA 142.

In Europe, there is a diversity of existing visual grading rules in use in different countries. This is a consequence of differences in species, geographic origin, dimensional requirements, quality of available material, historic influences and traditions, and varying requirements for different uses (EN 14081-1). However, many nationally applied visual grades are, on the basis of EN 1912, assigned to the common European strength classes defined as *C-classes* in EN 338.

As regards machine strength grading, a paradigmatic shift was begun in the late 1990s when the non-destructive measurement technique based on axial dynamic excitation was introduced. A longitudinal vibration is generated in a board by a hammer blow at one of the board ends and information about the induced vibrations is captured by a microphone, a laser vibrometer or an accelerometer. The first one measuring the "sound" of the board and the two latter ones capturing the axial oscillation of one of the board ends. On the basis of measured vibrations and by application of so called *Fast Fourier Transformation* (FFT), resonance frequencies corresponding to axial modes of vibration are determined. On the basis of such frequencies, and in combination with measured length and determined density, a mean axial dynamic MOE of a board can be determined from Equation (7). On a world-wide basis, many bending machines are still in use, but utilization of the axial dynamic technique is gradually increasing. At the time of writing, a total of about 25 models of different makes of grading machines are approved for grading on the European market, and axial dynamic excitation is applied in about 60 % of them. What is particularly attractive about this technique is that the equipment needed is installed in production lines where the timber is transported transversely, which means that the grading is carried out at a moderate feed speed. Furthermore, the equipment is fairly simple and the space needed for its installation is limited. Attention should also be brought to the fact that even if the described method only delivers the mean MOE of a board, the accuracy of the predicted strength is about the same as what is obtained from bending machines (see for example Table 2 and Betzhold 1999), despite the latter type being able to deliver information about MOE variation along a piece of timber.

Two grading machines that are based on axial dynamic excitation are the Dynagrade and the Precigrader (see Figure 14), both developed and marketed by the Swedish company Dynalyse AB. The main difference between these machines is that the Dynagrade applies an average density for a certain species, whereas the Precigrader measures the weight and calculates the density of each board to be graded. Since the first of these machines was introduced in 1997, they have gained large market shares and are today sold on the markets of *e.g.* Scandinavia, Russia, USA and Australia.

The simplicity of the axial dynamic excitation technique is underlined by the fact that a handheld and wireless measuring instrument called Timber Grader MTG from the Dutch company Brookhuis is approved for strength grading of structural timber intended for the European market. In addition to the actual axial dynamic grader (see Figure 15, left), a grading set (see Figure 15, right) includes a balance and a computer in which relevant software is installed. Such a set was utilized in the research presented in Paper II in which a more detailed description of the grading equipment is also found.

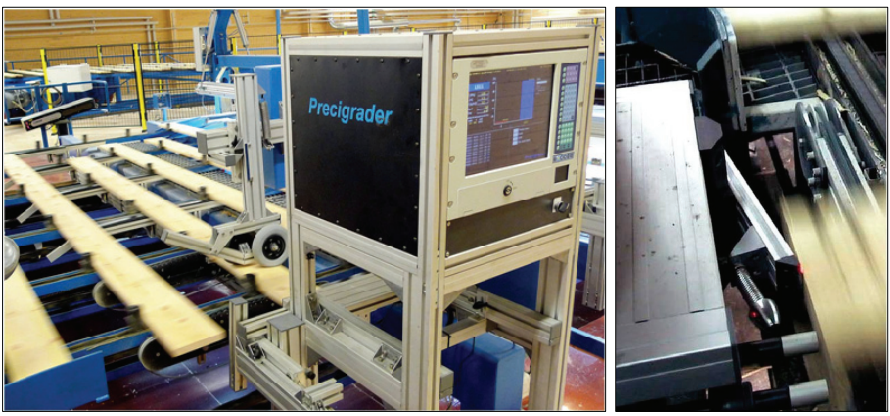

Figure 14. Precigrader grading machine in a sawmill production line with a length measuring device at the opposite side of the line (left), and dynamic excitation hammer (right). Photos by courtesy of Dynalyse AB, Sweden.

Figure 15. Timber Grader MTG (left) and grading set including grader, balance and computer with applicable software (right).

Grading accuracy can be improved by combining axial dynamic MOE with other indicating properties. One machine that combines this kind of MOE with information obtained from X-ray scanning is *Goldeneye 706* from the Italian company *Microtec*, see Figure 16. The X-ray scanning provides information about the density of a piece of timber and since there is a density difference between knots and clear wood, the scanning also gives information about knot size and knot position. When knot measures determined on the basis of the X-ray scanning was combined with axial dynamic MOE, a coefficient of determination as high as 0.69 was achieved between indicating properties and tensile strength (Bacher 2008). A relationship of R^2 = 0.58 between tensile strength and an IP based on axial dynamic excitation only was also reported.

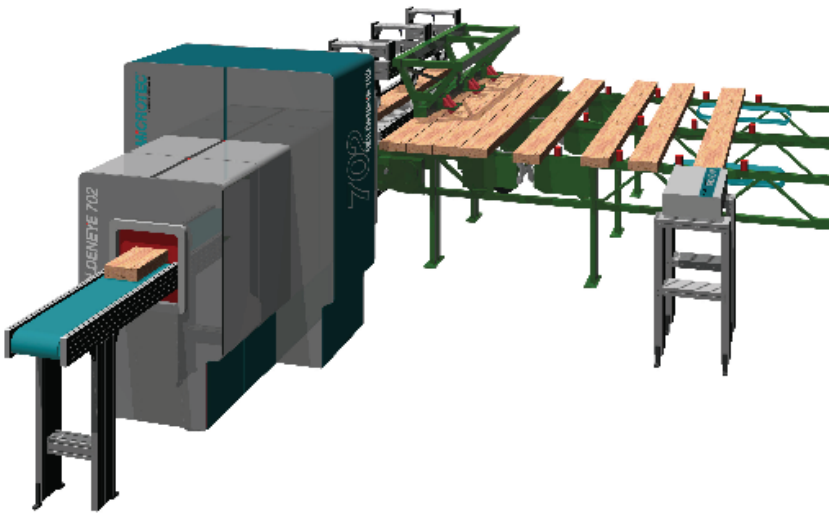

Figure 16. Set-up for GoldenEye 706 including axial dynamic excitation (right) and X-ray scanning left). Picture by courtesy of Microtec GmbH/srl, Italy.

On the market there are also grading machines that utilize other techniques than those described above. For example, the stiffness can be determined on the basis of a relationship between MOE and ultrasonic wave velocity, knots are detected by microwaves, density is determined from attenuation of γ-rays or microwaves, and grain angle deviation can be measured using either microwaves or the tracheid effect achieved when a board surface is illuminated by a dot laser. Even bending resonance frequencies are applied for MOE determination, but the utilization of this technique is, however, limited.

A grading method that is not applied in Europe today is so called *proof-loading*, which means that a board is loaded up to a stress level equal to the strength required for the intended strength class. If the board stands the test, it is accepted for structural use and classified accordingly. Ziethén (2006), who investigated different aspects of this method, claimed that it is mainly in Australia that proof loading is presently applied for strength grading.

3.3 European standards and approval of grading machines

3.3.1 Standards

Regulations for strength grading of structural timber intended to be put on the European market is found in a number of interrelated European standards most of which has already been referred to. The core standard is *EN 14081 Timber structures – Strength graded structural timber with rectangular cross section* which consists of four parts:

- Part 1 – General requirements, (EN 14081-1)
- Part 2 – Machine grading; additional requirements for initial type testing (EN 14081-2),
- Part 3 – Machine grading; additional requirements for factory production control (EN 14081-3), and
- Part 4 – Machine grading – Grading machine settings for machine controlled systems (EN 14081-4).

The general requirements laid down in EN 14081-1 comprise, as mentioned in section 1.1, both visual and machine strength grading, the latter also including visual override requirements. The rules concerning machine strength grading apply to grading systems that are either *machine controlled* or *output controlled*. Both types are based on so called *machine settings* which are determined on the basis of different procedures depending on which control system that is applied. The concept of settings, as defined in EN 14081-2,

refers to values of parameters that are used to set a machine to grade timber. They are mathematically related to indicating properties which, in turn, are related to one or several of the grade determining properties of the C-classes defined in EN 338, *i.e.* bending strength, MOE and density. Settings for a certain machine type define boundaries between different strength classes to be graded simultaneously by one machine in one production pass. Thus, the relationship between indicating properties measured for individual timber pieces and the settings for a machine determines to which strength class an individual piece shall be assigned. For some machine types, values of indicating properties are directly applied as settings, without the need of any further parameters.

The settings of a machine are dependent on species, grade, grade combinations, board dimensions and geographic origin of the timber to be graded. If, for example, several species are to be graded by a certain grading machine, different settings are required.

Machine control means that the grading is controlled only by the grading machine's settings which are derived on the basis of a rather comprehensive initial type testing (ITT) procedure laid down in EN 14081-2 and described in section 3.3.2 below. The results of such a procedure carried out for a specific machine type are evaluated by a technical group (TG1) set up under a technical committee (TC 124) within the European Committee for Standardization. Settings that are accepted by TG1 for a certain machine controlled system are constant for all machines of the same type and they cannot be influenced by neither sawmills nor grading machine manufacturers. Also for grading systems based on output control, settings are determined on the basis of initial type testing, but in this case they are considered as being merely *initial* since they can be adjusted in the run of sawmill production. The basis for such adjustments is proof-loading of pieces sampled on a daily basis from the sawmill production output. The consequence of the adjustment possibilities is twofold. First, the extent of testing required for determination of initial settings is much less than for determination of settings for machine controlled systems. Second, different output controlled machines of the same type can have different settings. Machine control systems are predominant on the European market, whereas output control is mainly used in North America, Australia and New Zealand.

The requirements in EN 14081-3 concern operation, calibration and maintenance of grading machines in current use, and EN 14081-4 contains grading machine settings that are accepted by TG1 for various machine controlled systems. However, the procedure of publishing machine settings in a European Standard was replaced in 2009 by a course of action implying that new machines or added settings can be introduced on the market as soon as acceptance has been obtained by TG1 and an ITT report has been issued. In a current proposal for a revised version of EN 14081, Part 4 is repealed.

Other important standards that are linked up with EN 14081 are

- *EN 338 Structural timber – Strength classes* (referred to in sections 1.2, 2.2.2.1, 2.2.2.4, 3.2 and 3.3.1),
- *EN 384 Structural timber – Determination of characteristic values of mechanical properties and density* (referred to in section 2.2.2.1),
- *EN 408 Timber structures – Structural timber and glued laminated timber – Determination of some physical and mechanical properties* (referred to in sections 2.1 and 2.2.2.1), and
- *EN 1912 Structural timber – Strength classes – Assignment of visual grades and species* (referred to in sections 1.1, 2.2.2.5, and 3.2).

3.3.2 Settings for machine controlled grading machines

3.3.2.1 Initial Type Testing

In the Introduction of EN 14081-2, it is stated that

> *The acceptability of grading machines and the derivation of settings rely on statistical procedures and the results will therefore depend on the method used. For this reason this document gives appropriate statistical procedures.*

These procedures are part of the initial type testing (ITT) that is described in the quoted standard. The settings accepted by TG1 for a specific type of machine refer to a single strength class or a combination of strength classes to be graded simultaneously in one production pass. The application of the settings is also limited by specified timber dimensions cut from trees of a certain species grown within a defined geographic area. One such area for which common settings often are applied consists of Sweden, Norway, Finland, Estonia, Latvia and northern parts of Russia west of the Urals. Another geographic area is Germany, Austria and the Czech Republic.

The ITT procedure for determination of settings can be divided into five main consecutive parts; sampling, grading, testing, determination of settings, and verification of settings.

3.3.2.2 Sampling

To derive machine settings that are valid for a new machine type, a minimum total number of 900 timber pieces originating from at least four different sub-samples shall, according to EN 14081-2, clause 6.2.2, be sampled. However, at the time of writing, the number of sub-samples required by TG1 as basis for settings derivation is often much larger. A number of eight is frequently applied (Ziethén 2012). Each sub-sample shall consist of at least 100 pieces, it

shall, in general, be sampled in full from one single sawmill, and it can include several board dimensions. The quality of the pieces shall be sawfalling, *i.e.* they must not be pre-graded. The sub-samples shall be distributed over the chosen geographic area with the purpose of reflecting the variation of growth conditions. The principles on which this distribution is based are, however, not laid down in detail in the standard, which may be regarded as a lack of transparency in the ITT procedure. To remedy this state of affairs, sampling guidelines has been issued by TG1 (Anon 2012).

It is in most cases sufficient to test three different board dimensions with varying width and thickness. The range of board sizes permitted to be graded on the basis of derived settings is ±10 % of the tested sizes. As an example, if a total sample of 900 boards includes the dimensions 35×150, 50×77 and 65×230 mm (see Table 3), the derived settings will be applicable for timber with dimensions ranging from 32×70 mm to 70×250 mm.

Table 3. Example of dimensions (marked with an "X") tested in an initial type testing resulting in settings valid for board sizes ranging from 32×70 mm to 70×250 mm.

Width [mm]	Depth [mm]		
	77	150	230
35		X	
50	X		
65			X

According to EN 14081-2, it shall be ensured that strength reducing characteristics that are not detected neither by the grading machine nor by the visual override inspection shall be present in the total sample in the same proportions as will exist in the sawmill grading. This may be relevant for characteristics such as top ruptures, rot and compression wood when optical scanners are applied for the visual override.

3.3.2.3 Grading

All pieces in the total sample are passed through the grading machine and the value of the indicating property (or properties) is recorded for each piece. Pieces that have defects that would be rejected by visual override inspection shall not be included in neither the total sample nor in any of the sub-samples (Anon 2012).

3.3.2.4 Testing – Determination of grade determining properties

The grade determining properties, *i.e.* bending strength, density and MOE, are determined at a selected critical section of each timber piece on the basis of tests and procedures described in EN 408 and EN 384, respectively. The section is "critical" in the sense that it should be assumed to be the weakest section along the piece. In four point bending tests, the critical section shall,

according to EN 384, clause 5.2, be positioned between the loads (see Figure 6). In the same clause it is also stated that the tension edge in bending shall be selected at random and that the grade of the piece shall be deemed to be the grade of the critical section. The MOE for this section is determined on the basis of a globally measured MOE, see Equation (6), that is subsequently adjusted to compensate for support indentation and shear deformations (see EN 384, clause 5.3.2). Density shall be determined from a small board section, cut as close as possible to the fracture obtained at a strength test (EN 408, clause 7).

For timber of Norway spruce, all measured values are adjusted to a moisture ratio of 12 %, since the characteristic and mean property values of the C-classes in EN 338 are defined for a climate that corresponds with an equilibrium moisture ratio of 12 % in Norway spruce. Furthermore, the bending strength is also adjusted to a reference board depth (or width) of 150 mm (see EN 384, clause 5.3.4.3), since the strength of structural timber is size dependent; the larger the depth, the lower the strength.

3.3.2.5 Determination of settings and assigned grades

The next step of the ITT procedure concerns development of mathematical models that describe the relationships between measured IPs and the values of the grade determining properties obtained from EN 408 tests. In general, one model is needed for each grade determining property. For example, simple regression models can be applied to describe the relationship between bending strength, σ_m, and an IP that often represents an average axial dynamic MOE. According to Equation (1), such models will follow the formula

$$\sigma_m = \beta_0 + \beta_1 \cdot IP \tag{14}$$

For a bending strength model as the one presented by Equation (14), settings in terms of IP values shall be determined for each grade to be graded together such that the required grade determining property, in this case σ_m, is achieved for each grade. The procedure for setting determination is rather comprehensive, but the principle is visualized in the scatter diagram shown in Figure 17 in which the setting for a grade combination of C24 and reject is exhibited. The setting value for C24, S_{C24}, is determined such that all pieces in the total sample with an IP larger than S_{C24} are assigned to C24, whereas pieces with a lower IP are assigned to reject. Grades determined in this way are called *assigned grades* and they reflect the performance of the investigated machine. Note that the setting value is chosen such that 5 % of the boards assigned to C24 do not fulfil the required strength of 24 MPa.

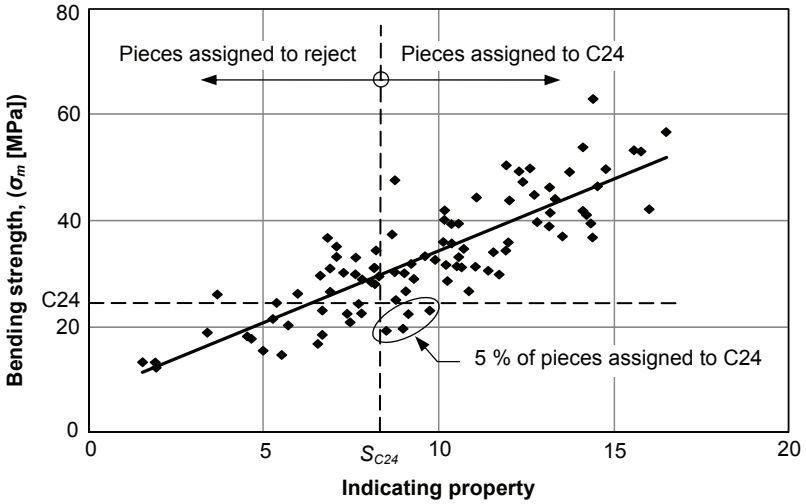

Figure 17. Determination of setting value, S_{C24}, and assignment of grades for a grade combination of C24 and reject.

3.3.2.6 Optimum grades and verification of settings

Verification of models and settings could be described as a course of actions in which the performance of the investigated grading machine is compared with an imaginary machine that is able to perform a perfect grading resulting in each timber piece being graded to its *optimum grade*, *i.e.* the highest possible grade of those for which settings are required. The optimum grade is determined on the basis of the results of the tests described in section 3.3.2.4. This means that the true values of the grade determining properties of each board shall equal or exceed the corresponding characteristic values (*i.e.* 5-percentile values of bending strength and density, respectively, and mean MOE) of the highest possible grade.

Each board in the total sample is arranged in a *Size matrix*, see example in Table 4, which shows to what extent boards are either wrongly up- or wrongly downgraded. The figures in the table indicate the number of boards arranged into each square.

Table 4. Example: Size matrix for a total sample of 900 boards graded to strength classes C30 and C18, and also reject.

Optimum grade	Assigned grade		
	C30	**C18**	**Reject**
C30	300	60	2
C18	16	429	8
Reject	8	12	65

Finally, the numbers in the Size matrix are divided by the total number of pieces in the assigned grade in question and multiplied with weighting factors that are pre-set in EN 14081-2 and dependent on the pieces being either wrongly upgraded or wrongly downgraded. The factors applicable to the former group are more severe than those applied for the latter one, since a wrongly upgraded board may jeopardize the strength of the structure in which it is installed, whereas the consequences of using boards that are wrongly downgraded are limited to the fact that larger dimensions than necessary are used.

The results of the described divisions and multiplications are presented in a *Global cost matrix*. The one achieved on the basis of the Size matrix in Table 4 is exhibited in Table 5.

Table 5. Example: Global cost matrix obtained from the Size matrix shown in Table 4.

Optimum grade	Assigned grade		
	C30	C18	Reject
C30	0	0.12	0.06
C18	***0.11***	0	0.12
Reject	***0.10***	***0.03***	0

For settings to be accepted, a number of requirements stated in EN 14081-2 have to be complied with. A crucial one is that none of the values in the squares of the Global cost matrix that reflect wrongly upgraded pieces must exceed 0.2. In Table 5, these values are shown in ***bold italics*** type. Another requirement is that characteristic values of the grade determining properties of the boards graded to a certain assigned grade shall fulfill the required values for that grade. If requirements are not fulfilled, the settings have to be adjusted and the assignment of grades and the procedure for verification of settings repeated.

3.3.2.7 Grading of one or several strength classes in a pass: Difference in setting values

According to EN 338, a strength class is defined by 5-percentile and mean values of different stiffness and strength properties. The application of 5-percentiles for the grade determining properties bending strength and density means that 5 % of the timber pieces assigned to a certain strength class do not have to fulfill the characteristic values of the class. This means that the setting, or IP value, for a certain class graded by a certain machine type vary depending on whether the class is graded as a single class or if it is graded together with other classes in the same production pass. In Figure 18, the setting/IP for boards graded to C24 as single class is illustrated. All boards for which the IP is larger than the setting, the latter denoted $S_{C24,single}$, are graded

to C24. Figure 19 shows settings for C24 and C30 when these classes are graded together. All boards with IP larger than the indicated setting $S_{C30,combi}$ are graded to C30, whereas all boards with IP between $S_{C24,combi}$ and $S_{C30,combi}$ are graded to C24. It is evident that the setting for C24 is more rigorous when C24 is graded together with C30 in comparison with the setting when C24 is graded as single class. This is an effect of the requirement that 95 % of the boards graded to a class have to fulfill the required 5-percentile values. It is also evident that the number of rejects is larger when several strength classes are graded together.

3.3.2.8 ITT procedure – Improvement potentials

In section 3.3.2.2 it is asserted that there is what may be regarded as a lack of transparency in the ITT procedure as regards the principles concerning sampling and geographic distribution of sub-samples. A part of the problem could possibly be explained by the terminology that is used in the interrelated standards as regards origin of timber. A number of partly overlapping terms (*e.g.* timber source, source, timber population, source country, source of production, growth area and accepted region) are used. Some of them are defined, but some are not. To understand the difference between many of them is, at least for researchers and engineers not involved in the work of TG1, difficult.

Another example of an issue that deserves to be highlighted is that the concept of settings is given two non-identical definitions; one in EN 14081-1 and another one in EN 14081-2. The terminology applied in the former definition emphasizes grading machine control, whereas the latter one lay stress upon the relationship between settings and indicating properties.

As regards the number of sub-samples in a total sample, it is mentioned in section 3.3.2.2 that at least four different sub-samples shall be sampled for derivation of settings for a new machine type, whereas the number required by TG1 is often much larger. On what grounds the required number is determined is, however, not fully transparent.

It should be mentioned that work concerning the revision of EN 14081 is ongoing.

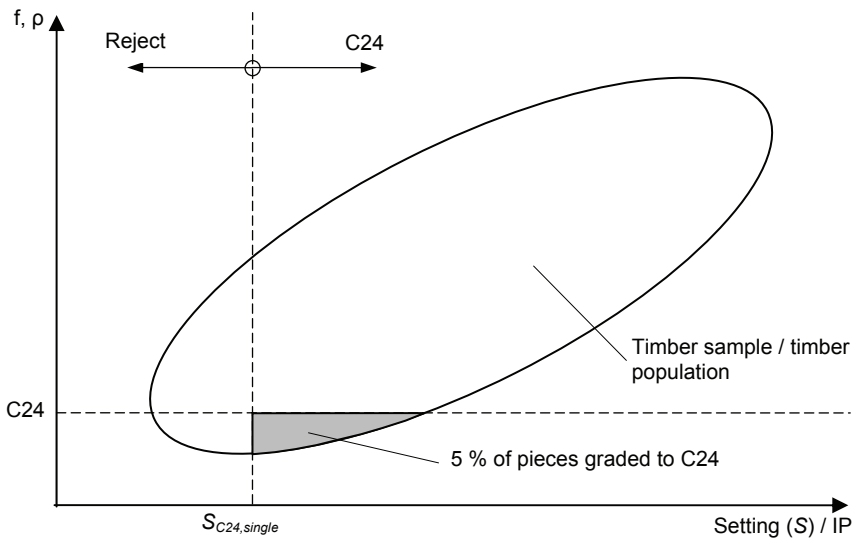

Figure 18. Setting when C24 is graded as single class.

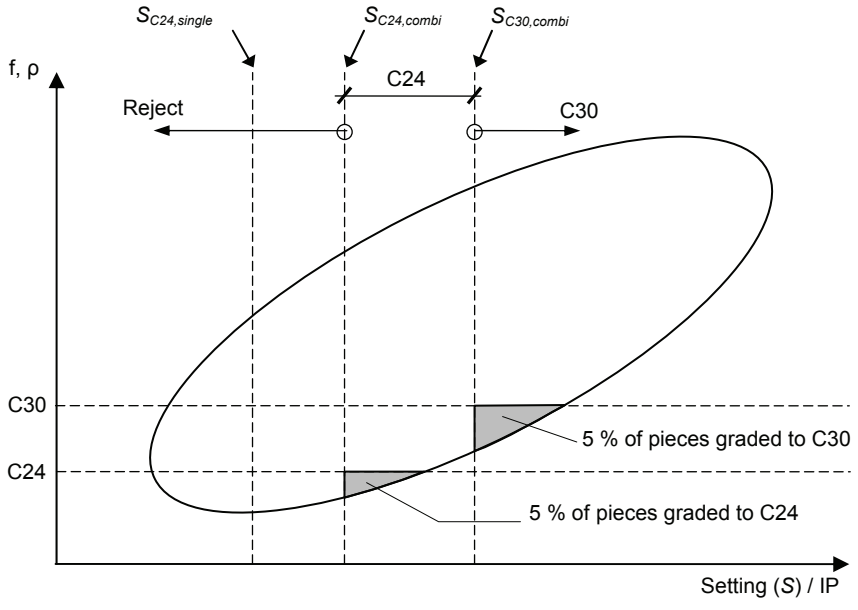

Figure 19. Settings when C24 and C30 are graded together in one pass.

4 Strength grading based on local stiffness – contributions of present research

4.1 Relationship between strength and occurrence of knots

From previous research and the results presented in appended Papers II and IV, it is evident that strength of timber pieces is, in general, dependent on the presence of knots. Results from bending tests of structural timber referred to in sections 1.1 and 2.2.2.2 have shown that more than 90 % of fractures in test pieces can be related to the occurrence of knots (Johansson 2003). In consideration of this, it may be found somewhat surprising that the relationship in terms of simple linear regression between strength and various indicating properties based on size and location of knots (*e.g.* TKAR and MKAR as defined in Figure 9) is rather weak.

The inherent contradiction between, on one hand, fractures being dependent on the presence of knots and, on the other hand, the knot measures being used up to now are poor predictors of strength can be explained by the fact that a fracture in a timber piece is in most cases *not* initiated precisely at an actual knot, but in wood fibres at some distance from it, see Figure 20 and Nagai *et al.* (2011). The orientation of such fibres deviates in general from the longitudinal direction of the piece. Thus, application of new IPs that not only take account of size and location of knots themselves, but also include effects exerted by surrounding clear wood fibres on structural properties of a timber piece, will be very useful for development of more accurate strength grading models. To be able to define such new IPs, detailed information about both fibre directions around knots and the joint structural behaviour of knots and surrounding fibres is needed. In this doctoral candidate project, two different measurement techniques was applied with the purpose of achieving such information; contact-free deformation measurements and laser scanning of fibre angles.

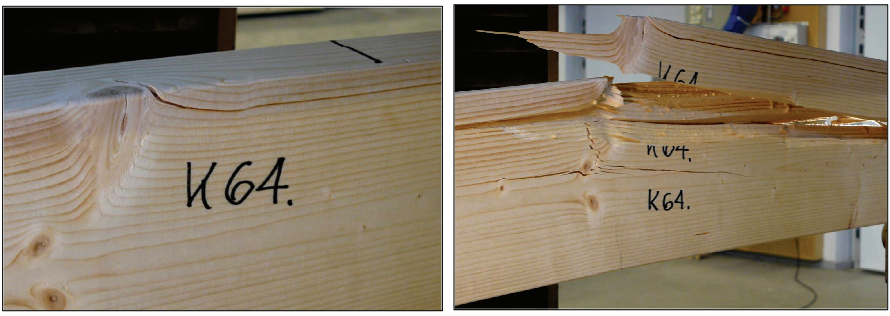

Figure 20. Typical initiation of bending fracture at an outbound arris knot (left) and fully developed fracture (right) in a timber piece of dimension 45×145×3600 mm.

4.2 Contact-free deformation measurements

4.2.1 DIC technique

A contact-free deformation measurement system based on white-light digital image correlation (DIC) was used in this doctoral project. The technique implies that strain fields occurring on a surface of a timber piece are calculated on the basis of deformations measured at a large number of pre-defined measuring points distributed over the surface. The strains fields, *i.e.* strains in lateral and longitudinal board directions and in shear, are determined and visualized as function of load level. In this research, DIC measurements were applied for determination of strain fields on both local and global level in timber pieces.

4.2.2 Strain fields around knots

Local tensile strain fields were determined around knots in a number of boards and test pieces. One such piece of dimensions 45×70×700 mm is shown in Figure 21. It includes a traversing edge knot and the longitudinal tensile strain fields occurring around the knot are shown in Figure 22.

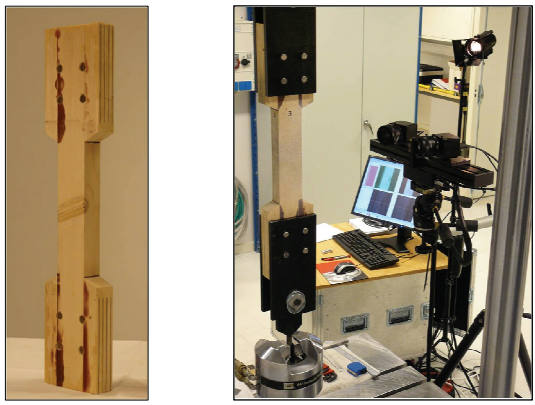

Figure 21. Test piece of dimensions 45×70×700 mm with traversing edge knot (left) and test set-up for contact-free deformation measurements (right).

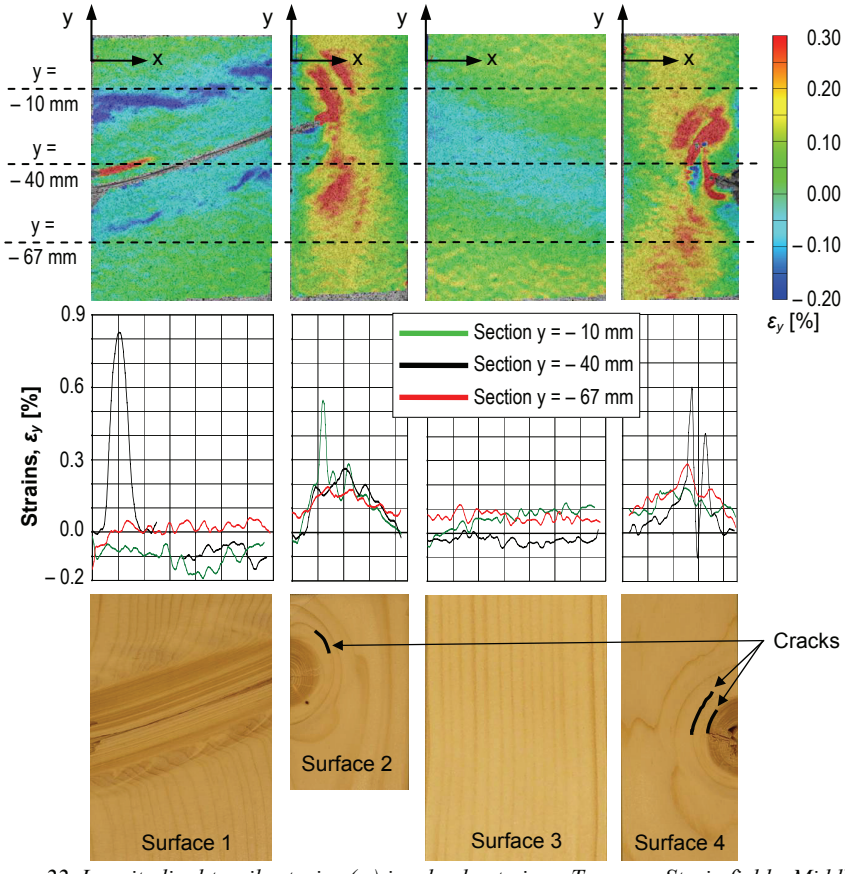

Figure 22. Longitudinal tensile strains (ε_y) in edge knot piece. Top row: Strain fields. Middle row: Strains along defined sections (dashed lines in top row). Bottom Row: Identified cracks.

The strains shown in Figure 22 correspond with a tension load of 30 kN. In the top row, three defined sections are exhibited as dashed lines and the strains along these are displayed in the diagrams of the middle row. Three distinct tensile peaks are found on Surfaces 2 and 4 and they correspond with cracks indicated in the bottom row. In strength testing, such cracks will most likely serve as indications of fracture. They were identified by use of a pocket lens since they could not be seen by the naked eye. The strain peak in the diagram of Surface 1 was caused by deformations at a crack within the knot, visible even before the testing was begun. It is shown as a thick red stripe in the top row of Figure 22.

The strain fields shown in Figure 22 were compared with those obtained from finite element (FE) calculations. The correspondence was surprisingly good, in spite of the fact that the utilized FE models were fairly simple.

4.2.3 Strains along narrow side boards

Strain fields in terms of tensile strains occurring along flat surfaces of side boards with cross-sectional dimension 25×56 mm were investigated. Such boards are utilized as laminations in the research concerning wet-gluing of laminated beams presented in Paper II. Results from one of the tested boards are exhibited in Figure 23. It is clearly shown to what extent the presence of knots affect the behaviour of the board. The most conspicuous observation is that the reduction of longitudinal stiffness at a knot is very local, limited to a length that according to Figure 23d can be estimated to about 50 mm for the board in question, in which the maximum knot size was 15 mm. An interesting comparison can be made with the required length over which a local tensile stiffness in terms of MOE parallel to the grain shall be measured according to EN 408. The stipulated length is five times the board width, which for the board shown in Figure 23a corresponds with a length of 280 mm. Thus, it can be concluded that a local MOE measured in accordance with EN 408 will overestimate the local stiffness at critical knots in narrow boards, since the measurement length will include parts of the board in which the stiffness is unaffected by the presence of the knots. Since stiffness in terms of MOE is correlated with strength, it is likely that such an overestimation will have a negative influence on the correlation. As a consequence, the correlation will be improved if MOEs determined on a very local scale is applied.

Another observation made from the measurement results in Figure 23c is that displacements perpendicular to the direction of applied load occur, revealing an uneven stress distribution over the board cross-section. The displacements were clearly visible with the naked eye. The maximum edgewise displacement was about 1.5 mm, see Figure 23c, and distinct peaks or irregularities coinciding with knots can be observed on the displacement curves.

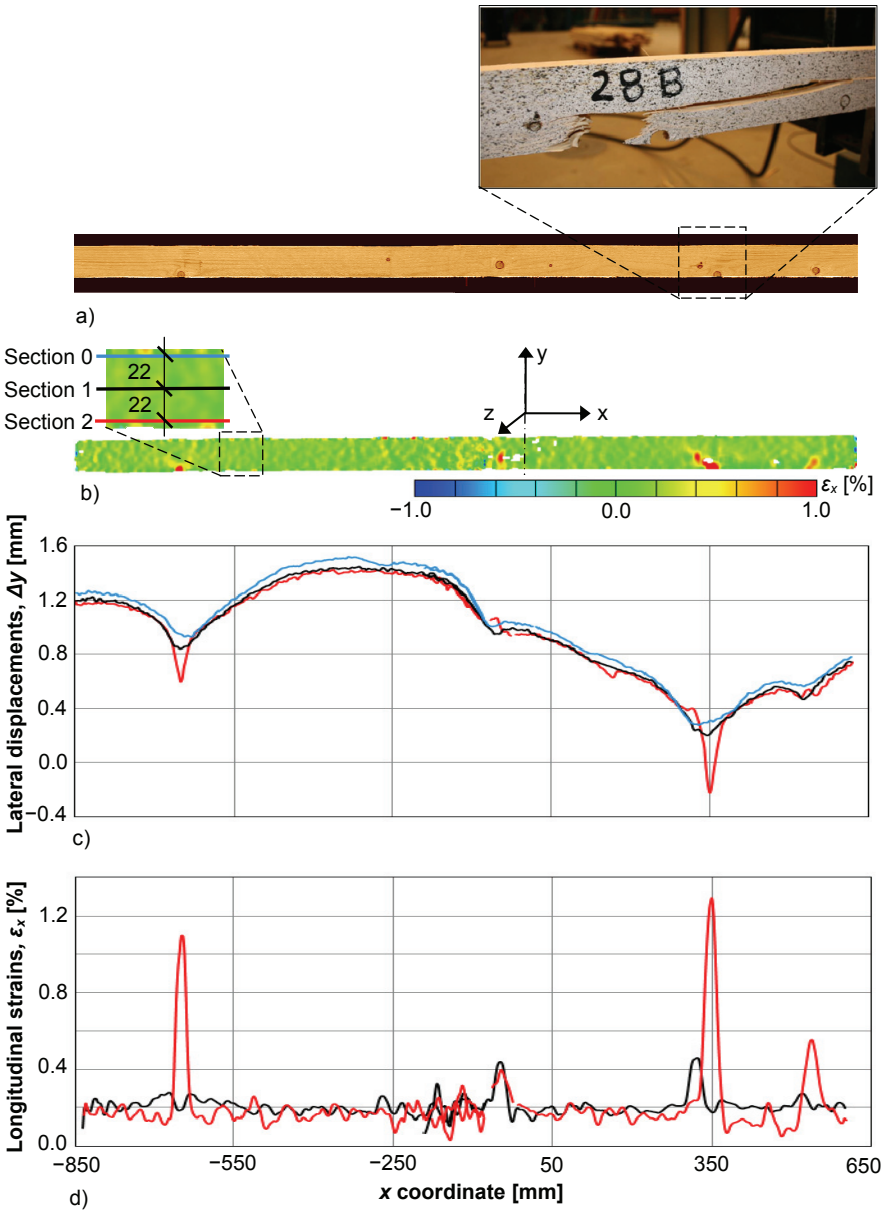

Figure 23. Displacements and tensile strains in a board of dimension 25×56 mm: a) measured flat surface, and board fracture, b) longitudinal strains, ε_x, and origin of coordinate system, c) lateral displacements, Δy, in edgewise board direction along Sections 0-2, and d) longitudinal strains, ε_x, along Sections 1-2.

4.3 Laser scanning of fibre angles

The relationship between grains deviating from the longitudinal direction of a timber piece and structural properties of the same piece has been discussed in section 2.2.2.3. Fibre inclination implies that the structural performance is severely impaired which is the reason why fracture in timber members is frequently initiated in fibres oriented in a direction that deviates from the longitudinal direction of the piece. From the research referred to in section 2.2.2.3, it is evident that information about local grain angles measured with high resolution has a great potential as regards development of more accurate strength grading methods.

Detailed information about fibre direction on the surfaces of a timber piece can be obtained by application of dot laser illumination and simultaneous tracheid effect scanning. A WoodEye scanner, see Figure 4, was utilized for this purpose. By application of dot lasers and cameras, fibre angles projected on the surfaces of scanned planks of dimension 45×145×3600 mm were measured with a resolution of about 0.8 mm in longitudinal and 3.6 mm in lateral direction of the timber pieces, respectively (see Paper IV). The angle projection on the surface means that the diving angle, *i.e.* the angle between the board surface and the direction of the wood fibres, is not regarded.

A typical result of tracheid effect scanning is shown in Figure 24. Each dash indicates the two-dimensional direction of the major axis of a measured laser dot which, due to the tracheid effect, has adopted an elliptic shape. It can also be observed that the dashes within the knot are randomly directed, due to the fact that the fibre direction within the knot in reality is perpendicular to the displayed surface.

The direction of each dash and its coordinates in both longitudinal and lateral board direction are documented in Windows txt-files that can be obtained from the WoodEye scanner.

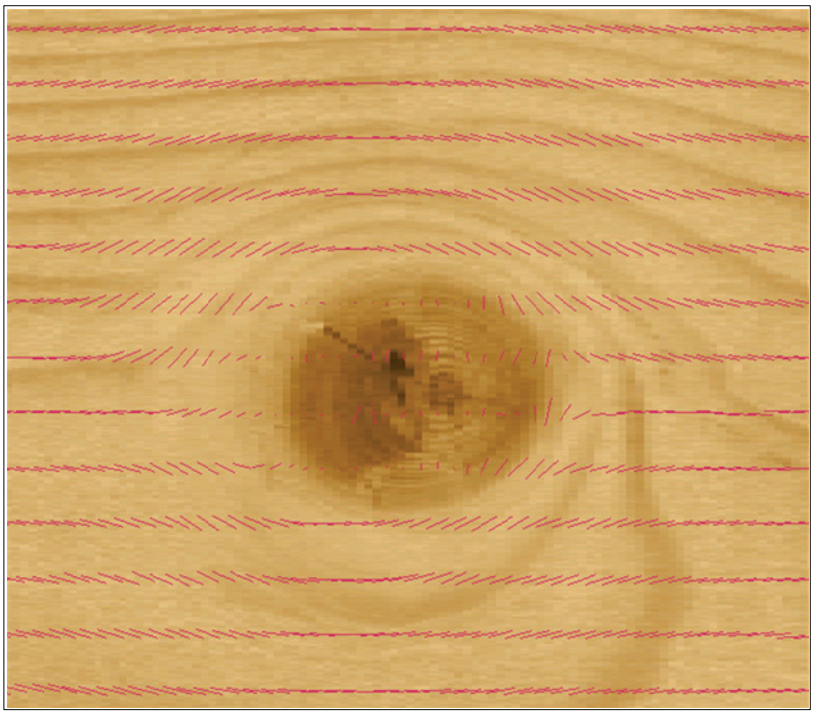

Figure 24. Fibre directions, measured on the basis of dot laser illumination and tracheid effect scanning, around a traversing knot (Ø=16 mm) in a board of dimension 19×95 mm.

4.4 New method for machine strength grading

The results obtained from DIC measurements and tracheid effect scanning have been utilized in the development of a new method for machine strength grading. Like most other grading methods, it is based upon a relationship between strength and stiffness and it also, just like the machines described in section 3.2, includes application of average longitudinal MOE values determined on the basis of axial dynamic excitation, board density and board length. It is, however, different from today's grading techniques in important aspects. It takes account of local fibre direction that is projected on the surfaces of a timber piece and measured using the scanning technique described in section 4.3. By combining information about average axial MOE and fibre direction, local MOE on the surfaces of a timber piece can be calculated with a resolution that corresponds with the tracheid effect measurements shown in Figure 24. On the basis of a model for integration over cross-sections, stiffness variation in terms of edgewise bending (EI) and axial stiffness (EA), respectively, can then be determined along the board.

New IPs are defined as the lowest bending MOE and the lowest axial MOE, respectively, found along a timber piece. The novel IPs were applied to a sample of 105 pieces of dimension 45×145×3600 mm (see Paper IV). An important issue was on what local scale the new IPs should be determined. Since the spatial resolution of scanned fibre angles was 0.8 mm in the longitudinal board direction, the IPs could be calculated with corresponding resolution. However, since critical knots or groups of knots have a certain extension in the longitudinal direction of a piece, different moving average values of bending and axial MOE, respectively, were also calculated over different length intervals along the pieces. The results, which are presented in Figure 25, show that the strongest relationship, amounting to R^2=0.68, between stiffness and bending strength was achieved for the IP represented by a moving average of the lowest bending MOE determined over an interval of about 80-100 mm. The highest R^2 value between lowest axial MOE and bending strength was 0.65 obtained for an interval of about 70-75 mm, see Figure 25, which is equivalent with half the board depth. For comparison, the frequently applied relationship between average axial dynamic MOE and bending strength was also calculated and it was found to be considerably lower, R^2=0.59, than those achieved by application of the new IPs.

Another important observation made on the basis of Figure 25 is that the R^2 value achieved for a moving interval of 725 mm, *i.e.* a length equivalent with five times the board depth which is the length over which local MOE in bending shall be determined according to EN 408, is considerably lower than the maximum R^2 value exhibited in the figure. This confirms the assumption made in section 4.2.3 regarding the possibility of improving strength grading correlations by application of MOEs determined on a more local scale.

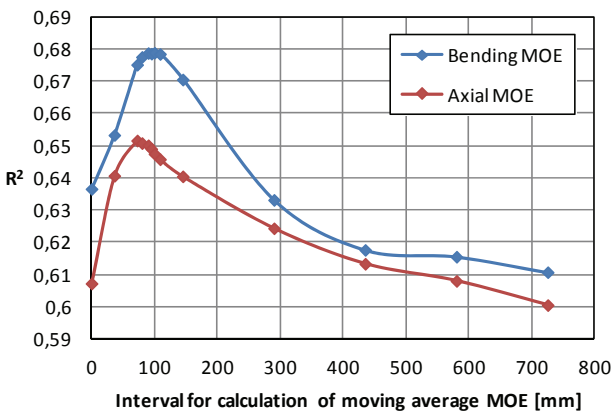

Figure 25. Relationship between interval for calculation of moving average MOE (x-axis) and coefficient of determination (R^2) between bending strength and the lowest moving average MOE (y-axis) for planks of dimension 45×145×3600 mm.

4.5 EWP development based on knowledge about local stiffness

As mentioned already in the last paragraph of section 1.1, glulam is a product that combines the EWP concept of gluing with strength grading of solid boards and planks. Since 2005, Linnæus University and the SP Technical Research Institute of Sweden have conducted research regarding development and manufacturing of wet glued laminated beams using Norway spruce side boards of narrow dimensions. The research has been carried out in close co-operation with the Södra Timber AB, which is one of the leading sawmilling companies in Sweden. The investigation presented in the appended Paper II, which concerns the possibility of grading side boards in a wet state by means of the grading technique based on axial dynamic excitation, was carried out within the scope of the described research. From the results presented in that paper, it was concluded that strength grading in the wet state was just as reliable as grading carried out after drying.

The strength of narrow timber pieces, such as the boards used in the wet gluing research, is even more dependent on the occurrence of large knots than what is the case for structural timber of dimensions representative for centre yield. This statement could be verified by a comparison of strength and stiffness properties for the two samples investigated in Paper II (boards with dimension 25×56×3000 mm) and Paper IV (planks with dimension 45×145×3600 mm), respectively, even if, firstly, the sampling of the two samples were not coordinated and, secondly, the applied strength tests differed between the two investigations. Nevertheless, the results exhibited in Table 6 indicate that the strength of the boards was considerably weaker and more scattered than for the planks. As regards average axial dynamic MOE, the results in the two investigations were similar.

Table 6. Mean values, standard deviations and coefficients of variation for axial dynamic MOE and strength of the timber samples investigated in appended Papers II and IV, respectively.

Sample	Axial dynamic MOE			Strength		
	Mean [GPa]	Stand.dev. [GPa]	CoV [%]	Mean [MPa]	Stand.dev. [MPa]	CoV [%]
Boards, Paper II (25×56×3000)	13.04	2.93	22.5	24.8[1]	13.5	54.4
Planks, Paper IV (45×145×3600)	12.4	2.6	21	38.4[2]	12.9	33.6

1. Tensile strength according to EN 408.
2. Bending strength according to EN 408.

The new grading method described in section 4.4 was applied to the sample of narrow boards investigated in Paper II. The MOE in longitudinal board direction calculated over the entire length (3000 mm) of the flatwise board surface the mid section of which is displayed in Figure 23a is shown in Figure 26a. Detail 1 in Figure 26a shows scanned fibre directions around the knot at the critical section. Corresponding longitudinal MOE are displayed in Detail 2.

For the sample of narrow boards, it was of particular interest to determine the calculation interval for which the relationship in terms of coefficient of determination between tensile strength and moving average IPs reached an optimum. In Figure 27, the relationship between the described R^2 and calculation interval is exhibited. In spite of the fact that the boards were tested in tension, it is evident that the strongest relationship was found for the lowest bending MOE determined as a moving average over an interval in the longitudinal direction of the board of about 25 mm, which is approximately half the board width. The relationship was actually as strong as $R^2 = 0.77$. The variation along the entire board length of moving average of lowest bending MOE, determined over the optimum interval of 25 mm, is exhibited in Figure 26b. The strong correspondence between knots and distinct dips in the graph should be noted.

For the other new IP, *i.e.* the lowest axial MOE along a board, the relationship between strength and IP was $R^2 = 0.72$ obtained for a moving interval of about 30 mm, see Figure 27.

The reason why the relationship was stronger for the IP based on bending stiffness, although the boards were tested in tension, is probably the fact that edge knots cause more unfavourable stress concentrations than what knots in the centre does, even if the load is applied in tension. These kinds of stress concentrations cause displacements in the directions perpendicular to the load direction. Such displacements in the edgewise direction are shown in Figure 23c.

The coefficient of determination between bending strength and average axial dynamic MOE was found to be $R^2 = 0.52$ (see Paper II). Thus, by applying the new grading method, it may be possible to add value to EWPs consisting of strength graded laminations of narrow dimensions.

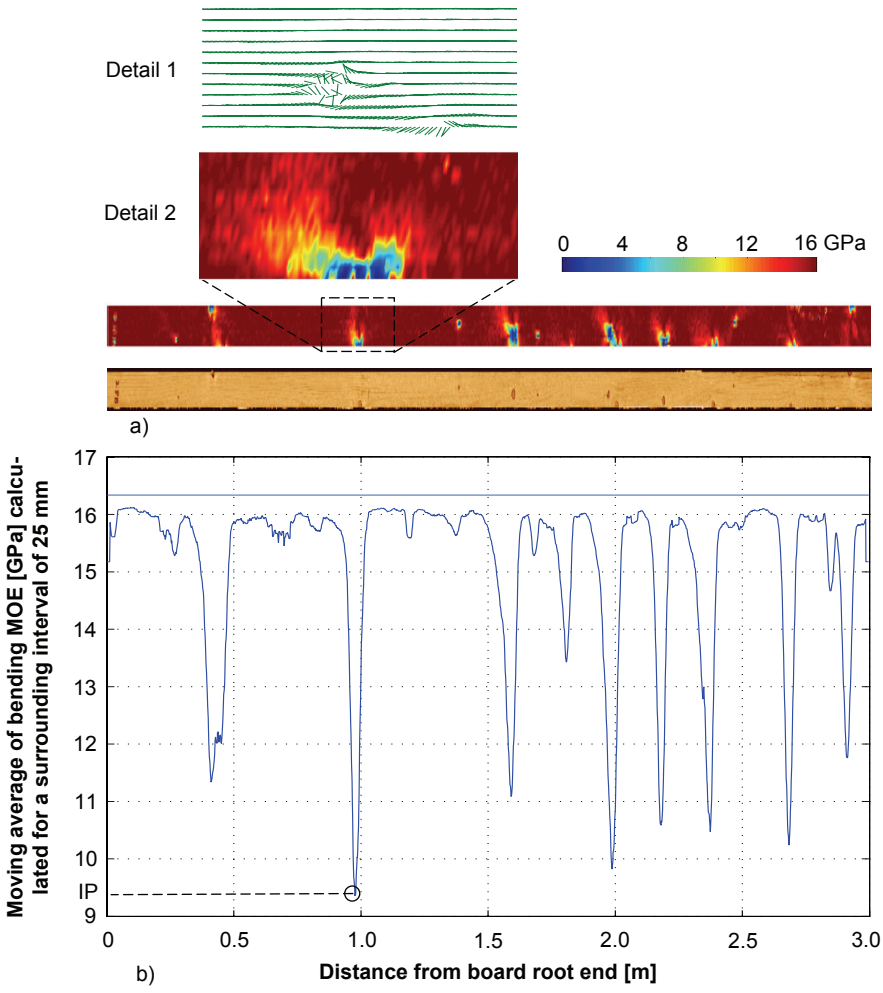

Figure 26. a) Image of flatwise board surface and contour plot of calculated MOE in longitudinal board direction (exaggerated width in both image and contour plot). Detail 1: Scanned fibre directions at critical section. Detail 2: Longitudinal MOE at critical section. b) Variation of moving average of bending MOE, determined over a surrounding interval of 25 mm, and indicated value (about 9.4 GPa) of the indicating property.

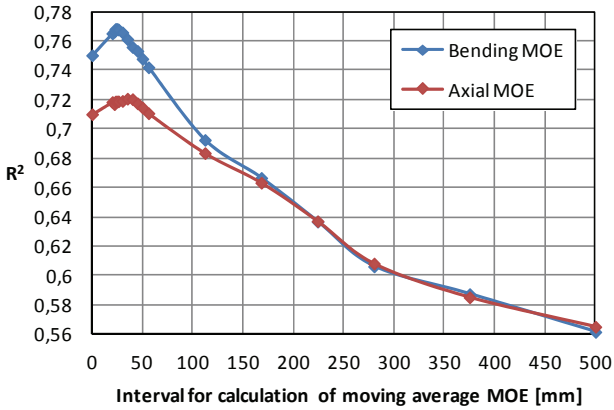

Figure 27. Relationship between interval for calculation of moving average MOE (x-axis) and coefficient of determination (R^2) between tensile strength and the lowest moving average MOE (y-axis) for boards of dimension 25×56×3000 mm.

4.6 Results and conclusions

The primary purpose that was formulated from the outset of this doctoral candidate project was to initiate a development towards more accurate methods for machine strength grading of structural timber. The research has included application of different measurement techniques, analysis of structural behaviour of timber pieces on both local and global level, strength tests in both bending and tension, development of algorithms for a new strength grading method, verification of the usefulness of the new method as regards different dimensions of boards and planks, and development of EWPs on the basis of machine strength grading of laminations. The most important findings can be summarized in the following way:

- The contact-free deformation measurement technique based on digital image correlation provides researcher with a tool by which the behaviour of wood pieces subjected to loading can be analyzed on both a global and a very close level. Such analysis provides substantial information about the structural behaviour of wood and knowledge about deformations and strains occurring at and around knots. The amount of achieved information is immense and it can be presented in many different ways, both qualitatively and quantitatively. The technique is an excellent means to be used for calibration of finite element models. It may also be useful for laboratory verification of new grading methods.

- Stiffness variation along timber pieces can be determined on the basis of dot laser scanning of local fibre angles projected on board surfaces. From such information, and in combination with board density and average axial dynamic MOE, the variation of local MOE in the longitudinal board direction can be calculated with a resolution that corresponds with laser scanned fibre angles.
- More accurate strength grading results in terms of coefficients of determination will be obtained for grading methods based on relationships between stiffness determined on a very local scale and strength. The relationship reaches optimum for stiffness measures determined as average values calculated over board lengths corresponding with approximately half the width of the investigated boards.
- A new machine strength grading method that applies indicating properties based on very locally determined stiffness measures was developed and assessed. For structural timber of cross-sectional dimension 45×145 mm, a coefficient of determination of 0.68 was achieved between stiffness and strength. An even better result (R^2=0.77) was obtained for narrow side boards of dimension 25×56 mm.
- Application of the new grading method should be particularly favourable for development of engineered wood products made of narrow laminations, since strength of such boards is even more dependent on the occurrence of large knots than what is the case for structural timber of larger dimensions, *i.e.* for timber intended to be utilized as *e.g.* joists or studs in timber framed buildings.
- The possibility of grading narrow side boards in a wet state and on the basis of axial dynamic excitation and weighing was investigated. It was found that such grading gives just as accurate grading results as corresponding grading carried out after drying.

4.7 Overview of appended papers

4.7.1 Paper I. Strain fields around knots

The overall purpose of Paper I was to obtain information about the joint behaviour of knots and surrounding clear wood fibres in timber pieces exposed to loading. Two-dimensional strain fields occurring on board surfaces were determined around knots in two test pieces of Norway spruce subjected to tension loading. One of the pieces included a traversing edge knot and the other one a traversing centric knot. The strain fields were achieved by

application of the DIC technique described in section 4.2. The measuring system ARAMIS was utilized. With this equipment, strains could be measured with an accuracy of up to 0.01 % strain. The measurement set-up consisted of two cameras placed in front of one of the test pieces installed in a testing machine. The cameras were positioned at angles and distances that depend on the size of the area to be measured. During a load test, surface deformations were measured and recorded by pictures taken simultaneously by the two cameras at fixed time intervals during the entire test. Pairs of pictures were taken at a time interval of two seconds, corresponding with a load increment of 400 N. Stereoscopic images were obtained from each pair of pictures, and current 3D-coordinates for a large number of defined points on the distorted surface were calculated relative to a coordinate system defined through a calibration procedure performed before the testing. By means of position changes of the defined points during a test, strain fields as function of load level occurring on the measured surface were determined.

In the research, strain fields on all four sides of each test piece were measured in the course of consecutive cyclic load tests, *i.e.* tests including both loading and unloading. One side of a specimen was studied during each cyclic test. The objectives were to examine to what extent the strain fields could be detected by means of the DIC technique, to investigate the correlation between strain fields on different sides of a specimen, and to analyze the strain distribution around the investigated knots.

Except for an initial test in which a crack in the edge knot specimen widened and propagated and internal stress release was observed close to the same knot, the loading was kept within the elastic range. In the initial test, the maximum loading was 40 kN, but in the following eight tests it was reduced to 30 kN. The load application was force-controlled, *i.e.* the load was both applied and detached with a constant load rate, in this case 200 N/second.

The results show that the applied technique is a very useful tool for catching both qualitative and quantitative information about the behaviour of knots in wood members subjected to loading. Clear wood defects that could not have been detected by neither visual inspection nor scanning were observed, and the release of internal stresses was considered as being of particular interest. Regarding the correlation between strain fields calculated on the basis of deformations measured on different surfaces of a specimen, it was shown that the strain match between adjacent surfaces was very good, given that only one surface was measured during each load test. Finally, the calculated strain fields were compared with those obtained from finite element simulations using the software ABAQUS. In these simulations, 3D elastic models of the test specimen's behaviour under loading were used. The correspondence between the different strain fields was surprisingly good, considering the fact that the finite element models were rather simple.

4.7.2 Paper II. Strength grading of wet side boards

The investigations behind both this paper and Paper III were carried out within the scope of the long-term research described in the first paragraph of section 4.5 concerning development of wet glued beams using narrow side board laminations of Norway spruce. Side boards, *i.e.* boards of narrow dimensions cut from the outer parts of a log, are regarded as products of low profitability due to a combination of low value and costly handling. At the same time it is well known that side boards possess excellent structural properties, and the idea behind the wet gluing research was that application of side boards as laminations in wet glued beams would result in an increase of the value of the boards. To optimize the structural performance of the glued beams, lamination with high quality in terms of measured stiffness and predicted strength should be placed in the outer parts of the cross-section and boards with low quality should be utilized as inner laminations. Such optimization requires strength grading of the laminations in a wet state. The investigation presented in Paper II concerns the possibility of grading narrow side boards in such a state by means of average dynamic MOE in the axial direction (MOE_{dyn}) determined on the basis of the first axial resonance frequency, board length and board density, *i.e.* on the basis of Equation (7).

For a sample of 58 wet side boards of dimension 25×125×3000 mm, density, length and MOE_{dyn} were determined. Each board was then split in the longitudinal direction into two boards and the procedure leading to a determined MOE_{dyn} was repeated for each split board, both before and after they were dried to a target moisture ratio of 12 %. After the sample of 116 split boards had been stored at a standard climate of 20 °C and 65 % relative humidity for about seven months, tensile strength was determined in accordance with test procedures described in EN 408. Finally, the relationship in terms of coefficient of determination (R^2) between strength and MOE_{dyn} for both wet and dried split boards was determined. For wet boards, the relationship was 0.55, whereas it was 0.52 for dried boards. The conclusion was that strength grading of narrow side boards in a wet state gives just as good results as grading performed after drying.

A so called *reversed lamination effect* on the stiffness of split side boards was also evaluated. This effect concerns to what extent the stiffness of such boards of narrow dimensions is reduced due to the splitting, relative to the stiffness of the corresponding un-split boards. The effect was found to be of low order.

4.7.3 Paper III. Tensile strain fields in narrow side boards

From previous research it is well known that the best single indicating property for both bending and tensile strength is the stiffness in terms of MOE determined on a rather local level at a critical section. Such sections coincide

with local defects, in most cases one or several knots. In section 4.1, development of new grading models based on IPs determined on a very local scale is discussed. Such development requires laboratory verification, and the investigation presented in Paper III concerns the possibility of using the same DIC technique as applied in Paper II for this purpose. Of the sample of 116 split boards applied in the research presented in the latter, nine boards were selected. Simultaneously as the tensile strength of each one of these were determined according to testing procedures described in EN 408, deformations along the entire visible length (*i.e.* the length between the grips of the tensile testing machine) of one of the flatwise surfaces were measured using two master-slave connected DIC systems. Each system measured deformations over about half the visible board length. Two cameras were applied in each system, and the master-slave application meant that pictures were taken simultaneously by all four cameras at fixed time interval during a load test.

Each DIC system performed a separate measurement project, implying that two separate 3D coordinate systems were applied. However, the deformations measured by each DIC system were subsequently transformed to a third coordinate system, which meant that the two measurement projects were combined, visualized and evaluated as one project.

To evaluate the intended application of the measurement technique, local MOE determined at an assumed critical section in each of the selected boards was determined in a traditionally way, *i.e.* on the basis of average transducer elongations measured in accordance with EN 408, and compared with equivalent MOE values achieved on the basis of detected strain fields and corresponding load level.

The accuracy of determined MOE values was assessed on the basis of regression analysis of sampled pair of observations along a chosen part of the straight line portion of the load-deformation graph. The correlation coefficient (R) achieved from such an analysis should according to EN 408 be of 0.99 or better.

Acceptable agreement was achieved between compared MOEs and the accuracy of MOE values determined on the basis of the DIC technique was on the same level as the regression requirement stipulated in EN 408. However, both investigated agreements and the accuracy of determined MOE values can with a high degree of probability be improve by modifications of the measurement procedures such as application of a load cell that is adjusted to current fracture load levels and filtering of load values sampled by the DIC system. On the basis of achieved results and potentials for measurement improvements, it was reasonable to conclude that the applied DIC technique can be applied for laboratory verification of new strength grading methods.

4.7.4 Paper IV. Prediction of bending strength on basis of local fibre orientations

As described in section 1.1 and 1.2, machine strength grading is, in general, based upon statistical relationships between indicating properties and bending strength, but such relationships applied on the market today are rather poor. This results in a maximum characteristic strength of 35-40 MPa for graded structural timber, although there is timber that is more than twice as strong. In this paper, a new grading method based upon new IPs resulting in more accurate strength predictions was presented.

The orientation of wood fibres in timber has a strong effect on stiffness and strength. In the new method, which is described in more detail in section 4.4, laser scanning was applied for identification of local fibre angles on face and edge surfaces of timber pieces. The fibre angle information was, in combination with average axial dynamic MOE, utilized for calculation of local MOE variation in the longitudinal direction of timber pieces. By integration over cross-sections along a board, an edgewise bending stiffness profile and a longitudinal stiffness profile, respectively, was calculated. New IPs were defined as the lowest bending stiffness and lowest axial stiffness, respectively, along a board. For a sample of 105 pieces of Norway spruce of dimension 45×145×3600 mm, a coefficient of determination of 0.68-0.71 was achieved between the lowest bending stiffness and bending strength. The corresponding relationship between average axial dynamic MOE and bending strength was only 0.59. It was also concluded that more accurate determination of stiffness profiles will lead to even better strength predictions.

A patent application has been filed for an invention corresponding to the new grading method, and industrial implementation is ongoing.

4.8 Future work

The basis for this doctoral candidate project was the limited possibility of grading timber with characteristic strength better than about 40 MPa by means of today's strength grading methods. During the course of the project, a general increase of interest from the sawmilling industry as regards development and application of strength grading have been noted. Furthermore, judging from papers presented at conferences and in scientific journals, the research efforts within this area are also intensified. Thus, a need for further improvement is foreseen, and there are a number of issues related to the research presented in this thesis that deserves to be investigated on a closer lever.

The possibility of enhancing the characteristics of the new strength grading method presented in Paper IV should be investigated. There are at least two different measures that may be beneficial for achieving such a purpose. The

first one concerns the resolution of the tracheid effect scanning of fibre angles. The dot laser scanning that has been applied so far in this doctoral project has been made with a resolution, *i.e.* distance between laser dots, of just below four mm in the lateral direction of scanned pieces. The effect that a doubled lateral resolution would have on the relationship between locally determined stiffness and board strength would be interesting to examine. The second measure also relates to the dot laser scanning. Currently, the new method utilizes two dimensional fibre angles that are obtained on board surfaces as a result of the projection of three-dimensional fibre directions. In consideration of the results of Hatayama (1984), see section 2.2.2.3, it can be assumed that knowledge about and application of the diving angle, *i.e.* the angle between the plane of the board surface and the 3D fibre direction, will considerably improve both the accuracy of calculated local stiffness and, consequently, also the relationship between this stiffness and board strength. The possibility of identifying the diving angle by means of optical laser scanning is therefore an interesting research task to be addressed.

The opportunities of utilizing the new strength grading method for development and optimization of high strength engineered wood products are deemed to be of great interest. Since the new method identifies weak and flexible section on a local longitudinal scale, it is highly appropriate for optimization of finger jointing of timber pieces, narrow glulam lamination in particular. An investigation concerning the potentials for such application is in progress.

An objective to be aimed at in a long-term perspective is development of strength grading methods based upon the actual fracture behaviour of individual timber pieces. The research idea is basically that the strength of a board can be accurately predicted by means of finite element analyses using models designed on the basis of scanned fibre angle information, relevant timber properties and fracture mechanics theory.

Further industrial application of optical fibre angle scanning should be investigated. On such area to probe into is to what extent fibre angle analysis can be of use for detection of serious defects such as top ruptures.

5 References

5.1 Standards and other normative documents

Anon (1981) *Instruktioner för sortering och märkning av T-virke* (*Instructions for grading and marking of T-timber).* Board of the T-timber Association (in Swedish).

Anon (2012) *Guidelines for sampling a growth area for deriving machine settings.* 5th DRAFT, 30 May. European Committee for Standardization / TC 124 / TG1.

BS 4978 (2007) *Visual strength grading of softwood – Specification*. British Standards Institution.

EN 338 (2009) *Structural timber – Strength classes*. European Committee for Standardization.

EN 384 (2010) *Structural timber – Determination of characteristic values of mechanical properties and density.* European Committee for Standardization.

EN 408 (2010) *Timber structures – Structural timber and glued laminated timber – Determination of some physical and mechanical properties*. European Committee for Standardization.

EN 1611-1 (1999) *Sawn Timber – Appearance grading of softwoods – Part 1: European spruces, firs, pines and Douglas firs.* European Committee for Standardization.

EN 1912 (2012) *Structural Timber – Strength classes – Assignment of visual grades and species*. European Committee for Standardization.

EN 1995 (2004) *Eurocode 5: Design of timber structures – Part 1-1: General – Common rules and rules for buildings.* European Committee for Standardization.

EN 14081-1 (2011) *Timber Structures – Strength graded structural timber with rectangular cross section – Part 1: General requirements.* European Committee for Standardization.

EN 14081-2 (2010) *Timber structures – Strength graded structural timber with rectangular cross section – Part 2: Machine grading; additional requirements for initial type testing*. European Committee for Standardization.

EN 14081-3 (2012) *Timber structures – Strength graded structural timber with rectangular cross section – Part 3: Machine grading; additional requirements for factory production control.* European Committee for Standardization.

EN 14081-4 (2009) *Timber structures – Strength graded structural timber with rectangular cross section – Part 4: Machine grading – Grading machine settings for machine controlled systems.* European Committee for Standardization.

INSTA 142 / SS 230120 (2010) *Nordic visual strength grading rules for timber.* Inter-Nordic standardization, Swedish Standards Institute (in Swedish).

5.2 Scientific publications

Bacher, M. (2008) *Comparison of different machine strength grading principles.* In: Proceedings of 2nd Conference of COST Action E53 – Quality control for wood and wood products, Delft, the Netherlands, October 29-30.

Baumann, R. (1922) *Die bisherigen Ergebnisse der Holzprüfungen in der Materialprüfungsanstalt an der Technichen Hochschule Stuttgart (Available wood testing results achieved at the Materials Testing Institution, Technical College, Stuttgart)*. Forschungsarbeiten auf dem Gebiete des Ingenieurwesens, Heft 231, Berlin, Germany (in German).

Beall, F. C. (2002) *Overview of the use of ultrasonic technologies in research on wood properties.* Wood Science and Technology, 36:197-212.

Bechtel, F. K., Allen, J. R. (1987) *Methods of implementing grain angle measurements in the machine stress rating process.* In: Proceedings of the 6th Nondestructive Testing of Wood Symposium, Washington State University, Pullman, USA.

Betzhold, D. (1999) *Maschinelle Festigkeitssortierung. Einfluss der Hochtemperatur-trocknung auf die elastomechanischen Eigenschaften des*

Schnittholzes (Machine strength grading. Influence of high-temperature drying on elastomechanical properties of sawn timber). Diplomarbeit, Fachhochschule Eberswalde, Germany (in German).

Blom, G. (1970) *Statistikteori med tillämpningar (Statistics theory with applications)*. ISBN 91-44-05591-9, Studentlitteratur, Lund, Sweden, p.13/25 (in Swedish).

Boström, L. (1999) *Determination of the modulus of elasticity in bending of structural timber – comparison of two methods*. Holz als Roh- und Werkstoff, 57:145-149.

Brundin, J. (2011) SP Technical Research Institute of Sweden, Stockholm, Sweden. Personal communication.

Brännström, M. (2009) *Integrated strength grading*. Doctoral thesis, ISBN 978-91-86233-12-9, Division of Wood Technology, Skellefteå Campus, Luleå University of Technology, Sweden.

Dahlblom, O., Persson, K., Petersson, H., Ormarsson, S. (1999) *Investigation of variation of engineering properties of spruce*. In: Proceedings of 6th International IUFRO Wood Drying Conference, Stellenbosch, South Africa, January 25-28, pp. 253-262.

Dinwoodie, J. M. (2000) *Timber: Its nature and behavior*. Second edition, E & FN Spon, London, UK.

Eliasson, L. (2005) *Automatisk egenskapsidentifiering av trä (Automatic identification of wood properties)*. Reports, no 18, School of Technology and Design, Växjö University, Växjö, Sweden (in Swedish with abstract in English).

Foley, C. (2003) *Modeling the effect of knots in structural timber*. Doctoral thesis, Division of Structural Engineering, Report TVBK-1027, Lund Institute of Technology, Lund, Sweden.

Foslie, M. (1971) *Norsk granvirkes styrkeegenskaper. Del 3 – Styrkeegenskaper for små, feilfrie prøver* (*Strength properties of Norwegian spruce. Part 3 – Strength properties of small, clear specimens)*. Report No. 42. The Norwegian Institute of Wood Working and Wood Technology (in Norwegian).

Glos, P., Heimeshoff, B. (1982) *Möglichkeiten und Grenzen der Festigkeitssortierung von Brettlamellen für den Holzleimbau (Possibilities and limitations regarding strength grading of board laminations for glulam*

construction). Ingenieurholzbau in Forschung und Praxis (Ehlbeck und Steck). Bruderverlag, Karlsruhe, Germany (in German).

Glos, P. (1995) *Strength grading.* STEP1, Lecture A6, Centrum Hout, The Netherlands.

Hankinson, R. L. (1921) *Investigation of crushing strength of spruce at varying angles of grain*. Air Service Information Circular, 3(259), Material Section Report No 130, US Air Service, USA.

Hatayama, Y. (1984) *A new estimation of structural lumber considering the slope of the grain around knots.* Bulletin of the Forestry and Forest Products Research Institute, Japan, No 326, pp 69-167 (in Japanese).

Herman, M., Dutilleul, P., Avella-Shaw, T. (1998) *Growth rate effects on temporal trajectories of ring width, wood density, and mean tracheid length in Norway spruce (Picea abies (L.) Karst.)*. Wood and Fibre Science, 30(1):6-17.

Hoffmeyer, P. (1984) *Om konstruktionstræs styrke og styrkesortering (About strength and strength grading of structural timber)*. I Skovteknologi. Et historiskt og perspektivisk strejftog. Dansk Skovforening (in Danish).

Hoffmeyer, P. (1990) *Failure of wood as influenced by moisture and duration of load*. Doctoral thesis, State University of New York, College of Environmental Science and Forestry, Syracuse, New York, USA.

Hoffmeyer, P. (ed.) (1995) *Styrkesortering ger mervärde, Del 2 – Tillgængelig teknik (Strength grading adds value, Part 2 – Available technique).* Laboratoriet for Bygningsmaterialer, Danmarks Tekniske Universitet, Teknisk Rapport 335-1995, ISSN 0908-3871 (in Danish, Norwegian and Swedish).

Huang, C.-L., Lindström, H., Nakada, R., Ralston, J. (2003) *Cell wall structure and wood properties determined by acoustics – a selective review.* Holz als Roh- und Werkstoff, 61:321-335.

Isaksson, T. (1999) *Modelling the variability of bending strength in structural timber – Length and load configuration effects*. Doctoral thesis, Division of Structural Engineering, Report TVBK-1015, Lund Institute of Technology, Lund, Sweden.

Johansson, C.-J. (1976) *Draghållfasthet hos limträlameller – Kvistars inverkan på draghållfastheten parallellt med fibrerna hos limträlameller av granvirke (Tensile strength of glulam laminations – The effect of knots on tensile strength parallel to the grain in glulam laminations of Norway spruce)*. Internal report no S 76:18. Chalmers University of Technology, Gothenburg, Sweden (in Swedish).

Johansson, C.-J. (2003) *Grading of timber with respect to mechanical properties*. In: Thelandersson, S. and Larsen, H. J. (editors) Timber Engineering, John Wiley & Sons, Ltd, Chichester, UK, pp. 23-43.

Johansson, C.-J., Brundin, J., Gruber, R (1992) *Stress grading of Swedish and German timber – A comparison of machine stress grading and three visual grading systems*. SP Swedish National Testing and Research Institute, SP REPORT 1992:23.

Johansson, C.-J., Boström, L., Bräuner, L., Hoffmeyer, P., Holmqvist, C., Solli, K. H. (1998) *Laminations for glued laminated timber – Establishment of strength classes for visual strength grades and machine settings for glulam laminations of Nordic origin*. SP Swedish National Testing and Research Institute, SP REPORT 1998:38.

Kliger, I. R., Perstorper, M., Johansson, G., Pellicane, P. J. (1995) *Quality of timber products from Norway spruce. Part 3. Influence of spatial position and growth characteristics on bending stiffness and strength.* Wood Science and Technology, 29:397-410.

Kliger, R., Johansson, M., Bäckström, M. (2003) *Dynamisk mätning av elasticitetsmodul på stockar – en möjlig sorteringsmetod? (Dynamic measurement of modulus of elasticity in logs – a possible grading method?)* Division of Structural Engineering, Report No. 03:5, Chalmers University of Technology, Gothenburg, Sweden (in Swedish).

Kollman, F. F. P. and Côté, W. A. (1968) *Principles of wood science and technology*. Springer Verlag, Berlin Heidelberg, Germany.

Källsner, B., Oja, J., Grundberg, S. (2002) *Prediction of timber strength by industrial X-ray scanning of Pinus Sylvestris saw logs.* In: Proceedings of the 7th World Conference on Timber Engineering, Shah Alam, Malaysia, August 12-15.

Källsner, B., Ormarsson, S. (1999) *Measurement of modulus of elasticity in bending of structural timber*. 1st RILEM Symposium on Timber Engineering, Stockholm, Sweden, September 13-15, pp 639-648.

Lackner, R., Foslie, M. (1988) *Gran fra Vestlandet – Styrke og sortering (Spruce from Western Norway – Strength, stiffness and grading)*. Report no. 74. The Norwegian Institute of Wood Technology (in Norwegian).

Lam, F., Prion, H. G. L. (2003) *Engineered Wood Products for structural purposes.* In: Thelandersson, S. and Larsen, H. J. (editors) Timber Engineering, John Wiley & Sons, Ltd, Chichester, UK, pp. 81-102.

Lam, F., Barrett, J. D., Nakajima, S. (2004) *Influence of knot area ratio based grading rules on the engineering properties of Hem-fir used in Japanese post and beam housing*. Wood Science and Technology, 38:83-92.

Larsson, D., Ohlsson, S., Perstorper, M., Brundin, J. (1998) *Mechanical properties of sawn timber from Norway spruce*. Holz als Roh- und Werkstoff, 56:331-338.

Lundgren, N., Brännström, M., Hagman, O., Oja, J. (2007) *Predicting the strength of Norway spruce by microwave scanning: A comparison with other scanning techniques.* Wood and Fibre Science, 39(1):167-172.

Lycken, A., Oja, J., Lundahl, C. G. (2009) *Kundanpassad optimering i såglinjen – Virkeskvalitet On-line (Customised optimisation in the saw line – Wood quality On-line)*. SP Technical Research Institute of Sweden, SP Report 2009:05 (in Swedish with abstract in English).

Madsen, B. (1992) *Structural behavior of timber.* Timber Engineering Ltd, North Vancouver, British Columbia, Canada, ISBN 0-9696162-0-1.

Metzler, B. (1997) *Quantitative assessment of fungal colonization in Norway spruce after green pruning*. European Journal of Forest Pathology, 27:1-11.

Montgomery, D. C. (2009) *Design and Analysis of Experiments*. John Wiley & Sons, Inc, Hoboken, NJ, USA. ISBN 978-0-470-39882-1, 7th Edition.

Mäkinen, H., Hein, S. (2006) *Effect of wide spacing on increment and branch properties of young Norway spruce*. European Journal of Forest Research, 125:239-248.

Nagai, H., Murata, K., Nakano, T. (2011) *Strain analysis of lumber containing a knot during tensile failure.* Journal of Wood Science, 57:114-118.

Nylinder, M., Fryk, H. (2011) *Timmer (Timber)*. Swedish University of Agricultural Sciences, Department of Forest Products, Uppsala, Sweden (in Swedish), ISBN 978-91-576-9030-2.

Nyström, J. (2002) *Automatic measurement of compression wood and spiral grain for the prediction of distortion in sawn wood products*. Doctoral thesis, Division of wood technology, Publication 2002:37, Luleå University of Technology, Luleå, Sweden.

Ohlsson, S., Perstorper, M. (1992) *Elastic wood properties from dynamic tests and computer modeling*. Journal of Structural Engineering, 118(10):2677-2690.

Oja, J., Källsner, B., Grundberg, S. (2005) *Predicting the strength of sawn wood products: A comparison between x-ray scanning of logs and machine strength grading of lumber*. Forest Products Journal, 55(9):55-60.

Olsson, A., Oscarsson, J., Johansson, M., Källsner, B. (2012) *Prediction of timber bending strength on basis of bending stiffness and material homogeneity assessed from dynamic excitation.* Wood Science and Technology, 46(4):667-683.

Ormarsson, S. (1999) *Numerical analysis of moisture-related distortions in sawn timber*. Doctoral thesis, Department of Structural Mechanics, Publication 99:7, Chalmers University of Technology, Gothenburg, Sweden.

Perstorper, M., Pellicane, P. J., Kliger, I. R., Johansson, G. (1995) *Quality of timber products from Norway spruce. Part 1. Optimization, key variables and experimental study.* Wood Science and Technology, 29:157-170.

Petersson, H. (2010) *Use of optical and laser scanning techniques as tools for obtaining improved FE-input data for strength and shape stability analysis of wood and timber.* In: Proceedings of V European Conference on Computational Mechanics, Paris, France, May 16-21.

Råberg, U., Edlund, M.-L., Terziev, N., Land, C. J. (2005) *Testing and evaluation of natural durability of wood in above ground conditions in Europe – an overview.* Journal of Wood Science, 51:429-440.

Sandoz, J. L. (1996) *Ultrasonic solid wood evaluation in industrial applications.* In: Proceedings of the 10th International Symposium on Nondestructive Testing of Wood, Lausanne, Switzerland, September 26-28, pp. 147-153.

Schajer, G. S., Bahar Orhan, F. (2006) *Measurement of wood grain angle, moisture content and density using microwaves.* European Journal of Wood and Wood Products, 64(9):483-490.

Serrano, E., Blixt, J., Enquist, B., Källsner, B., Oscarsson, J. (ed.), Petersson, H., Sterley, M. (2011) *Wet glued laminated beams using side boards of Norway spruce.* Report No 5, School of Engineering, Linnæus University, Växjö, Sweden.

Skog, J., Vikberg, T., Oja, J. (2010) *Sapwood moisture-content measurements in Pinus sylvestris sawlogs combining X-ray and three-dimensional scanning.* Wood Material Science and Engineering, 5:91-96.

Skog, J., Lundgren, N., Oja, J. (2011) *Detecting top rupture in Pinus sylvestris sawlogs.* In: Proceedings of the 20th International Wood Machining Seminar, Skellefteå, Sweden, June 7-10, pp. 132-140.

Steffen, A., Johansson, C.-J., Wormuth, E.-W. (1997) *Study of the relationship between flatwise and edgewise moduli of elasticity of sawn timber as a means to improve mechanical strength grading technology.* Holz als Roh- und Werkstoff, 55:245-253.

Stenman, B. (2012) SP Technical Research Institute of Sweden, Borås, Sweden. Personal communication.

Svensson, A. (2012) Vida Vislanda AB, Vislanda, Sweden. Personal communication.

Säll, H. (2002) *Spiral grain in Norway spruce*. Doctoral Thesis, Acta Wexionensia No 22/2002, Växjö University Press, Växjö University, Växjö, Sweden.

Thörnqvist, T. (2011) Linnaeus University, Växjö, Sweden. Personal communication.

Wang, X., Carter, P., Ross, R. J., Bradshaw, B. K. (2007a) *Acoustic assessment of wood quality of raw forest materials – A path to increased profitability*. Forest Products Journal, 57(5):6-14.

Wang, X., Ross, R. J., Carter, P. (2007b) *Acoustic evaluation of wood quality in standing trees. Part I. Acoustic wave behavior*. Wood and Fibre Science, 39(1):28-38.

Wormuth, E.-W. (1993) *Untersuchung des Verhältnisses von flachkant zu hochkant ermitteltem Elastizitätsmodul von Schnittholz zur Verbesserung der maschinellen Festigkeitssortierung (Study of the relationship between flatwise and edgewise moduli of elasticity of sawn timber for the purpose of improving machine strength grading technology)*. Master's thesis. Department of Wood Technology, University of Hamburg, Germany (in German).

Ziethén, R. (2006) *Proof loading – a new principle for machine strength grading of timber*. Licentiate thesis, School of Technology and Design, Reports, No. 33, Växjö University, Växjö, Sweden.

Ziethén, R. (2012) SP Technical Research Institute of Sweden, Borås, Sweden. Personal communication.

I

Wood Sci Technol (2012) 46:593–610
DOI 10.1007/s00226-011-0429-8

ORIGINAL

Strain fields around knots in Norway spruce specimens exposed to tensile forces

Jan Oscarsson · Anders Olsson · Bertil Enquist

Received: 10 June 2010 / Published online: 27 May 2011

Abstract Two-dimensional strain fields around knots in two Norway spruce specimens subjected to tension loading were detected using a contact-free measuring technique based on white-light digital image correlation. The first specimen included a traversing Edge knot, and the second one, a Centric knot. The development of strain fields as a function of load level was measured by consecutive cyclic load tests where one side of the specimen was studied during each test. The objectives were to examine to what extent the strain fields could be detected, to investigate the correlation between strain fields measured on different sides of a specimen and to analyse the strain distributions around the knots. The results show that the applied technique is useful for catching both overall and detailed information about the behaviour of knots in wood members exposed to loading. Clear wood defects that could not have been detected by neither visual inspection nor scanning were observed, and conclusions could be drawn regarding the release of internal stresses. The correlations between strain fields on different sides of the specimens were excellent, and the correspondence between measurement results and comparative finite element calculations was surprisingly good considering the fact that the employed FE models were fairly simple.

Introduction

Strength grading of structural timber means that strength, modulus of elasticity and density of individual timber members are predicted or measured by visual

J. Oscarsson (✉)
SP Technical Research Institute of Sweden, Videum Science Park, 351 96 Växjö, Sweden
e-mail: jan.oscarsson@sp.se

A. Olsson · B. Enquist
Linnæus University, 351 95 Växjö, Sweden

inspection or non-destructive machine testing. The market is, today, dominated by machine grading techniques that involve the determination of either flat-wise bending stiffness or dynamic stiffness in axial direction of a board. From previous research carried out by, *inter alia*, Johansson et al. (1992) and Larsson (1997), it is well known that the mentioned stiffnesses are, to a certain degree, correlated with the bending strength of a board. These relations are used to predict the latter property.

Present-day methods for machine grading result in a maximum characteristic strength of 40–45 MPa, but there are boards that in fact have a strength that exceeds 80 MPa. The reason why structural timber with characteristic strength higher than 45 MPa is not graded is that the prediction of a board's load-bearing capacity by the use of any available technique is not particularly good due to the somewhat limited correlation between stiffness and strength. Thus, to be able to utilize the potential of high strength timber, better grading methods are needed.

Mechanical properties of timber are, to a large extent, dependent on the occurrence of defects in the wood material. The degree of importance that different defects have on strength and stiffness has been investigated by, *inter alia*, Johansson et al. (1998) and Johansson (2003). It was found that knots were by far the type of defects that had the largest influence on visual grading and that the major cause of fracture was the presence of knots. Hence, it follows that a thorough knowledge and understanding of the behaviour of knots and the surrounding wood fibres in timber members exposed to loading is of great importance for the development of more accurate strength grading methods. Studies have been carried out concerning the effect of knots on the mechanical behaviour and mechanical properties of branch junctions. In an investigation carried out by Müller et al. (2006), it was found that the strain distribution of a mechanically loaded Norway spruce branch junction was very homogeneous, due to a combination of naturally optimized shape and optimized mechanical properties in the junction area. Jungnikl et al. (2009) measured the microfibril angle and density distribution at branch junctions of pine using computer tomography and X-rays, respectively, and found that the material properties vary locally as a response to different mechanical demands.

For studying the effect of knots on the strain distribution, techniques for contact-free deformation and strain measurement on surfaces of timber members could be useful. One such method, today widely used in, for example, the vehicle and aviation industries, is based on white-light digital image correlation (DIC). The use of DIC techniques in connection with wood or wood-based products is, however, rather limited. A review of research carried out up to the year 2005 is found in Serrano and Enquist (2005) where results from an investigation into strain distribution along wood adhesive bonds using DIC technique are presented. In recent years, the technique has been used for the measurements of, for example, strain in steel-to-timber dowel joints (Sjödin et al. 2006), strain in bi-axially loaded sheathing-to-framing connections (Vessby et al. 2008), strain distribution in timber subjected to four-point bending tests (Murata et al. 2005), strain-softening behaviour of wood under tension perpendicular to the grain (Miyauchi and Murata 2007) and tensile properties of early wood and late wood of loblolly pine (Young Jeong et al. 2009).

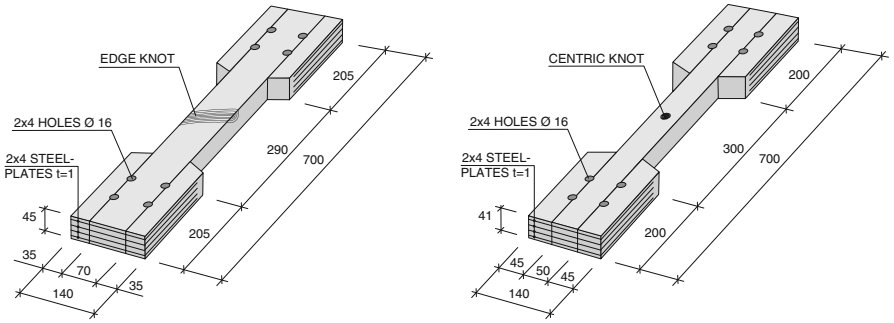

Fig. 1 Test specimens with Edge knot (*left*) and Centric knot (*right*)

Aim and scope

In this paper, findings from an investigation into two-dimensional strain fields around knots in wood members subjected to tensile forces are presented. Two test specimens of Norway spruce, one with a traversing Edge knot (henceforth denoted *Edge knot*) and one with a Centric knot (see Fig. 1), were studied using a non-contact optical 3D deformation measurement system of white-light DIC type. The aims were to examine 1. to what extent the strain fields could be detected, 2. the correlation between the strain fields measured on different sides of a specimen, and 3. the strain distribution around the knots. The development of strain fields was followed and measured by consecutive cyclic load tests consisting of both loading and unloading. Only one side of a specimen was studied during each test. Except for an initial test in which a crack in the Edge knot specimen widened and propagated, the loading was kept within the elastic range. Thus, the strain fields as a function of load level were detected in a comparable manner on all four sides of each specimen, even though only one side was studied during each test. The experimental results were also compared with those obtained from finite element (FE) simulations.

Test set-up and measurement equipment

The test set-up that was used for the experiments is shown in Fig. 2. The test specimens were fixed in a material testing machine of fabricate MTS with a 322 test frame, a control system of type FT60 and a maximum force capacity of ± 100 kN. The cyclic load that was applied during each test ranged from 0 to 30 kN, except for one test in which the maximum load was 40 kN. The load developed by the MTS machine was transferred to the test specimens by pin-ended steel yokes, each connected to the specimens by four steel dowels.

The two-dimensional strain fields in longitudinal and lateral directions and in shear occurring on the surfaces of the test specimens were detected using the measuring system ARAMIS^{TM}. It includes two charge-coupled device (CCD) cameras, in this case with a resolution of 2,048 $\times$ 2,048 pixels, placed in front of the specimen at angles and distances in accordance with a calibration procedure

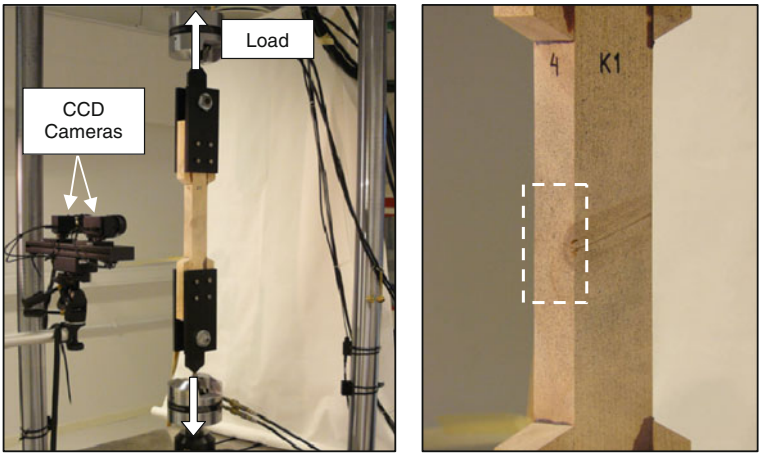

Fig. 2 Test set-up for the measurement of strain fields on one side of the Edge knot specimen (*left*) and corresponding measurement area (*right*)

carried out prior to the tests. With this equipment, strains in the range of 0.01–200% could be measured with an accuracy of up to 0.01% strain (GOM 2007).

During loading, the surface deformations and displacements are measured and recorded by pictures taken simultaneously, but from different angles, by the two cameras at fixed time intervals during the entire load test. Stereoscopic images are obtained from each pair of pictures, and current 3D-coordinates for a large number of points on the distorted surface are calculated relative to a coordinate system defined through the calibration procedure. In this research, pairs of pictures were taken at a time interval of 2 s, corresponding with a load increment of 400 N. Thus, each pair of pictures represents a unique load stage.

To be able to determine the displacements of a distinct point on the surface, each picture is divided into partially overlapping square or rectangular image subpictures, so-called facets. The size in pixels of both facets and overlap could be adjusted and chosen due to the spatial resolution and measurement accuracy needed for the test in question. In this case, the system's default settings, which are square 15 × 15 pixel facets and two pixel overlapping areas along the border of adjacent facets, see Fig. 3 (left), were chosen. This resulted in a facet step of 13 pixels, corresponding to a spatial resolution of about 0.67 mm. The default values are chosen as a compromise between measurement accuracy and computational time (GOM 2007). During a load test, each facet is identified for every subsequent stereoscopic image in the recording. This requires that the surface of the test object has an identifiable pattern, in this case a random speckled pattern of sprayed paint, see Fig. 3 (middle and right). During a test, the pattern deforms along with surface distortions, see Fig. 3 (right), and by the use of correlation algorithms, the 3D facet coordinates are calculated as the mean value of the coordinates of the facet corners. In Fig. 4, the coordinates of nine facets are shown as red and blue dots. These coordinates also define and coincide with the measuring point of the facet. Displacements of facet coordinates in a 3 × 3 facet mesh are used to calculate the strains in the measuring

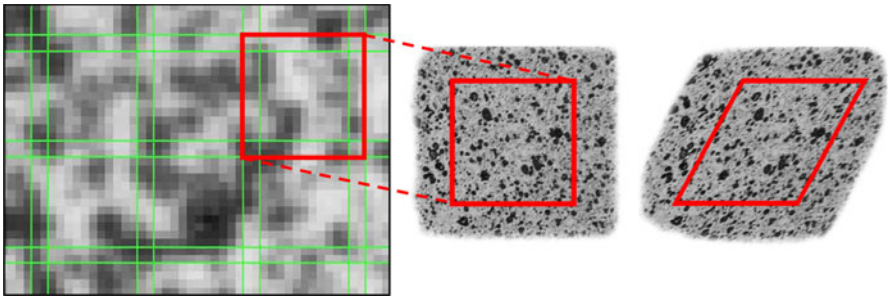

Fig. 3 Pixel facets of size 15 × 15 pixels with a two pixel overlap (*left*, GOM 2007), and random speckled pattern of a facet before loading (*middle*) and under loading (*right*)

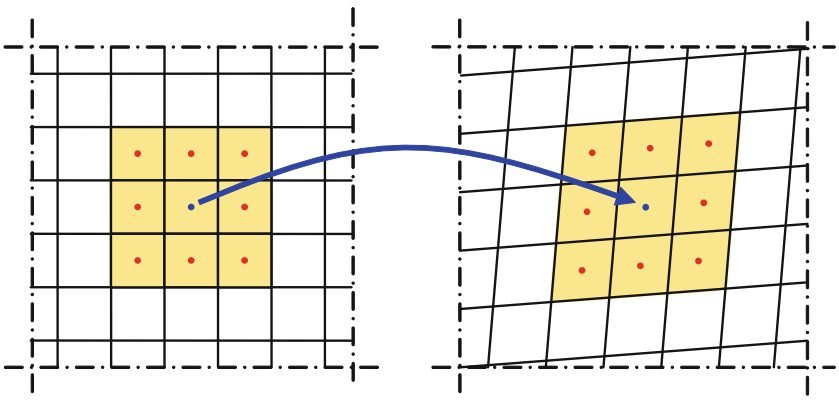

Fig. 4 Facet mesh before loading (*left*) and distorted facet mesh under loading (*right*)

point (blue dot in Fig. 4) of the centre facet of the mesh. By following the position changes of a large number of facets, the strain field as a function of load level can be determined and visualized.

Test specimens and loading

Drawings of the test specimens are shown in Fig. 1, and the dimensions and positions of the Edge knot and the Centric knot, respectively, are shown in Figs. 5 and 6. The experimental part of the research was divided into two test series, one for each test specimen. The Edge knot specimen was exposed to five load tests, numbered A0–A4, and the Centric knot specimen was exposed to four tests, numbered B1–B4.

In order to keep the stresses and strains within the elastic range, a maximum tension load of 30 kN was chosen for the Centric knot specimen, equal to an average tensile stress of about 15 MPa. For the Edge knot specimen, a higher load level was selected as the cross-section area of this specimen was more than 50% larger than the corresponding area of the Centric knot specimen. Since the presence

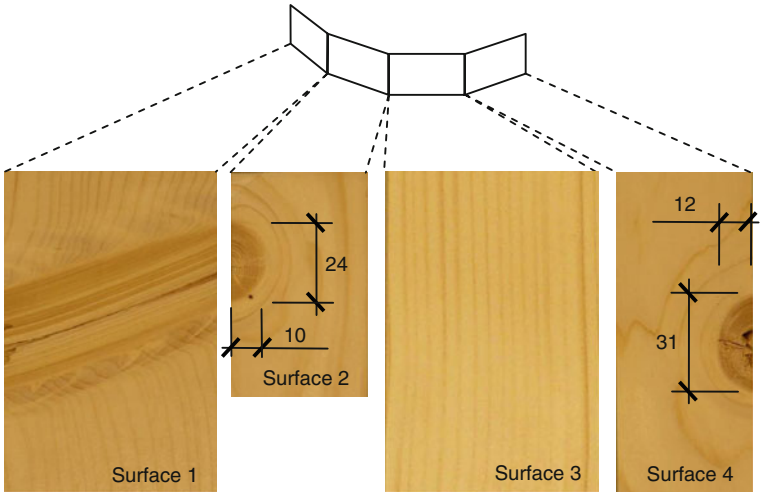

Fig. 5 Knot dimensions (mm) in Edge knot specimen

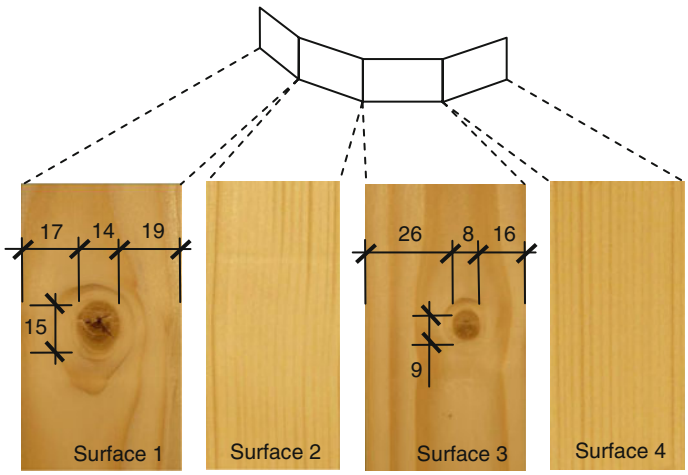

Fig. 6 Knot dimensions (mm) in Centric knot specimen

of the Edge knot caused a load eccentricity e of about 5.5 mm in the section through the knot, see Fig. 7 (left), the increase in the load level was limited to 10 kN resulting in a tension load of 40 kN for the Edge knot specimen. However, during the first load test (no. A0), an initial crack at the pith of the Edge knot expanded and propagated to the full depth of the knot, see Fig. 7 (left). Because of this, the load level was reduced to 30 kN, a load for which the strains on the surfaces of the Edge knot specimen were measured in tests A1–A4.

The load application in all tests was force-controlled, i.e., the load was both applied and detached with a constant load rate, in this case 200 Newton/s. The load–time relations for the different tests are shown in Fig. 7 (right).

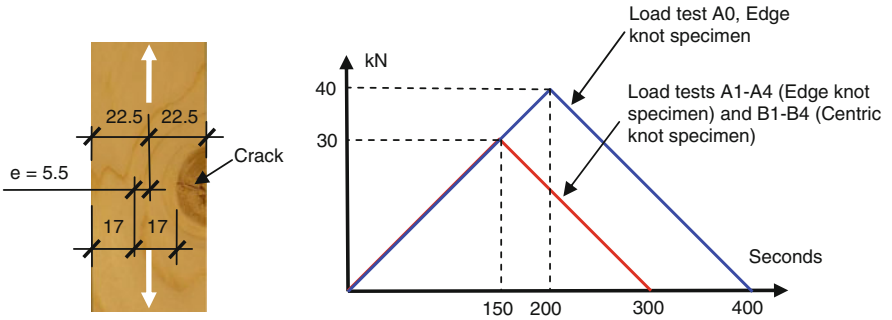

Fig. 7 Load eccentricity e (mm) in Edge knot specimen (*left*), and load–time relations for performed load tests (*right*)

Test results and evaluation

Two ARAMIS^{TM} post-processing tools, contour plots and section diagrams, were used to visualize the strain measuring results. By the first tool, a camera image of a measured surface is overlaid with coloured strain contour plots showing the strain distribution, for a defined load stage, over the measured surface. Such plots offer a qualitative and easily conceivable impression of the specimen's behaviour under loading. To obtain quantitative information with a higher degree of accuracy, sections can be defined in surface camera images and the strain variation along such sections can be shown in section diagrams. The position of a section is denoted in a local *xyz*-coordinate system defined in the camera image of each specimen surface. The results that are presented below concern the in-plane (*xy*-plane) strains that occurred on the surfaces of the test specimens. To be able to relate the four different coordinate systems on a specimen to each other, small marks of ink were applied on each surface. Since all marks were located at the same position in the longitudinal direction of a specimen and since the origin for each local coordinate system was located at such a mark, the measurement results for different surfaces of a specimen could easily be related to each other.

Load test no. A0: Edge knot specimen, load 40 kN

As described under the heading *Test specimens and loading* above, a tension load of 40 kN was chosen for this test where the strains on the specimen surface that shows a split section of the knot were measured, i.e. Surface 1 in Fig. 5.

Longitudinal strains (ε_y) for certain load stages are presented in Fig. 8. Stages 0–4 represent the undeformed and unloaded reference state, and the specified load level of 0.10 kN is considered as measuring noise. The load application started at stage 5 for which, at a load level of 0.59 kN, the widening of the initial crack in the pith of the knot is clearly visible.

Load stages 102–105 (see Fig. 8) illustrate the strain field just before and after the maximum load level of 40.1 kN was reached at stage 103. At this load, the crack had propagated and widened to such an extent that it was no longer possible to

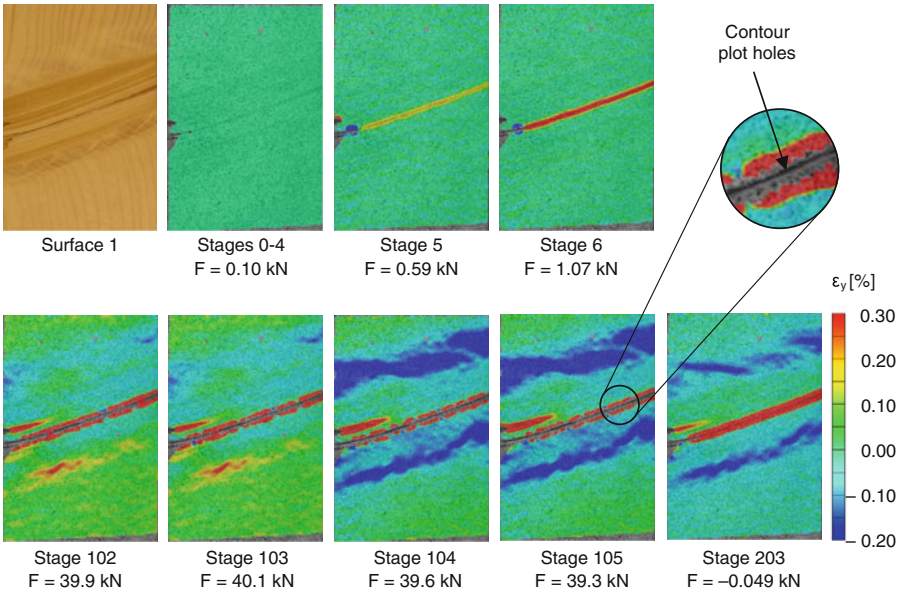

Fig. 8 Contour plots for longitudinal strains (ε_y) on surface 1, Edge knot specimen, load test no. A0, load stages no. 0–6, 102–105 and 203

identify displacements and deformations of facets in the crack area by means of the surface pattern of sprayed paint. Surface points that were not possible to identify are shown as holes in the contour plots, see detail in Fig. 8. During the unloading phase, the crack was gradually closed and the pattern restored to a degree where the facet displacements across the crack area were again possible to measure. However, considerable deformations, caused by crack propagation, remained in the crack after completed unloading at load stage 203. These deformations were represented by the ARAMIS^{TM} system as remaining longitudinal strains across the crack area, and they are shown as a thick red stripe in the contour plot for load stage 203, see Fig. 8.

In addition to the described crack deformations, large remaining negative (compressive) strains appeared in the wood fibres close to the knot. In general, strain changes measured by the ARAMIS^{TM} system from one load stage to another are rather small and more or less foreseeable, but in this test, the negative strains along the knot appeared instantly, at load stage 104, immediately after the maximum load of 40.1 kN was reached. During the 2 s that elapsed between the moments when pictures of load stages 103 and 104 were taken, the strain field was completely changed and areas of considerable negative strains emerged. A large portion of these remained after unloading, see load stage 203. A reasonable explanation for the sudden strain field changes is that crack growth during the test led to the release of internal stresses. After the test, the specimen was carefully examined and by using a pocket lens, two longitudinal clear wood cracks along the curvature of the fibre direction around the knot and one crack at the edge of the knot were discernible on Surfaces 2 and 4. The cracks are highlighted in the section diagrams of Figs. 9 and

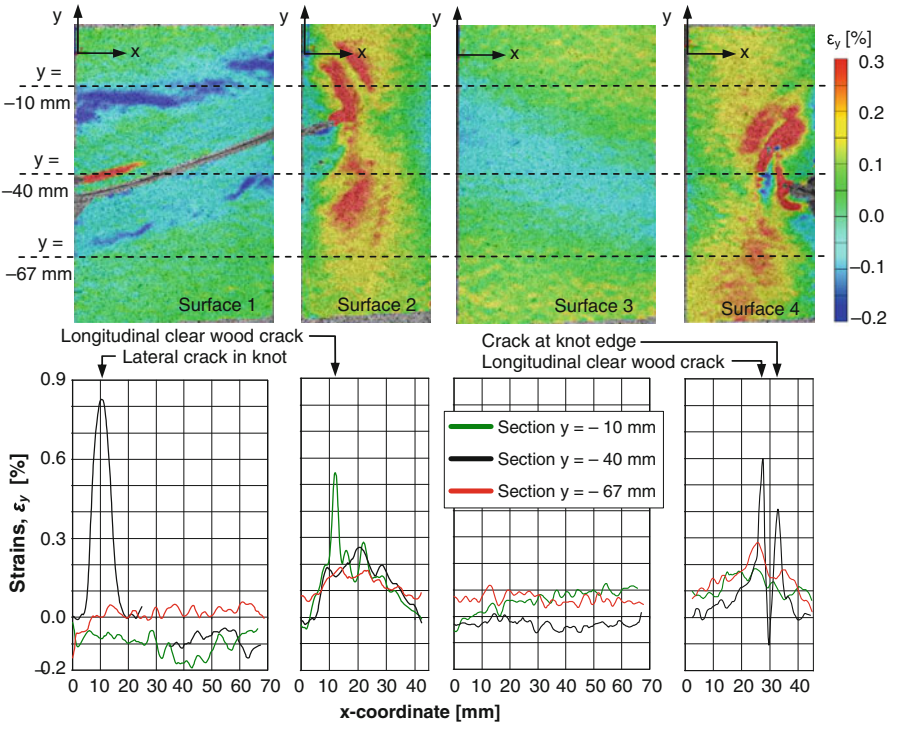

Fig. 9 Longitudinal strains (ε_y), Edge knot specimen, maximum load 30 kN, load tests A1–A4. *Top row* contour plots. *Bottom row* section strain diagrams for defined sections (*dashed lines*)

10. It should also be noted that the stress release occurred between the load stages 103 and 104, i.e. just *after* the maximum load level was reached. This indicates that the release was, to some extent, triggered by the change of sign of the load–time graph derivative, see Fig. 7 (right).

Load test no. A1–A4: Edge knot specimen, load 30 kN

In Load tests A1–A4, where the final strain stage of Load test A0 was used as unloaded reference stage (stage 0), the Edge knot specimen was exposed to a tension load of 30 kN for which the entire specimen displayed an elastic behaviour. Strain contour plots and section diagrams referring to the load stages for which the maximum load of 30 kN was reached are shown in Figs. 9 and 10.

The longitudinal strains (ε_y) are exhibited in Fig. 9. In spite of the fact that the specimen was exposed to tension loads, longitudinal negative strains were visible on Surfaces 1 and 3. The negative strains on Surface 1, measured during Load test A1, appeared in the same fibres as those where internal stresses were released in Load test A0. The appearance of these negative strains during Load test A1 was confirmed by a numerical analysis based on a 3D linear elastic model, see description under the heading "Numerical analyses" below. A possible explanation

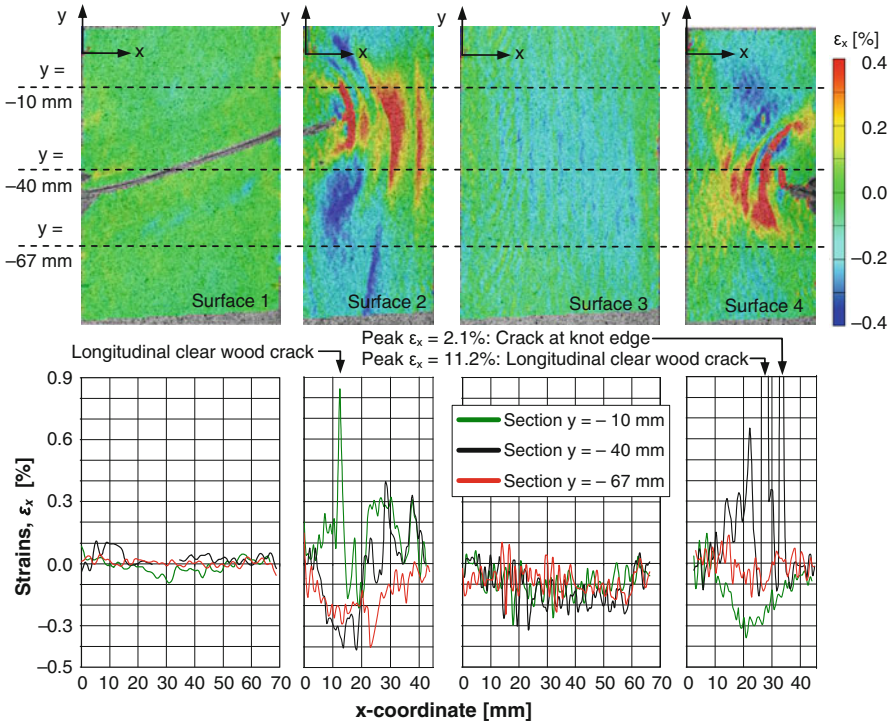

Fig. 10 Lateral strains (ε_x), Edge knot specimen, maximum load 30 kN, load tests A1–A4. *Top row* contour plots. *Bottom row* section strain diagrams for defined sections (*dashed lines*)

for this phenomenon is related to the behaviour of stress flow lines, i.e. imaginary lines showing how load is transferred between neighbouring material points. Such lines could be thought of as occurring in the vicinity of defects in specimens exposed to loading (Karihaloo 1995), and they create a biaxial stress and strain state. This effect is enhanced by deviating fibre directions around knots in timber members. The stress flow lines in the Edge knot specimen under tensile loading are exhibited in Fig. 11. The flow lines that develop under limited loading are shown as continuous lines. When the load increases, the eccentricity e shown in Fig. 7 creates a lateral deformation of the specimen that straightens the flow lines to the shapes represented by the dashed lines. From Fig. 11, the negative longitudinal strains occurring close to the knot on Surface 1 could be understood by studying the distances denoted a and b, measured between the tips of two lines drawn perpendicular to the flow line closest to the knot. The distance is reduced ($a > b$) when the line is straightened, and this may explain the negative strains in the clear wood fibres closest to the knot. The lateral deformation of the specimen, caused by the load eccentricity e, also explains the minor longitudinal negative strains in Section $y = -40$ mm on Surface 3, see Fig. 9.

The contour plots for Surfaces 2 and 4 in Fig. 9 exhibit large longitudinal tensile strains close to the knot. These strains are, like the strains discussed in the previous paragraph, related to the eccentricity e. Since hardly any stresses in the longitudinal

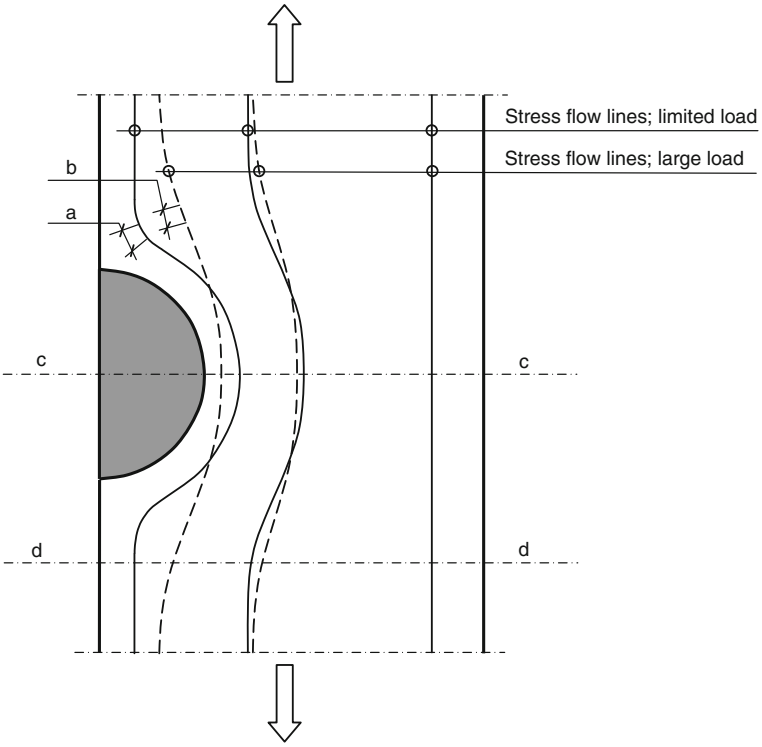

Fig. 11 Edge knot specimen under loading: straightening of imaginary stress flow lines

direction could be transferred through the knot, equilibrium requires higher longitudinal stresses and strains close to the knot than on the edge opposite to the knot. Furthermore, the fibre direction in the vicinity of the knot deviates considerably from the loading direction, and this difference probably contributes to increasing longitudinal tensile strains close to the knot.

The three strain peaks ($\varepsilon_y \geq 0.4\%$) in the section diagrams for Surfaces 2 and 4 in Fig. 9 are related to the previously described cracks that were observed by using a pocket lens. What is represented as surface strain peaks are, in fact, displacements caused by gradual widening of the cracks as load is applied.

A local tensile strain of about 0.82% was registered at Section $y = -40$ mm on Surface 1. As for the three strain peaks on Surfaces 2 and 4, this large strain value was also caused by the widening of a crack, in this case located within the knot and shown as a red stripe in the contour plot.

The lateral strains (ε_x) are presented in Fig. 10. They were insignificant on Surface 1, since the clear wood contraction was prevented by the presence of the knot. From a comparison of the contour plot of Surface 3 in Fig. 10 and the corresponding surface photo in Fig. 5, a correlation between the annual ring width and the wave-like pattern of the plot can be observed. This indicates a difference

between the Poisson's ratios of early wood and late wood of Norway spruce. Such a difference has been observed for loblolly pine by Young Jeong et al. (2009).

On Surfaces 2 and 4, lateral tensile strains developed beside the knot and compressive (negative) strains emerged in areas above and below the knot. As for the previously discussed longitudinal compressive strain shown on Surface 1, these lateral strains could also be understood from a study of the behaviour of the stress flow lines shown in Fig. 11. In section *c*, the lateral distance between the two flow lines that bend around the knot increases with increasing load and this indicates tensile strains in lateral direction. In section *d*, the lateral distance between the bending flow lines decreases corresponding to a lateral contraction. The huge apparent strains that coincide with the previously described cracks highlighted in the section diagrams in Fig. 10 are in fact lateral displacements caused by widening of the cracks.

Load tests no. B1–B4: Centric knot specimen, load 30 kN

Measurement results from tests carried out on the Centric knot specimen are shown in Fig. 12 (longitudinal strains, ε_y) and Fig. 13 (lateral strains, ε_x). All contour plots and section diagrams refer to the load stage for which the maximum load 30 kN was reached.

The contour plots for Surfaces 1 and 3 show large local strains, both longitudinal and lateral, in the vicinity of the knot. In the longitudinal direction (see Fig. 12), they could possibly and in a similar way as for the Edge knot be explained by a combination of stress flow line concentrations and deviation between fibre and loading directions. Regarding the strains in lateral direction, see Fig. 13, the expected contraction due to longitudinal tension loading is visible on both sides of the knot. The concentrations of large negative (compressive) lateral strains close to the knot are most likely caused by the curvature in the fibre directions and stress flow lines around the knot. The areas of tensile lateral strains visible above and below the knot on Surfaces 1 and 3 in Fig. 13 are similarly explained by an opposite curvature in fibres and stress flow lines.

From the lateral strain contour plots of Surfaces 2 and 4 in Fig. 13 and the photographs of the same surfaces shown in Fig. 6, the difference in Poisson's ratios between early wood and late wood is once again observed.

The contour plots and section diagrams in Fig. 12 reveal a concentration of longitudinal tensile strains in a section 20 mm below the local x-axis on Surface 4. According to the corresponding section diagram, there are strains as large as 0.95%, which is highly improbable. From the contour plots in Figs. 12 and 14 (left), it should be noted that just above the area where the large longitudinal strains occur, there are two zones where the longitudinal strains are approximately zero. In the same section as the large longitudinal strains appear on Surface 4, there are also, on an even more local scale, extreme contractions and expansions measured in the lateral direction of that surface, see Figs. 13 and 14 (right). A microscopic picture of the relevant area is shown in Fig. 14 (middle) where grain disturbances along a line on the surface are displayed. What is actually seen is the free edge of a surface chip and the concentration of large apparent strains described above are caused by

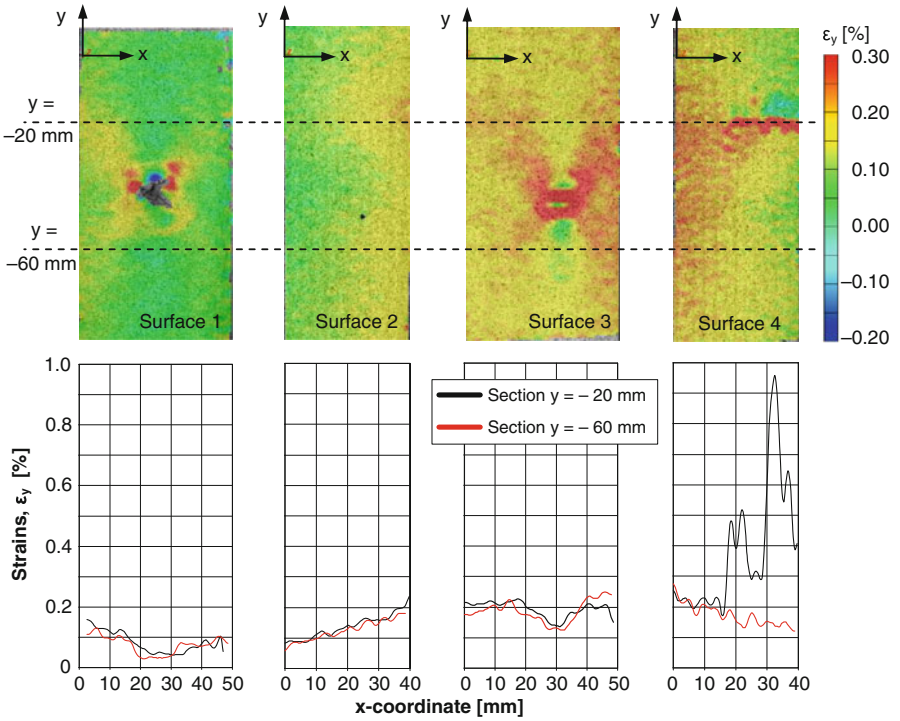

Fig. 12 Longitudinal strains (ε_y), Centric knot specimen, maximum load 30 kN, load tests B1–B4. *Top row* contour plots. *Bottom row* section strain diagrams for defined sections (*dashed lines*)

longitudinal and lateral translation of this edge. The presence of a chip clarifies why large apparent longitudinal strains are measured along a line on Surface 4 at the same time as there are large differences between the strains measured in areas on opposite sides of that line. The zero tensile strains in the area above the line are due to a rigid body translation of the chip.

Two more observations from Figs. 12 and 13 require comments. The first one concerns the fact that strains on both sides of a test specimen corner generally do not offer a perfect match. Computation of 3D coordinates and strain values for the measuring point of a facet requires that the previously described stochastic pattern of sprayed paint covers the entire area of the facet and that the entire pattern within the facet is visible from both the left and the right cameras. These requirements are not fulfilled for square facets that cover a corner of a test specimen. Consequently, on each side of a specimen corner, there are narrow areas where no strains could be calculated. However, with the exception of the corners themselves, the strain match between adjacent surfaces is very good considering the fact that they were established during different load tests. The second observation is that small areas of large lateral strains, both contraction and expansion, are found on the right-hand side of the contour plot of Surface 1 in Fig. 13. On this part of the specimen, the surface is rough due to minor maltreatment. According to the user manual for the

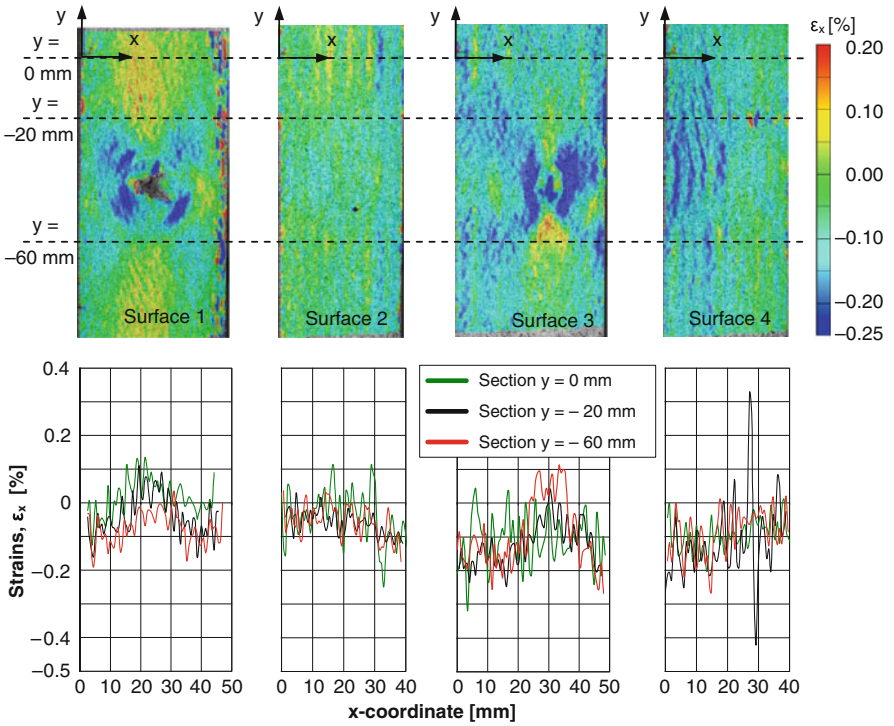

Fig. 13 Lateral strains (ε_x), Centric knot specimen, maximum load 30 kN, load tests B1–B4. *Top row* contour plots. *Bottom row* section strain diagrams for defined section (*dashed lines*)

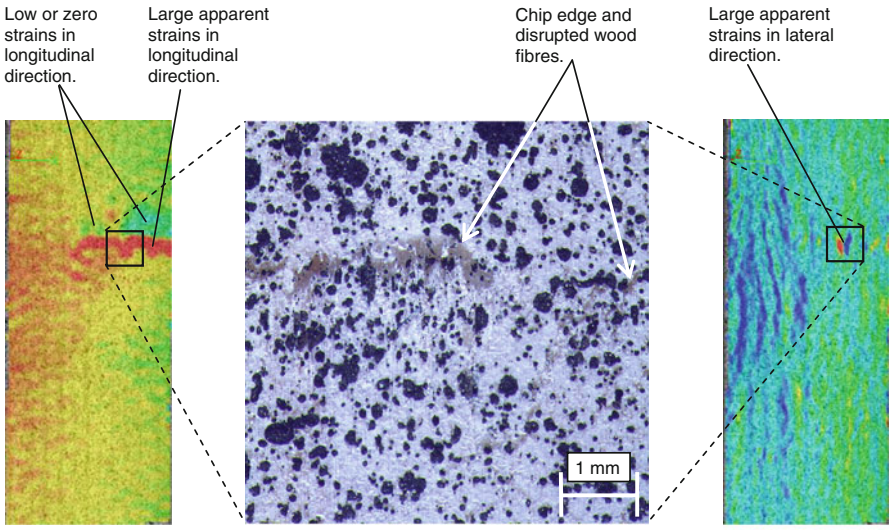

Fig. 14 Surface 4, Centric knot specimen: longitudinal strains (*left*), lateral strains (*right*) and microscopic picture showing disrupted wood fibres and chip edge (*middle*)

ARAMIS system (GOM 2007), an optimum specimen surface is smooth since highly structured surfaces may cause problems in facet identification and 3D point computation. Thus, the large strains identified on the rough part of the specimen surface are caused by incorrect measurement results and calculations.

Numerical analyses

The results of the experiments were compared with those obtained from FE simulations using the software ABAQUS (ABAQUS Inc. 2008). In the FE calculations, 3D linear elastic models of the test specimen's behaviour under loading were used. The model of the Edge knot specimen comprised about 113,000 2nd order elements and 483,000 nodes resulting in 1,449,000 degrees of freedom. Corresponding numbers for the Centric knot specimen model were 33,300 2nd order elements, 146,100 nodes and 438,200 degrees of freedom. In all simulations, a tension load of 30 kN was applied as a distributed load over the end surfaces of the specimens.

The material data needed for the numerical calculations, expressed in terms of elastic constants for spruce with a moisture ratio of 12%, were obtained from literature (Kollman and Côté 1968). The constants used for both clear wood and knots were $E_L = 13{,}500$, $E_R = 893$, $E_T = 481$, $G_{LR} = 716$, $G_{LT} = 500$ and $G_{RT} = 29$ MPa for the moduli of elasticity and the shear moduli and $\upsilon_{LR} = 0.43$, $\upsilon_{LT} = 0.53$ and $\upsilon_{RT} = 0.42$ for Poisson's ratios. The indices L, R and T refer to the longitudinal, radial and tangential directions, respectively, of the modelled orthotropic wood material. The longitudinal direction of the clear wood was oriented parallel to the longitudinal direction of the specimens, whereas the longitudinal direction of the knots was oriented perpendicular to the mentioned clear wood direction.

The applied FE models were fairly simple. The crack that widened and propagated in the pith of the Edge knot during load test no. A0 was included, but the material orientation deviations that always occur in clear wood close to knots were not regarded. Nevertheless, the simulation results presented in Figs. 15, 16 and 17 show, on an overall and qualitative level, a degree of correspondence with the experimental results shown in Figs. 9 and 10 and Figs. 12 and 13 that is surprisingly good. In terms of strain features on a closer level, several similarities deserve attention. For Surface 1 of the Centric knot specimen, calculated and measured strain fields in the vicinity of the knot strongly resemble one another, see Figs. 12, 13 and 15. This resemblance remains even if the knot is replaced by a hole, see Fig. 15, which is in accordance with assumptions made in, for example, the Nordic visual strength grading rules for timber, INSTA 142 (1998), namely that knots in structural timber should be equalized with holes (personal communication, Jan Brundin, SP Technical Research Institute of Sweden, 2008). INSTA 142 is referred to in the European Standard EN 1912 (2008) where nationally applied visual strength grades for visual grading of structural timber are assigned to common European strength classes established in the European Standard EN 338 (2003).

For the Edge knot specimen, the longitudinal negative strains measured on Surfaces 1 and 3, see contour plots in Fig. 9, could also be found in the

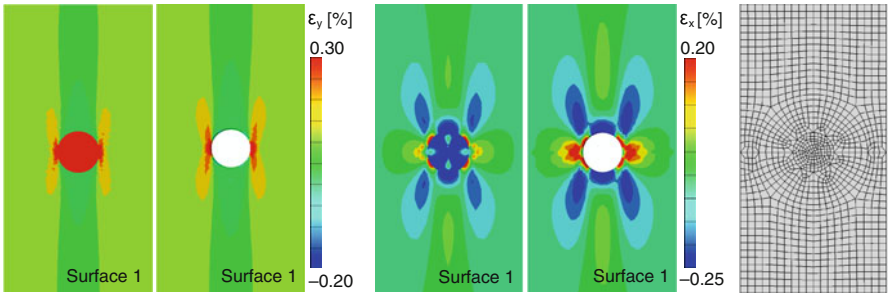

Fig. 15 Results from FE simulations, Centric knot specimen: longitudinal strains with and without knot (*left*), lateral strains with and without knot (*middle*) and FE mesh (*right*)

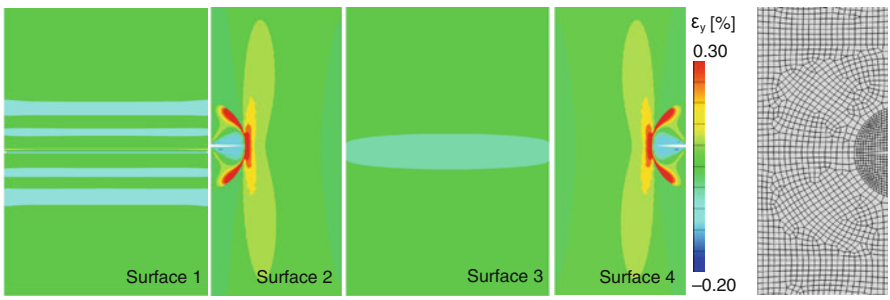

Fig. 16 Results from FE simulation, Edge knot specimen: longitudinal strains and FE mesh

corresponding plots in Fig. 16 and the areas of lateral compressive and tensile strains measured by the ARAMIS^{TM} system were also verified, see Fig. 17. However, the lateral strains are less evident in the FE simulations than in the ARAMIS^{TM} contour plots. The reason for this is probably that the curvature in the fibre direction around the knots increases the lateral strains measured on the surfaces of the test specimens, whereas no such effect is found in the FE calculations, since fibre curvatures are not included in the models.

The most conspicuous difference between measured and calculated strains concerns the large apparent tensile strains, both longitudinal and lateral, that occurred close to the knot in the Edge knot specimen. These apparent strains, which in fact were displacements caused by the cracks that were identified by using a pocket lens, could not be seen in the results of the simulations since these cracks were not included in the model.

Conclusion and future work

The objectives of this research were to investigate to what extent strain fields around knots could be detected by the use of DIC technique, to analyse the strain distribution around the investigated knots and to examine the correlation between

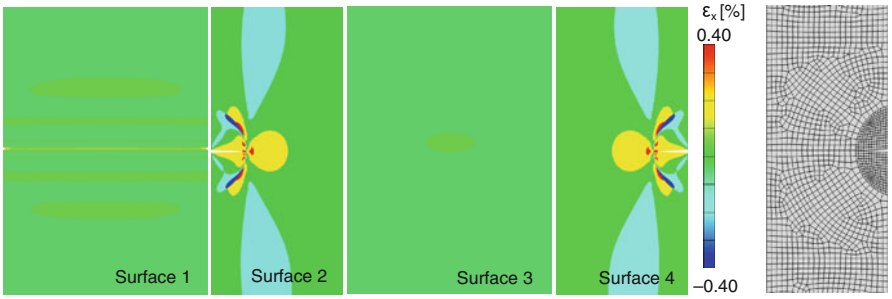

Fig. 17 Results from FE simulation, Edge knot specimen: lateral strains and FE mesh

the strain fields measured on different sides of a test specimen. Regarding the two first objectives, it could be concluded that the DIC technique is a useful tool for catching both qualitative and quantitative information about the behaviour of knots in wood members exposed to loading. The observation of release of internal stresses close to the knot in the Edge knot specimen must be considered as rather interesting. The graphical representations of the strain measuring results by the use of contour plots and section diagrams for different load stages in a load test provide valuable information about the strain distribution and development around knots. It is also possible to detect clear wood defects that are difficult to identify otherwise. For example, the chip on Surface 4 of the Centric knot specimen and the three cracks on Surfaces 2 and 4 of the Edge knot specimen could not have been detected neither by scanning nor by visual inspection. It is very likely that the discovered cracks will serve as indications of fracture and in the plans for future work, fracture tests are included. In such tests, the progress of fracture of the two specimens will be measured and documented by the use of the ARAMIS^{TM} system.

With reference to the objective concerning correlation between strain fields on different specimen surfaces, it has been demonstrated that the strain match between adjacent sides is very good, taken into account that only one specimen surface was measured during each load test.

Finally, the correspondence between the measurement results and the FE simulations is, indeed, promising, especially considering the fact that the applied models were rather simple. The DIC technique used in this research will, with a high degree of probability, be of great interest for the calibration of finite element models for, for instance, the analyses of fracture mechanical behaviour of knots in wood members. Such models would be of great importance for the development of more accurate strength grading methods based on scanned information concerning the occurrence of knots liable to initiate fractures in wood members to be graded.

Acknowledgments This research was made possible by the financial support from The Knowledge Foundation and The Swedish Research Council for Environment, Agricultural Sciences and Spatial Planning.

References

ABAQUS Inc. (2008) ABAQUS/Standard and ABAQUS/CAE version 6.8, User's manuals

European Standard EN 1912:2004+A2 (2008) Structural timber—strength classes—assignment of visual grades and species

European Standard EN 338 (2003) Structural timber—strength classes

GOM mbH (2007) ARAMIS User Manual—Software, aramis_v6_1st_en_rev-c, 25 April 2007

Inter-nordic standardisation INSTA 142/SS 23 01 20 (1998) Nordic visual strength grading rules for timber (in Swedish)

Johansson C-J (2003) Grading of timber with respect to mechanical properties. In: Thelandersson S, Larsen HJ (eds) Timber engineering. Wiley, Chichester, pp 23–43

Johansson C-J, Brundin J, Gruber R (1992) Stress grading of Swedish and German timber—a comparison of machine stress grading and three visual grading systems. SP Swedish National Testing and Research Institute, SP REPORT 1992:23

Johansson C-J, Boström L, Bräuner L, Hoffmeyer P, Holmqvist C, Solli KH (1998) Laminations for glued laminated timber—establishment of strength classes for visual strength grades and machine settings for glulam laminations of Nordic origin. SP Swedish National Testing and Research Institute, SP REPORT 1998:38

Jungnikl K, Goebbels J, Burgert I, Fratzl P (2009) The role of material properties for the mechanical adaptation at branch junctions. Trees 23(3):605–610

Karihaloo BL (1995) Fracture mechanics & structural concrete. Longman Group Ltd, Harlow

Kollman FFP, Côté WA (1968) Principles of wood science and technology. Springer, Berlin

Larsson D (1997) Mechanical characterization of engineering materials by modal testing. Dissertation D97:4, Chalmers University of Technology, Gothenburg

Miyauchi K, Murata K (2007) Strain-softening behaviour of wood under tension perpendicular to the grain. J Wood Sci 53(6):463–469

Müller U, Gindl W, Jeronimidis G (2006) Biomechanics of a branch-stem junction in softwood. Trees 20(5):643–648

Murata K, Masuda M, Ukyo S (2005) Analysis of strain distribution of wood using digital image correlation method—four-point bend test of timber including knots. Trans Visual Soc Jpn 25(9):57–63

Serrano E, Enquist B (2005) Contact-free measurement and non-linear finite element analyses of strain distribution along wood adhesive bonds. Holzforschung 59:641–646

Sjödin J, Serrano E, Enquist B (2006) Contact-free measurements and numerical analyses of the strain distribution in the joint area of steel-to-timber dowel joints. Holz Roh Werkst 64:497–506

Vessby J, Olsson A, Enquist B (2008) Contact-free strain measurement of bi-axially loaded sheathing-to-framing connection. In: Proceedings (CD) of the 10th world conference on timber engineering, Miyazaki, Japan

Young Jeong G, Zink-Sharp A, Hindman DP (2009) Tensile properties of earlywood and latewood from Loblolly Pine (Pinus Taeda) using Digital Image Correlation. Wood Fibre Sci 41(1):51–63

II

Strength grading of narrow dimension Norway spruce side boards in the wet state using first axial resonance frequency

J. Oscarsson*[1], A. Olsson[2], M. Johansson[2], B. Enquist[2] and E. Serrano[2]

Strength grading of Norway spruce [*Picea abies* (L.) Karst.] side boards in the wet state was investigated. For a sample of 58 boards, density and dynamic modulus of elasticity in the axial direction (MOE_{dyn}) were determined in the wet state. The boards were then split into two parts and the procedure of determining MOE_{dyn} was repeated both before and after the boards were dried to a target moisture content of 12%. Finally, tensile strength of the split boards was measured and its relationship to MOE_{dyn} for both wet and dried split boards was determined. The investigation also included an evaluation of a so called reversed lamination effect on the stiffness caused by the splitting of boards into two parts. The results show that strength grading of split boards in the wet state can give just as good results as grading performed after drying. The reversed lamination effect on the stiffness of split boards was found to be of lower order.

Keywords: Strength grading, Axial stiffness, Side boards, Wet state, Green state

Introduction

Approximately 30% of the volume of sawn timber produced at a typical Swedish sawmill consists of side boards, i.e. boards of narrow dimensions sawn from the outer parts of a log. Large production volumes and small dimensions imply that considerable numbers of side board pieces have to be handled in the sawmilling process and the costs for production, storage and sales are, in many cases, not met by the selling price on the market.

Previous research has shown that several wood characteristics that influence the structural properties of sawn timber vary considerably in the radial direction, i.e. from pith to bark. For example, the modulus of elasticity (MOE) in softwood trees increases significantly from the pith and outwards (Wormuth 1993) and similar behaviour has also been found for density of Norway spruce (Steffen *et al.* 1997; Dahlblom *et al.* 1999). Accordingly, side boards possess excellent structural properties but due to their small dimensions, they are very seldom used for load bearing purposes. Since 2005, Växjö University (from 1 January 2010 named Linnæus University) and SP Technical Research Institute of Sweden have conducted research regarding the development of high-value products utilising softwood side boards. The research carried out by the University and the Institute concerns the possibility to use undried Norway spruce [*Picea abies* (L.) Karst.] side boards as laminations in wet-glued laminated beams for load-bearing applications. The beams consist of flatwise glued wet boards with cross-section dimensions of 25×120 mm. For wet boards, the moisture content (MC) could vary from the fibre saturation point, which for Norway spruce occurs at $\sim$30%, to $\sim$150% (Boutelje and Rydell 1995). After gluing, each beam is split, dried and planed into two new beams with a width of 50 mm (*see* Fig. 1).

Structural properties of these split beams have been measured and analysed, and the results obtained so far are promising (Petersson *et al.* 2009; Serrano *et al.* 2010). Despite the fact that the beams have been produced from batches of un-graded boards, their stiffness and strength properties are consistent with both glued laminated timber of strength class GL32h, as defined in EN1194 (CEN 1999), and structural timber of strength class C35, as defined in EN338 (CEN 2009). Furthermore, by gluing boards in the wet state, directly after sawing, a higher yield and a much more cost-efficient handling in the sawmill production process would be obtained.

To improve the structural properties of the beams even further, defect elimination by finger jointing and strength grading of the wet side boards before gluing has been proposed. Grading of structural timber into different strength classes means that the grade-determining properties (namely bending strength, MOE and density of timber members) are predicted or measured by visual inspection or non-destructive machine testing. The market is, today, dominated by machine strength grading based on the relationship between a determined MOE value, which is used as the indicating property, and the other two grade-determining properties. One such approach is based upon dynamic excitation and measurement of the first resonance frequency f_{A1} (Hz) in

[1]SP Technical Research Institute of Sweden, Videum Science Park, SE-351 96 Växjö, Sweden
[2]School of Engineering, Linnæus University, SE-351 95 Växjö, Sweden

*Corresponding author, email jan.oscarsson@sp.se

Received 31 October 2010; accepted 27 August 2011
DOI 10.1179/2042645311Y.0000000015

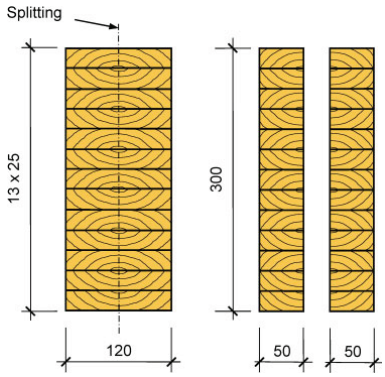

1 Wet-glued beams before (left) and after (right) splitting, drying and planing (Petersson *et al.* 2009; Serrano *et al.* 2010)

the axial direction. The relationship between this frequency and the board length L (m), density ρ (kg m^{-3}) and dynamic modulus of elasticity E_{An} (Pa) in the axial direction is expressed by equation (1) (e.g. Ohlsson and Perstorper 1992)

$$E_{An} = 4\rho\left(\frac{f_{An}L}{n}\right)^2 \quad (1)$$

where n denotes the mode number used to evaluate MOE. Thus, from equation (1), it is made clear that MOE could also be evaluated on the basis of resonance frequencies of higher modes. However, the research reported in this paper is based upon measurement and application of the first resonance frequency. This is due to the fact that industrially applied strength grading techniques that are based upon axial dynamic excitation and listed in EN14081-4 (CEN 2009) utilise only one resonance frequency, i.e. the first resonance frequency, for assignment of timber to strength classes defined in EN338 (CEN 2009). In such industrial applications, the E_{A1} value obtained from equation (1) is used to predict the board's bending strength. This prediction also decides to which strength class the board is graded. Other relevant strength properties such as tensile strength are either defined in the strength class, or calculated in accordance with EN384 (CEN 2010) from the bending strength determined for a sample, or determined from tests described in EN408 (CEN 2010). In this context, it should be noted that MOE is a material property that varies along the length of a board. Thus, the axial dynamic MOE, determined using either f_{A1} or a resonance frequency corresponding with a higher mode, is an apparent MOE that reflects an average MOE value in a board.

The approach described above is generally used for strength grading of structural timber in the dried state, i.e. typically timber with an MC of about 16–18%, but recently grading systems based on axial excitation have also been approved for wet state grading of structural timber (e.g. Initial type testing report; CEN 2010). In previous research carried out by Glos and Burger (1998), similar yields were found when structural timber with thickness >50 mm was graded in both the green state and after kiln-drying to ~12%MC using a bending and radiation type machine. Unterwieser and Schickhofer (2007) investigated the possibility of grading sawn timber, both centre-cuts and side boards with thickness >41 mm, in the wet state. They found that the axial dynamic MOE showed no dependence on the MC above the fibre saturation point and that the relationship in terms of coefficient of determination R^2 between wet and dried axial dynamic MOE was as strong as R^2=0·96.

In this paper, the results from a study to investigate the possibility to grade narrow dimension side boards in the wet state by axial dynamic excitation are presented. For a sample of boards, E_{A1} was determined by dynamic excitation under both wet and dried conditions. Subsequently, tensile strength and local static MOE in tension were measured in the dried state and the correlation between results in wet and dried states was analysed. The reason why the tests were carried out in tension was that laminations in outer parts of the type of split beam that is shown in Fig. 1 are mainly loaded in this mode and, subsequently, the tension properties of such laminations are in most cases determinant for the bending strength of a beam.

In the context of wet-glued laminated split beams made of narrow side boards, the issue of a so called reversed lamination effect on the stiffness of split boards was also raised. The effect concerns to what extent the stiffness of such boards of narrow dimensions is reduced due to the splitting, relative to the stiffness of the corresponding un-split board. This paper includes an evaluation of such an effect.

Methods and materials

A sample consisting of 58 wet Norway spruce side boards of dimensions 25 × 120 × 3900 mm was used in this project. The length of the boards was reduced to 3000 mm by removing 450 mm from each end and a small specimen of 100 mm length was cut from one of the sections removed from each board. The MC of these specimens was determined according to the oven dry method described in EN13183-1 (CEN 2002). Boards and specimens were marked in corresponding consecutive orders from no. 1 to 58.

The first axial resonance frequency f_{A1} was then measured for each board using a Timber Grader MTG which is a handheld and wireless measuring instrument for strength grading of structural timber (Brookhuis Micro-Electronics BV 2009). A grading set includes grader, balance and computer software and hardware. When measuring f_{A1}, the Grader is held against one of the board ends and longitudinal modes of vibration are excited by the blow of a metal piston incorporated in the Grader. Vibration data are measured by a sensor in the Grader and sent via a Bluetooth connection to the PC. From installed software, several axial resonance frequencies could be obtained, but only the first one is employed for determining the dynamic axial MOE. The Grader is approved as a machine grading system with settings listed in EN14081-4 (CEN 2009) and the approval concerns timber with mean MC between 10 and 25%. In this investigation, a board's weight and f_{A1} were obtained from the balance and the Grader respectively. Density and E_{A1} were calculated manually: the latter parameter from equation (1).

In the next step, each board was split in the longitudinal direction into two parts. One of them, randomly

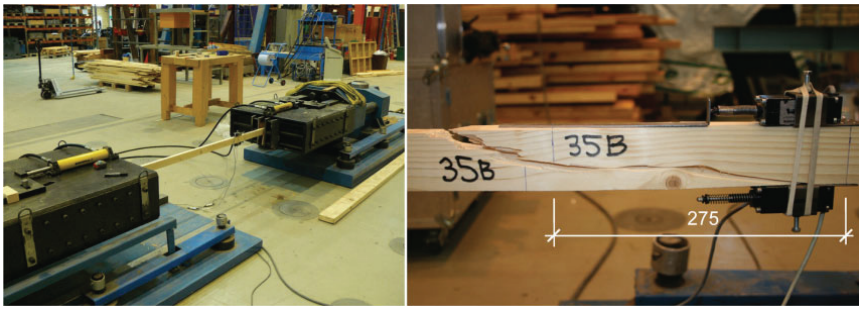

2 Test set-up for tension tests (left) and transducers and measurement length (275 mm) for elongation measurement (right)

chosen, was marked with an 'A' and the other one with a 'B' to supplement the marking from the previous step. The procedure for determination of resonance frequency, density and E_{A1} was then repeated for each split board. After drying to an MC varying between 12 and 14%, the measurement procedure was carried out once again.

Finally, after the boards had been stored at standard climate 20°C/65% relative humidity for ~7 months, tensile strength and local static MOE in tension were measured in accordance with procedures described in EN408 (CEN 2010). The test set-up is shown in Fig. 2 (left). The testing machine was of make MFL with hydraulic force generation, maximum load 3·0 MN and 2000 mm length of stroke. Wedge type grips were used, which prevented rotation of the board ends, and the distance between the grips was 1500 mm. The load

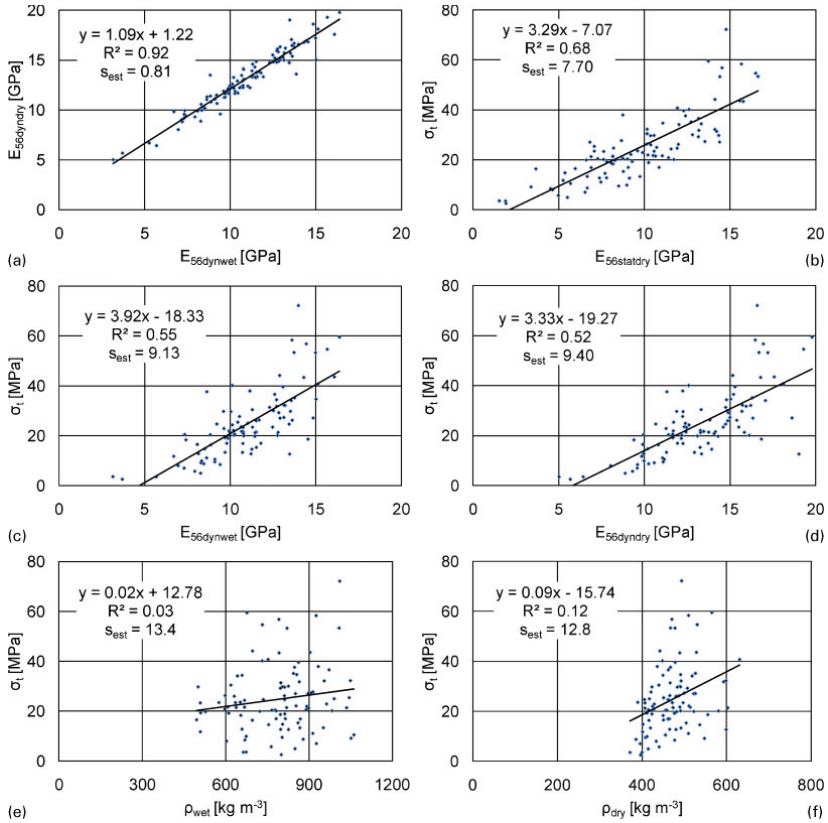

3 Relationship between *a* $E_{56dynwet}$ and $E_{56dyndry}$, *b* $E_{56statdry}$ and σ_t, *c* $E_{56dynwet}$ and σ_t, *d* $E_{56dyndry}$ and σ_t, *e* ρ_{wet} and σ_t and *f* ρ_{dry} and σ_t

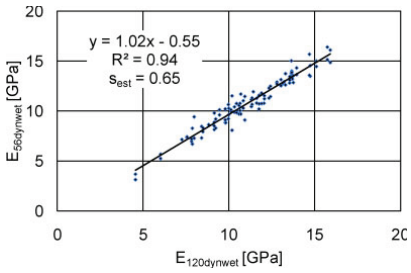

4 Relationship between $E_{120dynwet}$ and $E_{56dynwet}$

application was force controlled with a constant loading rate of 7–8 kN min^{-1} and the average time to failure for the tested boards was 304 s.

The local static MOE was determined from the elongation, measured by two transducers, between two points 275 mm apart, corresponding to a length of five times the width of the boards. The transducers were placed on opposite narrow board edges [*see* Fig. 2 (right)], at the worst defect, i.e. at the board section where the fracture was expected to occur. This critical section was, in most boards, chosen as the one including the largest single knot. For boards that contained traversing edge knots or several potential critical knots of similar size, the grain disturbances around the knots were also considered.

The measurement results were analysed using simple linear regression. To evaluate the possibility of grading wet boards, the following relationships in terms of coefficients of determination R^2 between different material parameters were calculated (indices '56' and '120' refer to the average widths of split boards and un-split boards respectively):

(i) axial dynamic MOE measured for split boards in the wet state, denoted $E_{56dynwet}$, in relation to axial dynamic MOE for split boards in the dried state (12–14%MC), denoted $E_{56dyndry}$ (Fig. 3*a*)
(ii) local static MOE measured for split boards in the dried state $E_{56statdry}$ in relation to the tensile strength for split boards in the dried state σ_t (Fig. 3*b*)
(iii) $E_{56dynwet}$ and $E_{56dyndry}$ respectively, in relation to σ_t (Fig. 3*c* and *d*)
(iv) density before drying ρ_{wet} in relation to σ_t (Fig. 3*e*)
(v) density after drying ρ_{dry} in relation to σ_t (Fig. 3*f*).

Table 2 Coefficients of determination R^2 of different properties of investigated boards

R^2	$E_{56dynwet}$	$E_{56dyndry}$	$E_{56statdry}$	σ_t	ρ_{wet}	ρ_{dry}
$E_{56dynwet}$	1	0·92	0·62	0·55	0·05	0·37
$E_{56dyndry}$		1	0·62	0·52	0·03	0·46
$E_{56statdry}$			1	0·68	0·01	0·14
σ_t				1	0·03	0·12
ρ_{wet}					1	0·06
ρ_{dry}						1

The reversed lamination effect was assessed on the basis of the relationship between $E_{56dyndry}$, as defined above, and $E_{120dynwet}$, i.e. axial dynamic MOE determined for un-split wet boards (Fig. 4).

In addition to the R^2 values presented in the figures referred to above, standard errors of the estimate s_{est} and equation of the regression lines y are also given in the same figures.

Results and discussion

Grading of wet side boards

A number of seven out of the 58 un-split boards and eight out of the 116 split board appeared to contain rot and were eliminated from the subsequent analysis (*see* explanatory notes in Table 1). The MC of the remaining 51 un-split boards in their green state varied considerably, from a minimum value of 28% to a maximum of 180%. The mean MC value was 93% with a standard deviation of 43%.

Mean values and standard deviations of determined parameters defined in the section on 'Methods and materials' are shown in Table 1. Relevant scatter plots are exhibited in Fig. 3*a–f* and the R^2 values for selected interrelationships are presented in Table 2. The mean value of $E_{56dynwet}$ was ~17% lower than $E_{56dyndry}$, which corresponds fairly well with results referred to in Dinwoodie (2000), and the mean value of $E_{56statdry}$ is 26% lower than $E_{56dyndry}$. The last observation is partly explained by the fact that the dynamically measured MOE of a board is related to an average MOE value of the entire board, whereas the local static MOE is measured locally, at the section where the worst defect is located. The difference is also related to the fact that the dynamically measured MOE of a board is, in general, larger than the corresponding statically measured MOE (Larsson *et al.* 1998).

There was a strong relationship between dynamic MOEs measured for split boards in wet and dried states (R^2=0·92, *see* Fig. 3*a*), similar to the one that was found

Table 1 Mean values and standard deviations of different properties of investigated boards

	Unit	Mean value	Standard deviation	Number of boards
$E_{120dynwet}$	GPa	11·10	2·57	50*
$E_{56dynwet}$	GPa	10·84	2·58	108†
$E_{56dyndry}$	GPa	13·04	2·93	108†
$E_{56statdry}$	GPa	9·59	3·40	106‡
σ_t	MPa	24·8	13·5	96§
ρ_{wet}	kg m^{-3}	785	141	108†
ρ_{dry}	kg m^{-3}	471	53	108†

*Eight boards disregarded due to rot (seven) and measurement error (one).
†Eight boards disregarded due to rot.
‡Ten boards disregarded due to rot (eight) and damage (two).
§Twenty boards disregarded due to rot (eight), damage (two) and failure in grips (ten).

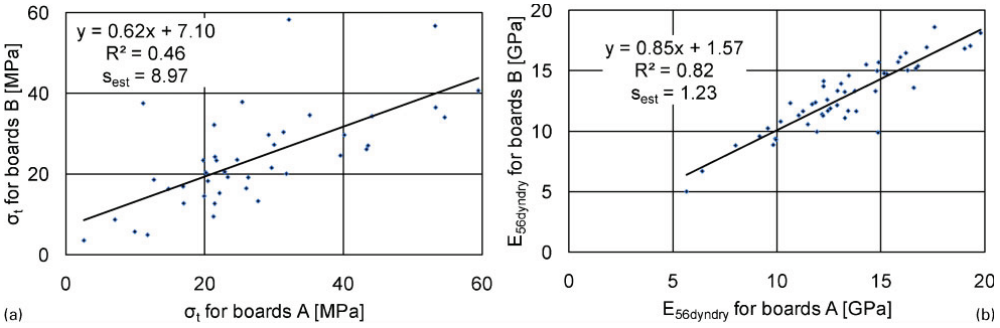

5 Relationship between *a* σ_t for pairs of split boards A and B and *b* $E_{56dyndry}$ for pairs of split boards A and B

by Unterwieser and Schickhofer (2007) for centre-cuts and side boards with thickness >41 mm.

A comparison of Fig. 3*c* and *d* shows that the relationship between dynamic MOE in wet condition and tensile strength was of similar strength as the corresponding relationship between dynamic MOE in dried condition and tensile strength (R^2=0·55 in wet state and R^2=0·52 in dried state). The coefficient of determination for the latter relationship increased to R^2=0·58 when the dried state density was included as a second prediction variable in a multiple linear regression analysis. The relationship between local static MOE, measured in the dried state at the assumed weakest board section, and tensile strength was stronger (R^2=0·68, *see* Fig. 3*b*) than the relationships between tensile strength and dynamic MOE in wet and dried conditions respectively (*see* Fig. 3*c* and *d*). This is presumably due to the fact that the local static MOE is measured at the board section where the fracture is expected to occur, whereas the dynamic MOEs reflect average values for the entire board.

There was a weak relationship between tensile strength and density in the dried state (R^2=0·12, *see* Fig. 3*f*), whereas no such relationship was established between density in the wet state and the tensile strength (R^2=0·03, *see* Fig. 3*e*). It was not surprising that the latter relationship was found to be even weaker than the former, since the density measured in the dried state is a good measure of the amount of wood cell material, whereas in the wet state at variable MC, it is not. Furthermore, the level of significance in terms of p values was calculated for the relationships between densities and tensile strength. The relationship in the dried state was found to be statistically significant (p<0·001), whereas the p value for R^2 between wet state density and strength was, as expected, considerably higher (p=0·12).

The results obtained in this study indicate that it is possible to grade split side boards in the wet state using axial dynamic excitation since, first, the dynamic MOE values measured in wet and dried states are strongly related and, second, the tensile strength is as strongly related to axial dynamic MOE measured in the wet state as it is to axial dynamic MOE measured in the dried state. However, the presented coefficients of determination require that the actual densities in wet and dried states respectively, are regarded when axial dynamic MOEs are calculated.

The idea of grading side boards in the wet state originates from ongoing research concerning wet-glued laminated split beams. For such beams, strength grading of laminations has to be carried out for un-split boards. Thus, the relationship between axial dynamic MOE measured for un-split wet boards $E_{120dynwet}$ and σ_t for dried split boards was also determined and it was found to be R^2=0·45 for the entire sample. However, since $E_{120dynwet}$ is related to σ_t of two split boards, each split board observation is not truly independent. From Fig. 5*a*, it is clear that σ_t of A boards and B boards are correlated to a certain degree. Because of this, the relationships between $E_{120dynwet}$ and σ_t of A and B boards respectively, were determined. For A boards only, the relationship between σ_t and $E_{120dynwet}$ was R^2=0·53 and for B boards it was R^2=0·39. From the calculated coefficients of determination, it could be concluded that the relationship between $E_{120dynwet}$ and σ_t for dried split boards was, as expected, slightly weaker than the relationship between $E_{56dynwet}$ and σ_t (R^2=0·55, *see* Fig. 3*c*).

In some of the split boards, there were knots larger than half the width of the board [*see* Fig. 6 (left and middle)], and in such cases strength values as low as 2·6 MPa were found. The strength of the strongest

6 Fracture in two of weakest split boards (left and middle) and in strongest split board (right)

board was 72·1 MPa [*see* Fig. 6 (right)]. Furthermore, there was a considerable amount of variation in σ_t for boards split from the same original board (R^2=0·46, *see* Fig. 5*a*). The strength of this relationship, together with the mean value and the standard deviation for σ_t given in Table 1, indicates that the scattering of measured strength values for the split boards could be considered as rather large, compared with other investigations of laminations for glued laminated timber (Johansson *et al.* 1998). This is not surprising as the boards examined here are of very narrow dimensions. In comparison, there was a much stronger relationship between values of $E_{56dyndry}$ for boards split from the same original board (R^2=0·82, *see* Fig. 5*b*).

Even if the strength of many of the boards was very low due to the occurrence of knots, this does not necessarily reflect the behaviour of the boards when they are used as flatwise glued laminations in the type of glulam beams shown in Fig. 1. For example, large deformations, both longitudinal and lateral, in flexible sections of a lamination are restrained by adjacent laminations, and tensile forces in weak laminations could, to a certain degree, be transferred via bond lines to other laminations. This, in combination with the fact that the beams consisted of side board laminations, explains why high performance wet-glued beams could be achieved from un-graded batches of split Norway spruce side boards.

Reversed lamination effect

From Table 1, the mean value and standard deviation of the stiffnesses, in the wet state, of split and un-split boards ($E_{56dynwet}$ and $E_{120dynwet}$) used in this investigation could be compared and the relationship between $E_{56dynwet}$ and $E_{120dynwet}$ is shown in Fig. 4. According to the obtained results, the mean value was 2% lower after splitting, the standard deviations were almost the same and the relationship was very strong (R^2=0·94). The two variables, before splitting ($E_{120dynwet}$) and after splitting ($E_{56dynwet}$), were compared with a paired *t*-test and the difference in MOE, although small, was found to be statistically significant ($p<0·01$). In the analysis, the value for an un-split board was compared with values for both split boards. Consequently, the $E_{56dynwet}$ observations are not truly independent, as the stiffnesses of A boards and B boards are correlated (*see* Fig. 5*b*). However, the effect is small. For the A boards only, the relationship between $E_{56dynwet}$ and $E_{120dynwet}$ was R^2=0·94, and for the B boards it was R^2=0·93, i.e. almost exactly the same R^2 values as was obtained for the entire sample of split boards.

Conclusions and future work

The objectives of this research were to investigate the possibility to grade Norway spruce side boards of narrow dimensions in the wet state using axial dynamic excitation, and to evaluate a possible reversed lamination effect on the stiffness caused by splitting wet boards longitudinally into two parts. According to the results, strength grading in the wet state using axial dynamic MOE as indicating property is just as reliable as grading carried out correspondingly after drying, provided that actual board density in both wet and dried states are measured and regarded when MOE values are determined. The relationship between axial dynamic MOE for split boards in the wet and dried states, $E_{56dynwet}$ and $E_{56dyndry}$, was found to be as high as R^2=0·92.

The results also show that the difference in strength between two split boards originating from the same un-split board could be considerable. However, the difference would most likely be reduced by implementation of defect elimination such as finger jointing of un-split side boards, since such a measure would result in a reduction in the inhomogeneity of material properties in both split and un-split boards. This is an issue to be addressed in future work.

Regarding the reversed lamination effect on the stiffness of split boards, it was in this investigation found to be of lower order.

Acknowledgements

This research was made possible by financial support from The Knowledge Foundation, The Swedish Research Council for Environment, Agricultural Science and Spatial Planning and CBBT – Centre for Building and Living with Wood.

References

Boutelje, J. B., and Rydell, R. 1995. Wood facts – 44 wood species in text and illustrations (in Swedish). Trätek – Swedish Institute for Wood Technology Research, Stockholm, Sweden. Publ. no. 8604028.

Brookhuis Micro-Electronics BV. 2009. Timber Grader MTG – operating instructions. Enschede: Brookhuis Micro-Electronics BV. MTG Manual GB 12062009-C.

CEN. 1999. EN1194 Glued laminated timber – strength classes and determination of characteristic values. European Committee for Standardization, Brussels, Belgium. CEN/TC124.

CEN. 2002. EN13183-1 Moisture content of a piece of sawn timber – Part 1: determination by oven dry method. European Committee for Standardization, Brussels, Belgium. CEN/TC175.

CEN. 2009. EN338 Structural timber – strength classes. European Committee for Standardization, Brussels, Belgium. CEN/TC124.

CEN. 2009. EN14081-4 Timber structures – strength graded structural timber with rectangular cross section – Part 4: machine grading – grading machine settings for machine controlled systems. European Committee for Standardization, Brussels, Belgium. CEN/TC124.

CEN. 2010. EN384 Structural timber – determination of characteristic values of mechanical properties and density. European Committee for Standardization, Brussels, Belgium. CEN/TC124.

CEN. 2010. EN408 Timber structures – structural timber and glued laminated timber – determination of some physical and mechanical properties. European Committee for Standardization, Brussels, Belgium. CEN/TC124.

CEN. 2010. Initial type testing report no. ITT/36/20/03. European Committee for Standardization, Brussels, Belgium. CEN/TC124/TG1.

Dahlblom, O., Persson, K., Petersson, H., and Ormarsson, S. 1999. Investigation of variation of engineering properties of spruce. Proc. 6th Int. IUFRO Wood Drying Conf. Stellenbosch, South Africa, January 1999. IUFRO. Pages 253–262.

Dinwoodie, J. M. 2000. Timber: its nature and behaviour. London: Second Edition, E & FN Spon.

Glos, P., and Burger, N. 1998. Maschinelle Sortierung von frisch eingeschnittenem Schnittholz (in German). Holz. Roh. Werkst. 56(5): 319–329.

Johansson, C.-J., Boström, L., Bräuner, L., Hoffmeyer, P., Holmqvist, C., and Sollie, K. H. 1998. Laminations for glued laminated timber – establishment of strength classes for visual strength grades and machine settings for glulam laminations of Nordic origin. SP Swedish National Testing and Research Institute, Sweden. SP report 1998:38.

Larsson, D., Ohlsson, S., Perstorper, M., and Brundin, J. 1998. Mechanical properties of sawn timber from Norway spruce. Holz. Roh. Werkst. 56(5): 331–338.

Ohlsson, S., and Perstorper, M. 1992. Elastic wood properties from dynamic tests and computer modeling. J. Struct. Eng. 118(10): 2677–2690.

Petersson, H., Bengtsson, T., Blixt, J., Enquist, B., Källsner, B., Oscarsson, J. (ed.), Serrano, E., and Sterley, M. 2009. Increased value yield by wet and dry gluing of sawn side boards into

property optimized wood products for the construction market (in Swedish). School of Technology and Design, Växjö University, Sweden. Reports no. 53.

Serrano, E., Oscarsson, J., Enquist, B., Sterley, M., Petersson, H., and Källsner, B. 2010. Green-glued laminated beams – high performance and added value. Proc. (Poster session) 11th World Conf. on Timber Engineering, Riva del Garda, Italy, June 2010. Trees and Timber Institute. Pages 829–830.

Steffen, A., Johansson, C.-J., and Wormuth, E.-W. 1997. Study of the relationship between flatwise and edgewise moduli of elasticity of sawn timber as a means to improve mechanical strength grading technology. Holz. Roh. Werkst. 55(2–4): 245–253.

Unterwieser, H., and Schickhofer, G. 2007. Pre-grading of sawn timber in green condition. Proc. 1st Conf. of COST Action E53 – quality control for wood and wood products. Warzaw, Poland, October 2007. European Science Foundation.

Wormuth, E.-W. 1993. Untersuchung des Verhältnisses von flachkant zu hochkant ermitteltem Elastizitätsmodul von Schnittholz zur Verbesserung der maschinellen Festigkeitssortierung (in German). Master's dissertation. University of Hamburg, Germany.

III

Determination of tensile strain fields in narrow Norway spruce side boards as a basis for verification of new machine strength grading methods

Jan Oscarsson[*,1]*, Anders Olsson*[2]*, Bertil Enquist*[2]

ABSTRACT

Today's methods for machine strength grading of structural timber result, in general, in strength predictions with a rather low accuracy. A need for development of more precise methods has been identified. Application of stiffness in terms of locally determined MOE as indicating property is an evident starting point for such a process. Development of new grading procedures and models require laboratory verification, and this research investigates the possibility of using contact-free deformation measurement technique based on white-light digital image correlation (DIC) for this purpose. A sample of nine Norway spruce (*Picea abies*) side boards of narrow dimensions was tested in tension according to the European Standard EN 408. Simultaneously, deformations along the entire length of one of the flatwise surfaces of each board were measured using two master-slave connected DIC systems. Strain fields were subsequently calculated. To evaluate the accuracy of the measurement technique, local MOE determined traditionally, *i.e.* on the basis of elongations measured in accordance with EN 408, was compared with corresponding MOE values calculated on the basis of DIC deformation measurements. Acceptable agreement between compared MOEs were achieved and the accuracy of MOE values determined on the basis of the DIC technique was on the same level as requirements laid down in EN 408. However, the resolution of the information supplied by the DIC technique can, in contrast to elongations measured traditionally, be used to gain detailed knowledge regarding local MOE in evaluated boards. Therefore, based upon achieved results, in combination with certain identified potentials for measurement improvements, it is concluded that DIC technique can be used as a tool for development and laboratory verification of new strength grading methods.

Keywords: contact-free, modulus of elasticity, side boards, strain distribution, strength grading, wood

INTRODUCTION

Strength grading of structural timber based on axial dynamic excitation is a method that has gained large market shares since it was introduced in the late 1990s. On the basis of measured longitudinal vibrations induced in a piece of timber by a hammer blow at one end, mean axial dynamic modulus of elasticity E_A is calculated by application of a relationship (*e.g.* Ohlsson and Perstorper 1992) between E_A, resonance frequency f_{A1} of the first axial mode of vibration, board density ρ and board length L. The strength σ in terms of predefined strength classes is then predicted on the basis of a statistical relationship between E_A and σ.

An important reason why the described method has been successful is its simplicity. The space that the equipment occupies is limited and it can be installed in existing production lines in which the boards are fed transversely, the latter implying that the grading is carried out at a limited feed speed. The accuracy of the method is on the same level as grading machines based on flatwise bending (*e.g.* Betzhold 1999). More precise grading may be achieved by systems based on axial excitation and X-ray scanning (Bacher 2008), but such systems are in general rather costly, and a need for more accurate, but yet inexpensive, grading methods has been articulated.

[1] SP Technical Research Institute of Sweden, Videum Science Park, SE-351 96 Växjö, Sweden.
[2] School of Engineering, Linnaeus University, SE-351 95 Växjö, Sweden.

* Corresponding author, email jan.oscarsson@sp.se

Previous research (*e.g.* Hoffmeyer 1995; Olsson *et al.* 2012) has shown that the best single predictor, or indicating property, of both bending and tensile strength is the stiffness in terms of modulus of elasticity (MOE) determined on a rather local level at a critical section, *i.e.* at a section at which stiffness and strength is expected to be reduced. In most cases, such sections coincide with knots (Johansson 2003). Thus, application of stiffness, determined on a local scale, as indicating property is an interesting starting point for development of more accurate strength grading methods.

The need for new grading techniques by which local defects can be identified, evaluated and possibly also eliminated has been made clear from research concerning development of glulam beams using wet glued laminations of narrow side boards of Norway spruce (*Picea abies*). Such research is since 2005 jointly conducted by the SP Technical Research Institute of Sweden, Linnæus University, previously named Växjö University, and the Södra Timber AB, which is one of the largest sawmilling companies in Sweden. Side boards, *i.e.* boards of narrow dimensions obtained from the outer parts of a log, are considered to be products of poor profitability owing to a combination of low value and costly handling. However, side boards possess excellent material properties (*e.g.* Wormuth 1993) and when applied as laminations in glulam beams, their value is expected to increase considerably.

The principal lay-up of investigated beams of side board laminations is exhibited in Figure 1 (left). After gluing, the beams were split, dried and planed to cross-sectional dimensions of 50×300 mm, see Figure 1 (middle). In two initial test series the beams were manufactured from ungraded boards, but in a third series, the three outermost boards at each beam edge were strength graded on the basis of E_A and visual inspection of knot size. The results of four point bending tests carried out in accordance with the European Standard EN 408 was found to be very promising (Serrano *et al.* 2011).

For narrow boards such as those applied in the split beams, the reduction of strength and stiffness due to local defects such as large knots, see Figure 1 (right), is more severe than if the same defects would occur in structural timber of more common dimensions. Consequently, and as mentioned above, the need for strength grading methods based on determination of local stiffness was underlined by results of the research concerning narrow side boards. Development of procedures and models for such grading is ongoing. In this process, laboratory verification is required.

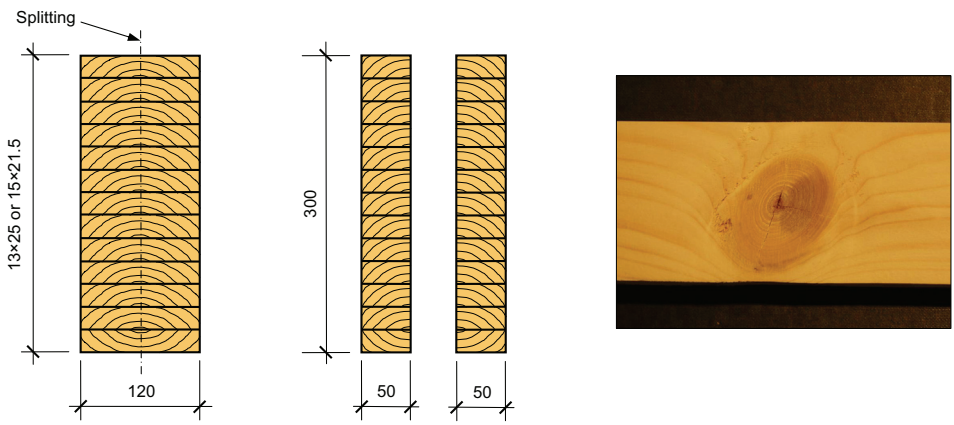

Figure 1. Principal lay-up of wet glued beams before (left) and after (middle) splitting, drying and planing, and crucial knot in a side board lamination (knot size $\emptyset_{max}$=39 mm in lateral board direction).

PURPOSE AND OBJECTIVE

The purpose of this research was to investigate the possibility of using contact-free DIC measurement technique as a means for laboratory verification of new strength grading methods based on application of locally determined MOE as indicating property. The objective was to evaluate the possibility of determining stiffness variation with high accuracy along the flatwise surfaces of timber pieces under tensile load. This was to be achieved on the basis of analysis of occurring strain fields calculated from deformations measured by DIC technique. To verify the ability of this approach, local MOE at an assumed critical section in each investigated board was determined in a traditional way, *i.e.* in accordance with EN 408, and compared with equivalent MOE values achieved on the basis of detected strain fields and corresponding load level.

MATERIALS

Nine boards of dimension 25×55×3000 mm were selected from a sample of 116 boards for which tensile tests according to EN 408 were carried out as part of the described research concerning wet-glued beams. The results of the tensile tests are found in Oscarsson *et al.* (2011). The 116 board sample were obtained from cutting and splitting an initial sample of 58 boards of dimension 25×120×3600 mm delivered from a sawmill in the south east part of Sweden. Before testing, the boards were stored in a climate room at a standard climate 20°C/65% relative humidity for about seven months.

The maximum knot dimension, $\varnothing_{max}$, measured in the lateral direction of the nine boards, varied between 8 and 24 mm, with an average value of 15 mm. The maximum knot size of each board is tabulated in Table 1.

TEST SET-UP AND MEASUREMENT EQUIPMENT

Simultaneously as each of the selected nine boards were subjected to tensile tests in accordance with EN 408, the deformations along one of the flatwise surfaces were measured using DIC technique and corresponding strain fields subsequently calculated. To evaluate the longitudinal stiffness variation in the boards, it was deemed necessary to measure the deformations over a considerable length. To ensure a high measurement resolution, two identical DIC systems were applied and connected in a master-slave fashion, each measuring the deformations of slightly more than half the visible board length, see Figure 3.

Set-up for tensile tests according to EN 408

The test set-up is shown in Figures 2-3. The testing machine was of make MFL with a hydraulic force generation, 2.0 m length of stroke and a 3.0 MN load cell. The distance between the wedge type grips was approximately 1500 mm. The load was applied in force control mode with a loading rate of 7-8 kN/minute. During a load test, corresponding load and deformation values were sampled by the data acquisition system of the MFL machine every half second. Each sampled value was determined on the basis of measurement signals being filtered by means of time integration, resulting in a reduction of measurement noise.

Transducers for determination of MOE according to EN 408

The local MOE in tension parallel to the grain was determined according to EN 408, *i.e.*

$$E_{EN408} = \frac{l_1(F_2 - F_1)}{A(w_2 - w_1)} \tag{1}$$

where $F_2 - F_1$ = increment of load on the straight line portion of the load-deformation graph, $w_2 - w_1$ = elongation corresponding to $F_2 - F_1$, l_1 = length, equivalent with five times the width (w_b) of the board, over which the elongation is measured, and A = cross-sectional board area. The load F_2 was set equal to 40 % of the fracture load, F_{max}, and F_1 was set equal to 10 % of F_{max}. The elongation was determined as the mean value of the elongations measured by two transducers positioned at the centre of opposite narrow edges, see Figure 2 (right). Since the width, w_b, was 55 mm, the length l_1 was 275 mm, see Figure 2 (right).

When local MOE in *bending* is determined according to EN 408, it is required that a regression analysis of sampled pair of observations along the chosen straight line portion of the load-deformation graph should result in a correlation coefficient R of 0.99 or better. A similar condition is, however, *not* explicitly expressed as regards determination of local MOE in *tension* parallel to the grain, but the same kind of regression analysis as the one described was still used for evaluation of the accuracy of the determined local tension MOE of the nine boards.

Digital image correlation for determination of strain fields

The board surface area for which two dimensional strain fields in lateral and logitudinal directions and in shear were determined was approximately 55×1500 mm. The surface deformations were measured using two DIC measurement systems named ARAMIS from GOM mbH, Germany (GOM 2009a). Each system separately measured a board length of approximately 800 mm, resulting in a measurement overlap of 113 mm (see Figure 3). Applied cameras were of Charge-Coupled Device (CCD) type with a resolution of 2048×2048 pixels. They were positioned at angles and distances that depend on the size of the object to be measured. Before the tests were carried out, separate 3D coordinate systems were defined for each measurement system through calibration procedures.

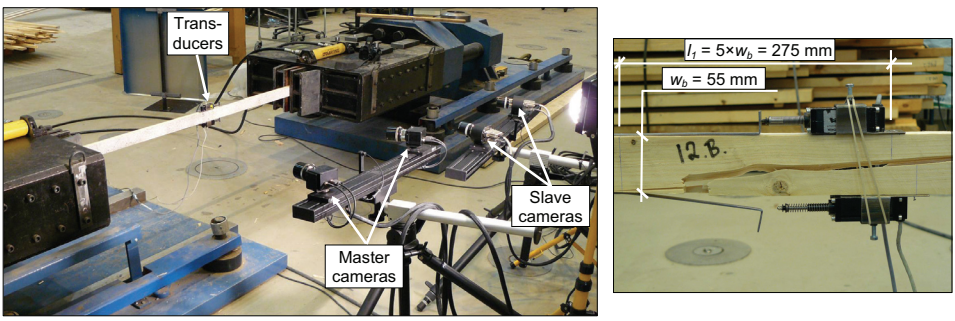

Figure 2. Set-up for tension tests according to EN 408 and for surface deformation measurement (left), and transducers for measurement of elongation at the assumed critical board section (right).

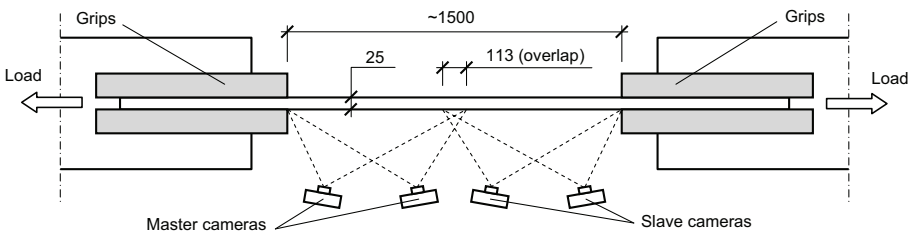

Figure 3. Camera set-up (plan) for surface deformation measurement.

The ARAMIS systems were applied in a master-slave fashion, implying that pictures were taken simultaneously by all four cameras at a fixed time interval of three seconds during a load test. Since the two cameras of each ARAMIS system were positioned at different angles, stereoscopic images of the measured surface were obtained separately from each system. Thus, the deformations occuring along the entire surface during a load test were recorded by pictures taken simultaneously by both pair of cameras. Each such double pair of pictures represented a unique so-called *load stage* to which similarly unique strain fields corresponded. The analog force signal of the MFL machine was acquired by the computer of the ARAMIS master system at each load stage, *i.e.* a load value was sampled for each double pair of pictures. However, the master computer's acquisition of these load values were momentary, without any filtering, which meant that they included more measurement noise than the load values sampled by the data acquisition system of the MFL machine.

Based on the stereoscopic images, 3D positions of a large number of points on the deformed surface could be determined for every load stage. Such coordinate determination is carried out based on the camera pictures being divided into partially overlapping square or rectangular image sub-pictures called *facets*. Each such facet represents a measuring point. The coordinates of each facet are identified for every load stage, which requires that the object's surface has an identifiable pattern that deforms along with the test object as the load changes. In this case, the pattern consisted of a white and black speckled pattern of sprayed paint.

The size, in pixels, of both facets and overlaps could be adjusted depending on the shape of the measured object and required spatial resolution of the measurements. To reflect the long and narrow shape of the measured boards, chosen facet shape and overlaps resulted in resolutions, *i.e.* facet step or distance between measuring points, of 3.6 mm in longitudinal board direction and 1.8 mm in the lateral direction. The strains of each facet were calculated on the basis of the coordinate displacements occurring in a 5×5 facet mesh surrounding the facet for which the strains were determined. More thorough descriptions of the ARAMIS system are found in Serrano *et al.* (2005) and Oscarsson *et al.* (2012).

To evaluate and visualize strains along the entire board length jointly and simultaneously, and since the ARAMIS systems performed separate measurement project based on separate coordinate systems, there was a need for a third coordinate system to which the other two could be transformed. Using yet another contact-free optical measurement system called TRITOP (GOM 2009b), such a coordinate system was defined on the basis of a set-up, see Figure 4 (left), including *orientation crosses*, 27 *reference point markers* fixed to a metal sheet, and a scale bar by which the dimensions of the coordinate system were determined. Digital pictures of the set-up were taken from several angles using a photogrammetric camera. From these pictures, 3D coordinates of the reference points were calculated using TRITOP software. These coordinates defined the third coordinate system, implying that the reference point markers on the metal sheet shared a fixed coordinate relationship. Thus, if the sheet was moved, the TRITOP coordinate system was moved along with the sheet. This characteristic was utilized for coordinate transformation from ARAMIS to TRITOP. When a master-slave ARAMIS measurement was prepared, the sheet was put just behind the board to be measured, see Figure 4 (right). It was positioned halfway between the grips, and consequently covering the overlap shown in Figure 3. As the pictures of the first load stage were taken, the reference points on the sheet were also caught and their positions in the ARAMIS projects were calculated. Accordingly, since the reference points on the sheet were defined in both the TRITOP and the ARAMIS coordinate systems, it was possible to transform ARAMIS coordinates to the TRITOP system. It should be noted that most of the reference points on the sheet were only identified in one of the ARAMIS projects, since the sheet was positioned to cover the measurement overlap. Nevertheless, the coordinate transformation from each

ARAMIS project to TRITOP was still possible. Finally, after transformation of facet coordinates from ARAMIS to TRITOP, the two projects were exported to a further GOM software called SVIEW (GOM 2009b) by which the projects were combined, visualized and evaluated as one project, see Figure 6.

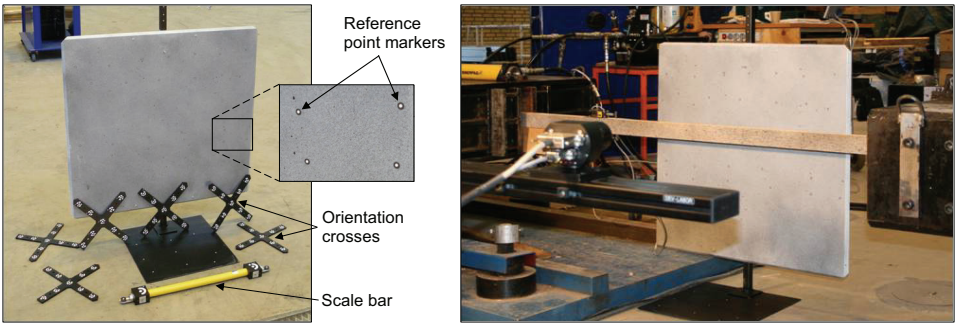

Figure 4. Set-up for determination of TRITOP coordinate system (left) and set-up for transformation of ARAMIS coordinates to TRITOP coordinates (right).

RESULTS AND DISCUSSION

Load-deformation graphs

Load-deformation graphs of the nine boards are shown in Figure 5. As mentioned in the section *Test set-up and measurement equipment* the deformation was determined as the average of the elongations of two transducers, see Figure 2 (right), located at the assumed critical section of a board. The tensile strength, denoted σ_{max}, varied conspicuously between the boards, ranging from 11.1 MPa (F_{max} = 15.2 kN) for board no. 39A, to 59.5 MPa (F_{max} = 81.1 kN) for board no. 34A. For the entire sample of 116 boards, the strength variation was even more striking, σ_{max} ranging from 2.6 to 72.1 MPa. This confirms, as asserted in the *Introduction*, that large defects have a severe strength reducing effect on narrow boards and that there is a need for strength grading methods based on local stiffness. Values of tensile strength and fracture load of the nine boards are presented in Table 1.

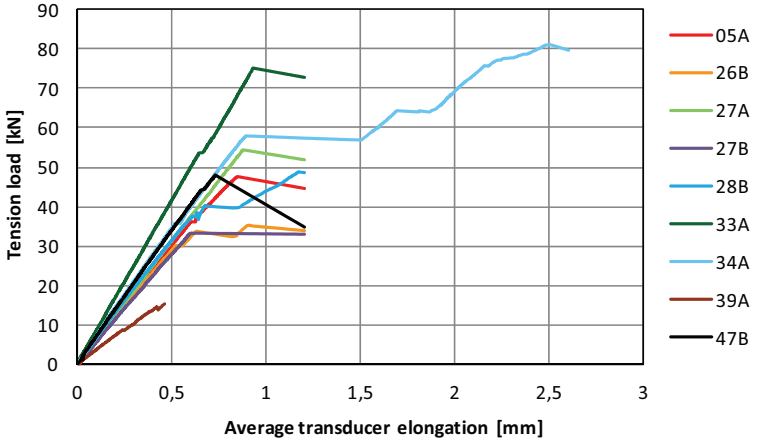

Figure 5. Load-deformation graphs of boards for which strain field measurements were carried out.

Table 1. Locally determined MOEs for boards used in the strain field measurement investigation.

Board	Maximum knot size	Fracture load	Tensile strength	MOE EN408	Coeff. of corr.	MOE lines	Coeff. of corr.	MOE area	Coeff. of corr.
	$Ø_{max}$	F_{max}	σ_{max}	E_{EN408}	R_{EN408}	E_{line}	R_{line}	E_{area}	R_{area}
	[mm]	[kN]	[MPa]	[MPa]	[−]	[MPa]	[−]	[MPa]	[−]
05A	14	47.8	35.1	12700	1.000	14400	0.994	13800	0.990
26B	19	35.4	26.2	12000	1.000	11400	0.984	11200	0.980
27A	8	54.5	39.6	12300	1.000	11900	0.995	12200	0.997
27B	19	33.1	24.6	11900	1.000	11200	0.984	11200	0.992
28B	15	48.8	36.6	13200	1.000	13200	0.994	13300	0.995
33A	8	75.2	54.6	16500	1.000	16200	0.997	16900	0.998
34A	15	81.1	59.5	13700	1.000	14200	0.997	13800	0.998
39A	24	15.2	11.1	7500	0.999	8800	0.972	8800	0.985
47B	13	47.9	34.4	13300	1.000	12600	0.989	13200	0.992

Strain field measurements

The results of the strain field measurements were graphically represented using so called *contour plots* and *section diagrams*, which are post-processing tools available in both ARAMIS and SVIEW. A contour plot means that the strain distribution in longitudinal or lateral direction or in shear over the measured surface is visualized, for a certain load stage, on the basis of a defined colour scaling. Such plots are powerful means for providing a qualitative and immediate impression of the strain distribution over the measured surface. To obtain more detailed strain information on a local scale, so called *sections*, defined in camera images as lines on the measured surface, can be used. The strains and displacements along such lines can be plotted in section diagrams.

As an example of achieved results, described plots and diagrams of one of the investigated boards, board no. 28B, are exhibited in Figure 6. Figure 6a shows an image of the measured surface. In Figure 6b, longitudinal tensile strains, ε_x, achieved by the two ARAMIS measurement projects are exhibited. The combination of these two projects by use of the SVIEW software is visualized in Figure 6c which also shows the positions of three defined longitudinal sections (left detail) and the position of the origin of the TRITOP coordinate system (right detail). Lateral displacements in edgewise board direction, Δy, and longitudinal strains, ε_x, along the sections are presented in Figures 6d-e.

The results in Figure 6 represent a load stage at which the load F was 36.9 kN, equivalent with $0.76 \times F_{max}$. This load stage is shown, since the contour plots for the following stages were disturbed, due to cracks occurring at the knot located at longitudinal coordinate $x \approx -650$ mm and at the two knots at $x \approx 350$ mm.

The appearance of longitudinal strain concentrations at the knots is clearly seen in the contour plots in Figures 6b-c and in the section diagram in Figure 6e. Such concentrations are explained by the fact that the orientation of clear wood fibres close to the knots deviate from the longitudinal board direction. Since the stiffness of wood fibres is much larger in the longitudinal fibre direction than in the perpendicular directions, longitudinal strains increase on board surface areas where fibres are inclined in relation to the longitudinal board direction. Since the entire fibre structure within a knot is rotated in relation to the clear wood fibre structure, large strains are also found on knot cross sections. The occurrence of cracks as described in the previous paragraph is in agreement with reasonable expectations, considering

that the presence of knots has a strong influence on crack propagation and fracture in sawn timber (*e.g.* Johansson 2003). For clarity, it should be noted that the longitudinal strains along Section 0 are excluded in Figure 6e, since their variation along this section was small.

The lateral displacements, Δy, shown in Figure 6d reveal distinct peaks at the knots, which indicate that edgewise lateral deflection occurring in a tension test can be used for identification of local defects. Similar results, but on the basis of bending tests, was found by Nagai *et al.* (2009), who investigated the possibility of detecting knots in lumber of Sitka spruce (*Picea sitchensis*) using bending deflection curves obtained from DIC measurements. The same research group investigated tensile strain distribution around knots in Japanese cedar (*Cryptomeria japonica*) using DIC technique and found that fractures was often initiated close to knots where the fibre-orientation changed in a three-dimensional manner (Nagai *et al.* 2011).

Each ARAMIS measurement project included a facet mesh that was created without consideration of the mesh in the other project. When the two projects were combined in SVIEW, each mesh was simply inserted into the TRITOP coordinate system, which implied that the overlapping area included measurement results from both projects. This is clearly seen in the overlapping area of the section diagrams in Figure 6e.

In the section *Materials* it was described that maximum knot dimension in the measured nine boards was 24 mm. However, boards with knots as large as $\varnothing$ = 42 mm were initially also measured. For such boards, fracture occurred within a limited space of time after loading had begun. Considering the sampling frequency (pictures taken every third second) and the chosen resolution of the facet mesh, the amount of strain information from such measurements was too limited for it to serve as a basis for any relevant analysis of strain behaviour.

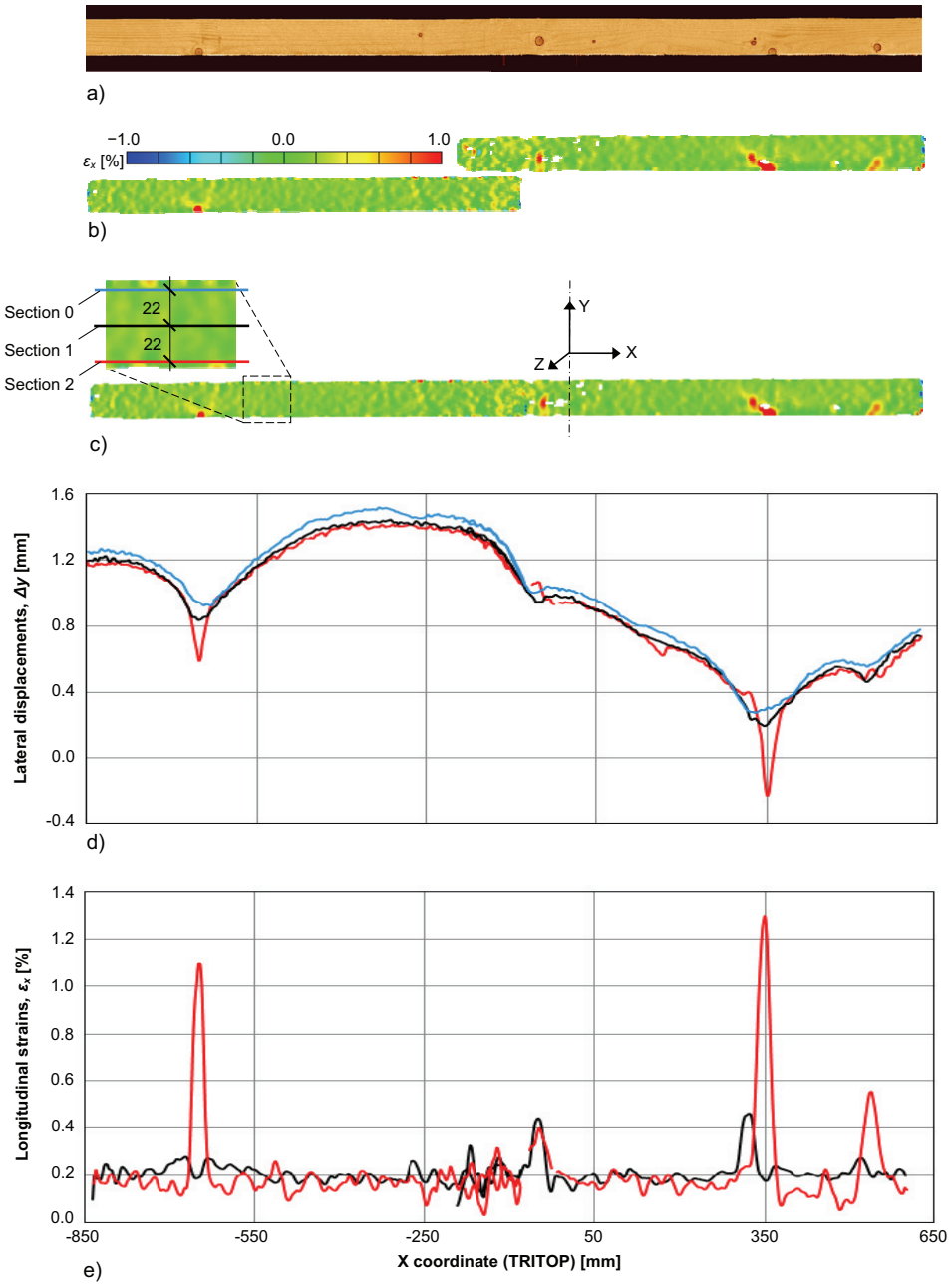

Figure 6. Displacement and strain field measurement results for board no. 28B at load stage no. 173 (F=0.76×F_{max}), just before the occurrence of cracks: a) image of board surface, b) contour plots of longitudinal strains, ε_x; master project (left) and slave project (right), c) SVIEW contour plot; positions of defined sections (left detail) and position of TRITOP coordinate system (right detail), d) lateral displacements, Δy, in edgewise board direction along Sections 0-2, and e) longitudinal strains, ε_x, along Sections 1-2.

Local modulus of elasticity

Local tensile MOE was determined in three ways. As described in the section *Test set-up and measurement equipment*, it was determined according to EN 408, *i.e.* according to Equation (1) and on the basis of average transducer elongations, see Figure 2 (right). It was also calculated in two different ways based upon DIC measurement. Firstly, it was determined on the basis of elongations of lines defined in camera images, see Figure 7 (left). The principle of this MOE determination, the values of which was denoted E_{line}, was the same as the one applied in EN 408, *i.e.* the relative displacement between the end points of each line was measured. The length of the lines and their position in the longitudinal board direction were the same as the length over which the transducer elongations were measured. The lines were positioned along the outermost facets, as close to the board edges as possible. Secondly, local MOE was also determined using average longitudinal strains measured over board surface areas, see Figure 7 (right). Both location and length of the area were the same as for the lines applied for E_{line} determination. The average area strains were plotted against the load, and the local MOE, denoted E_{area}, was determined as

$$E_{area} = \frac{(F_2 - F_1)}{A(\varepsilon_2 - \varepsilon_1)} \tag{2}$$

where F_2-F_1 = the same load increment as applied in Equation (1), $\varepsilon_2-\varepsilon_1$ = change of average longitudinal area strain corresponding to F_2-F_1 and measured over the defined surface area, and A = the cross-sectional board area.

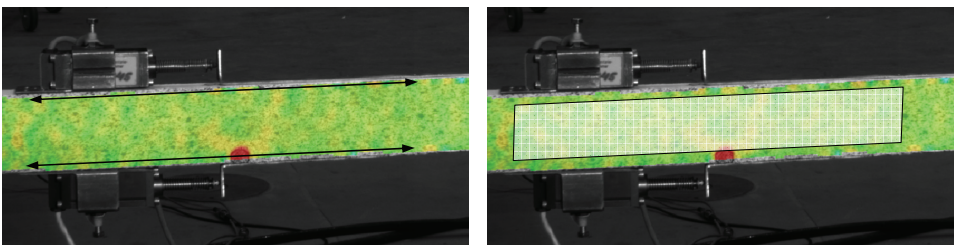

Figure 7. Elongation measurement lines (left) and average strain measurement area (right) for determination of local MOEs denoted E_{line} and E_{area}, respectively.

Values of E_{EN408}, E_{line} and E_{area} and corresponding correlation coefficients R determined from regression analysis of load-deformation graphs are shown in Table 1. To assess the accuracy of the determined MOEs, the achieved R values were compared with the regression requirement of EN 408 ($R \geq 0.99$) discussed in the section *Test set-up and measurement equipment*. Such a comparison showed that R_{EN408} fulfilled, by a wide margin, the regression requirement for all nine boards, which was not the case for R_{line} or R_{area}. The main reason for this was that sampled load and deformation values upon which calculation of E_{EN408} was based were determined on the basis of filtered measurement values obtained from the MFL machine, whereas E_{line} and E_{area} were calculated on the basis of ARAMIS measurement values that were obtained momentarily. Consequently, the measurement values upon which the two latter MOEs were based included measurement noise that was much larger than the noise that E_{EN408} values were contaminated with. However, the noise could have been reduced by applying a load cell with a maximum load that was better adjusted to the size of measured fracture loads. The largest fracture load exhibited in Table 1 was 81.1 kN, only representing 3 % of the load cell's capacity. A load cell with a more limited capacity would result in a decrease of absolute noise in load values sampled by both the MFL machine and the ARAMIS system. However, even if the noise in load values obtained by the ARAMIS

systems was considerable, determined R_{area} for eight of the boards fulfilled the regression requirement stated in EN 408. As for R_{line}, the results were somewhat less accurate.

The relationship between E_{EN408} and E_{line} in terms of coefficient of determination was R^2=0.86, whereas R^2 between E_{EN408} and E_{area} was 0.91. The difference could probably be explained by difficulties inherent in the DIC technique. Determination of coordinates, displacements and strains on facet level require that the board surface is smooth, since irregularities may cause problems as regards facet identification and coordinate calculations (GOM 2009a). Since the lines shown in Figure 7 (left) are located very close to board edges that might be rough or round in shape, it is most likely that the accuracy of the measured line elongations is impaired, resulting in a reduction of R^2 between E_{EN408} and E_{line}.

Since the total number of pair observations was limited, the accuracy of the obtained R^2 values was investigated by repeated regression analyses in which one pair of observations was eliminated in turn. The relationship between E_{EN408} and E_{line} was reduced to R^2=0.77 when the stiffest board (no. 33A) as well as the most flexible one (39A) were eliminated. As regards the relationship between E_{EN408} and E_{area}, it was only reduced (R^2=0.85) when board no. 33A was eliminated. In all other elimination cases, the relationships were either slightly improved or unchanged.

According to EN 408, local MOE in tension parallel to the grain should be determined on the basis of elongations measured by two extensometers positioned to minimize the effect of distortions such as bending or other local displacements in flatwise or edgewise board direction. Distortions are considered as being regarded if local board elongation is determined as the average value of elongations measured by two transducers positioned at the centre of opposite narrow edges, as shown in Figure 2 (right). Correspondingly, if local MOE is to be determined on the basis of longitudinal strain fields determined on flatwise board surfaces, and if requirements in EN 408 should be fulfilled, effects of flatwise distortions must be eliminated. This could be achieved if local tensile MOE is calculated as the average of either E_{line} or E_{area} values determined on opposite flat surfaces and on the basis of deformations measured simultaneously on both sides. However, the values of E_{line} and E_{area} reported in Table 1 are based on ARAMIS measurements performed on only *one* of the flat surfaces, which means that the exhibited MOE values might be affected by flatwise deformations. Thus, it is most likely that the R^2 values reported above will be improved by means of a measurement set-up eliminating the effects of flatwise distortion.

CONCLUSIONS

The purpose of this research was to investigate the possibility of using a contact-free DIC measurement system as a tool for development and laboratory verification of new strength grading methods based on the relationship between local stiffness and board strength. The objective was to evaluate the possibility of determining stiffness variation with high resolution and high accuracy along timber member under tensile load. This was to be verified by comparing local MOE determined in a traditional way with corresponding MOE values calculated on the basis of surface deformations measured by contact-free measurement technique.

It could be concluded that the DIC technique is a forceful tool for providing both qualitative and quantitative information about the strain distribution over a surface for which the ratio between length and width is large.

As regards the comparison of different local MOE measures, acceptable agreements were achieved and the accuracy of MOE values determined on the basis of DIC measurements were on the same level as requirements stipulated in EN 408. However, both agreement and

accuracy could most likely be further improved by application of a load cell that is better adjusted to current fracture load levels, by filtering load values sampled by the ARAMIS system, and by simultaneously measuring surface deformations on both flatwise surfaces of a board. On the basis of achieved results, in combination with suggested measurement improvements, it is reasonable to conclude that DIC technique can be applied for laboratory assessment of local MOE of boards, which for example is of great value when developing and verifying new methods for strength grading.

In boards including large knots, *i.e.* in boards with low strength, the sampling frequency applied and chosen resolution of facet meshes were not sufficient. Thus, adjustments in these respects would be needed in order to assess such boards sufficiently well.

ACKNOWLEDGEMENTS

This research was made possible by financial support granted by *CBBT – Centre for building and living with wood* and *FORMAS – The Swedish Research Council for Environment, Agricultural Science and Spatial Planning*.

REFERENCES

EN 408 (2010) *Timber structures – Structural timber and glued laminated timber – Determination of some physical and mechanical properties*. European Committee for Standardization.

GOM mbH (2009a) *ARAMIS User Manual – Software*. aramis-v6-1, 7-Aug-2009.

GOM mbH (2009b) *TRITOP User Manual – Software*. tritop_v62, 30-Jul-2009.

Bacher, M. (2008) *Comparison of different machine strength grading principles.* In: Proceedings of 2nd Conference of COST Action E53 – Quality control for wood and wood products, Delft, the Netherlands, October 29-30.

Betzhold, D. (1999) *Machinelle Festigkeitssortierung. Einfluss der Hochtemperatur-trocknung auf die elastomechanischen Eigenschaften des Schnittholzes (Machine strength grading. Influence of high-temperature drying on elastomechanical properties of sawn timber).* Diplomarbeit, Fachhochschule Eberswalde, Germany (in German).

Hoffmeyer, P. (ed.) (1995) *Styrkesortering ger mervärde, Del 2 – Tillgængelig teknik (Strength grading adds value, Part 2 – Available technique).* Laboratoriet for Bygningsmaterialer, Danmarks Tekniske Universitet, Teknisk Rapport 335-1995, ISSN 0908-3871 (in Danish, Norwegian and Swedish).

Johansson, C.-J. (2003) *Grading of timber with respect to mechanical properties*. In: Thelandersson, S. and Larsen, H. J. (eds) Timber Engineering, John Wiley & Sons, Ltd, Chichester, England, pp 23-43.

Nagai, H., Murata, K. and Nakano, T. (2009) *Defect detection in lumber including knots using bending deflection curve: comparison between experimental analysis and finite element modeling*. Journal of Wood Science, 55:169-174.

Nagai, H., Murata, K. and Nakano, T. (2011) *Strain analysis of lumber containing a knot during tensile failure*. Journal of Wood Science, 57:114-118.

Ohlsson, S. and Perstorper, M. (1992) *Elastic wood properties from dynamic tests and computer modeling.* Journal of Structural Engineering, 118(10):2677-2690.

Olsson, A., Oscarsson, J., Johansson, M., Källsner, B. (2012) *Prediction of timber bending strength on basis of bending stiffness and material homogeneity assessed from dynamic excitation.* Wood Science and Technology, 46(4):667-683.

Oscarsson, J., Olsson, A., Johansson, M., Enquist, B., and Serrano, E. (2011) *Strength grading of narrow dimension Norway spruce side boards in the wet state using first axial resonance frequency*. International Wood Products Journal, 2(2):108-114.

Oscarsson, J., Olsson, A. and Enquist, B. (2012) *Strain fields around knots in Norway spruce specimens exposed to tensile forces*. Wood Science and Technology, 46(4):593-610.

Serrano, E. and Enquist, B. (2005) *Contact-free measurement and non-linear finite element analyses of strain distribution along wood adhesive bonds*. Holzforschung, 59:641-646.

Serrano, E., Blixt, J., Enquist, B., Källsner, B., Oscarsson, J. (ed.), Petersson, H. and Sterley, M. (2011) *Wet glued laminated beams using side boards of Norway spruce.* School of Engineering, Linnæus University, Växjö, Sweden. Report No 5, ISBN: 978-91-86491-79-6.

Wormuth, E.-W. (1993) *Untersuchung des Verhältnisses von flachkant zu hochkant ermitteltem Elastizitätsmodul von Schnittholz zur Verbesserung der maschinellen Festigkeitssortierung (Study of the relationship between flatwise and edgewise moduli of elasticity of sawn timber for the purpose of improving machine strength grading technology*. Master's thesis, Department of Wood Technology, University of Hamburg, Germany (in German).

IV

Prediction of timber bending strength and in-member cross-sectional stiffness variation on basis of local wood fibre orientation

Anders Olsson[1], Jan Oscarsson[2], Erik Serrano[3], Bo Källsner[4], Marie Johansson[5] and Bertil Enquist[6]

Abstract Machine strength grading of structural timber is based upon relationships between so called indicating properties (IPs) and bending strength. However, such relationships applied on the market today are rather poor. In this paper, new IPs and a new grading method resulting in more precise strength predictions are presented. The local fibre orientation on face and edge surfaces of wooden boards was identified using high resolution laser scanning. In combination with knowledge regarding basic wood material properties for each investigated board, the grain angle information enabled a calculation of the variation of the local MOE in the longitudinal direction of the boards. By integration over cross-sections along the board, an edgewise bending stiffness profile and a longitudinal stiffness profile, respectively, were calculated. A new IP was defined as the lowest bending stiffness determined along the board. For a sample of 105 boards of Norway spruce of dimension 45 × 145 × 3600 mm, a coefficient of determination as high as 0.68-0.71 was achieved between this new IP and bending strength. For the same sample, the coefficient of determination between global MOE, based on the first longitudinal resonance frequency and the board density, and strength was only 0.59. Furthermore, it is shown that improved accuracy when determining the stiffness profiles of boards will lead to even better predictions of bending strength. The results thus motivate both an industrial implementation of the suggested method and further research aiming at more accurately determined board stiffness profiles.

Keywords Machine strength grading, Bending stiffness, Laser scanning, Fibre angle, Grain angle, Wood, Structural timber, Lumber, Dynamic stiffness, MOE

List of symbols

σ_m	bending strength
E_m	local MOE based on measured deflections in static bending
$E_{m,g}$	global MOE based on measured deflections in static bending
ρ	board (average) density
f_{a1}	resonance frequency of first longitudinal mode of vibration
E_{a1}	MOE calculated on basis of f_{a1} and ρ
$E_{a,min}$	MOE calc. for longitudinal dir. in the weakest section, based on fibre orient. and f_{a1}
$E_{b,min}$	MOE calc. for bending of the weakest section, based on fibre orientation and f_{a1}
$E_{b,min,\delta}$	MOE calc. for bending of the weakest δ mm long part of the beam

[1] School of Engineering, Linnaeus University, SE-351 95 Växjö, Sweden. Email: anders.olsson@lnu.se
[2] SP Technical Research Institute of Sweden, Vidéum Science Park, 351 96 Växjö. Email: jan.oscarsson@sp.se
[3] School of Engineering, Linnaeus University, SE-351 95 Växjö, Sweden. Email: erik.serrano@lnu.se
[4] School of Engineering, Linnaeus University, SE-351 95 Växjö, Sweden and SP Technical Research Institute of Sweden, Box 5609, 114 86 Stockholm. Email: bo.kallsner@lnu.se
[5] School of Engineering, Linnaeus University, SE-351 95 Växjö, Sweden. Email: marie.johansson@lnu.se
[6] School of Engineering, Linnaeus University, SE-351 95 Växjö, Sweden. Email: bertil.enquist@lnu.se

$E_{b,min,\delta,w}$	MOE calc. for bending of the weakest δ mm long part of the beam in relation to a weight function w
R^2	Coefficient of determination

Introduction

Structural timber is classified into specific strength grades using various methods available on the market. A brief description of the most important of these is given below. However, the statistical relationships being utilized today between the indicating properties (IP) and the target bending strength are rather weak. In commercially available machine strength grading systems, the coefficient of determination, R^2, between the IPs and the bending strength typically lies in the range of 0.5-0.6 for Norway spruce. With the most advanced systems known to the market, using a multitude of sensors and measurement principles, values above R^2=0.7 can be achieved but such systems are rarely used in practice. Improvements of the coefficient of determination between the IPs and the bending strength have a considerable commercial potential as higher accuracy would make it possible to efficiently grade timber into higher strength classes than what can be done today, and a better yield would be achieved in the more common strength classes.

The basic principle for machine strength grading of structural timber is generally to determine a modulus of elasticity (MOE) of a board and to use this property as an IP for prediction of bending strength. Dynamic excitation can, in combination with density and board length, be used to determine a global, longitudinal MOE directly, see e.g. Larsson (1997). This method is frequently applied using relatively inexpensive machines. It could also be utilized without determination of the actual board density. In such cases, an average density of the graded wood species is used.

A literature review carried out by Olsson et al (2011) showed that the bending stiffness correlates better to bending strength than what the longitudinal stiffness does. Olsson el al (2011) also showed that a set of resonance frequencies corresponding to higher modes of vibration can be used for assessing the homogeneity of a board. A measure of inhomogeneity (MOI), corresponding to the variation of stiffness along a board, was suggested as a complementary IP, i.e. to be used in combination with the MOE, for prediction of bending strength.

Flatwise bending machines have been used since the 1960´s and are still available on the market. Over a span of about one metre, and moving along the board, the bending stiffness is measured and on basis of this a MOE valid for *flatwise* bending representing a certain part of the board is calculated. Thus, such machines give some information regarding the stiffness variation along the board.

The sizes and locations of knots can be detected with rather high precision using X-ray techniques. The benefit of such detection is underlined by the fact that fracture testing of a sample of about 1000 pieces of timber has shown that more than 90% of the failures were caused by knots (Johansson 2003). Schajer (2001) was able to make better predictions using an X-ray technique than what could be done using a bending machine in a comparative study. There are grading machines on the market today that combine X-ray techniques with either flat-wise bending or measurement of the dynamic longitudinal stiffness. The information added by the X-ray technique compared to the other techniques is a high resolution in measuring the variation of the density within a board.

The orientation of wood fibres in timber has a large effect on stiffness and strength and there are techniques to identify the fibre orientation locally on the surface or within wooden members. An early attempt to utilize such information for strength grading purposes was presented by Bechtel and Allen (1987). The fact that the dielectric constant is higher in the fibre direction, or

actually in the direction of fibres projected on a surface, than across the fibres was utilized. Fibre angles were identified over the two face surfaces of boards and it was shown that the detected grain field could be used for identifying knots. Three different methods aiming at actually calculating the crack path and the tensile strength of boards were also suggested. The methods were based on the Hankinson formula by which the local tensile strength in the direction of the board was expressed as a function of the tensile strength in the fibre direction and the local fibre angle. For a small sample consisting of 24 specimens it was shown that a coefficient of determination between calculated and true tensile strength exceeding 0.8 could be reached. However, the coefficient of determination between global MOE and true tensile strength was for the same sample 0.77, which is very high compared with what has been presented in other studies and also compared with what is reached in grading utilizing global MOE as indicating property to strength. Two possible explanations for the high R^2 values were offered. First, the tensile test was carried out over a short span (70 cm) and, second, usual statistical procedures for material sampling were not followed. Recently Moore and Baldwin (2011) discussed the method suggested by Bechtel and Allen and concluded that nowadays it is possible to identify the grain angle field on basis of the dielectric constant in a speed corresponding to the production speed at sawmills. They also suggested an improved version of one of the methods suggested by Bechtel and Allan, but it was only verified on a very small sample consisting of nine planed fir boards two of which had to be excluded because of twist causing difficulties when applying the dielectric method.

Laser techniques utilizing the so-called tracheid effect for detecting fibre orientation are available and have been implemented in high speed, high resolution wood-scanners already on the market. However, the technique is not yet utilized for strength grading purposes in a sophisticated way. Petersson (2010) showed that size and location of knots can be determined on basis of the grain-angle distribution detected using this technique. In addition, he presented research aiming at accurately predicting the stiffness on basis of end scanning, including information about the pith location and the annual ring width.

In a study presented by Jehl et al (2011), the influence of fibre angles in the prediction of both MOE and tensile strength was evaluated. The fibre angle fields were examined over the face surfaces of 350 boards. Also the diving angle, i.e. the angle between the board surface and the wood fibres, was evaluated by examining the shape of the elliptic laser dot, which due to the tracheid effect is stretched in the direction of the projected fibre angle. The authors claim that the diving angle can be determined in this way but they also say that the results achieved are rather uncertain. Furthermore, it was assumed that the MOE is an affine function of the density. Thus, a map of the local board density, averaged through the thickness of each board, was obtained from an optical scanner equipped with an X-ray source. From such maps, the fraction of the thickness occupied by a knot was computed on pixel level and the corresponding clear wood area ratio (CWAR) was determined. To take the effect of fibre angle fields into account, local CWAR values were modified using Hankinson's formula. Finally, a board's MOE was determined either from axial dynamic excitation or as the product of modified CWAR and the clear wood's MOE. The tensile strength was similarly estimated as the product of modified CWAR and clear wood tensile strength. By application of the described method, it was possible to predict tension strength with very high accuracy, at best with a coefficient of determination of 0.78.

As previous research has pointed out, high resolution information regarding fibre angles has a very interesting potential for strength grading purposes. However, whereas the research referred to above are based mainly upon empirical relationships, a theoretically sound base for the relationship between wood material properties, fibre orientation in timber and local MOE in the direction of the board is presented in this paper. A suitable IP to bending strength is also defined

and the potential for further improvements of the concept of utilizing local stiffness for strength grading purposes is evaluated. A patent application has recently been filed for an invention corresponding to the method presented herein.

Sampling of material for evaluation

The sampling of timber for the investigation took place in Långasjö, Sweden, on December 11-12, 2007, at a sawmill owned by the company Södra Timber. The timber consisted of sawn boards of Norway spruce (*Picea Abies*) of nominal dimensions 50 × 150 mm and of length 3900 mm or 4500 mm. In the sampling, a sample with large variation in strength was aimed for. Thus, boards with high and low expected strength were included. For this purpose a grading machine of type Dynagrade® was employed with settings for grading of timber to be used for roof trusses (strength class TR26) on the UK market. Both boards fulfilling (61 pieces) and boards not fulfilling the requirements (44 pieces) were selected for further investigation. A visual assessment was performed in order to identify the weakest section of each board according to instructions in the European standard EN 384 (CEN 2010a). This standard prescribes that the weakest section should be located in the maximum bending moment zone, i.e. between the two point loads in a four point bending test, and that the tension edge shall be selected at random after the weakest section has been chosen.

All the boards were planed to dimension 45 × 145 mm immediately after selection. Then the boards were cut to the length 3600 mm and placed in a climate room holding a temperature of 20°C and 65% relative humidity (RH). Small pieces of wood were also saved and stored in the climate room for assessment of the moisture content.

Methods and measurements

The research involves laboratory testing including laser scanning, dynamic excitation and static loading. Quantities measured in the laboratory were the weight and dimensions of the boards, high resolution fibre orientation fields on the surfaces of the boards, resonance frequencies corresponding to longitudinal modes of vibration, static edgewise bending stiffness (determined in two different ways, giving a local and a global measure, respectively) and the bending strength. The arrangements and carrying through of the scanning and the dynamic and static tests are described below.

In addition to the laboratory work, the research also involves analytical and numerical calculations and common regression analysis using the software Matlab®.

Scanning for detection of fibre angles on surfaces

A WoodEye scanner (by the company Innovativ Vision AB) equipped with four sets of multi-sensor cameras, dot and line lasers and conveyor belts for feeding boards in the longitudinal direction through the scanner was used for face and edge scanning. Figure 1 shows the WoodEye-scanner (left) and an overview of the WoodEye system with lasers, light and multi-sensor cameras (right). The notation ”IN” marks the cross section of a scanned board. The laser scanning makes use of the so-called tracheid effect where one of the principal axes of the light intensity distribution around a laser dot is oriented in the direction of the wood fibres (Nyström 2003). This provides a practical method for measuring variations in grain angle on a wood surface. Figure 2 shows a piece of wood including a knot (left), an image showing how the light

from the dot lasers spread on the wood surface (middle) and the fibre orientation on the wood surface (right) calculated by identifying the major principal axis of each light spot using image analysis. Within knots, where the shape of the light spots is close to circular, the calculation of the fibre direction becomes uncertain. This is indicated in Figure 2 (right) by the dotted lines drawn for the calculated fibre orientations corresponding to such laser dots.

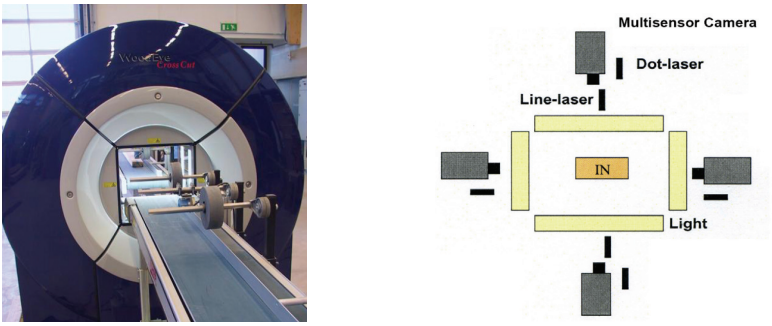

Figure 1 WoodEye-scanner (left) and overview of the WoodEye system with lasers, light and multisensor cameras (right). The notation ”IN” marks the cross-section of a scanned board. [Images originate from Petersson (2010).]

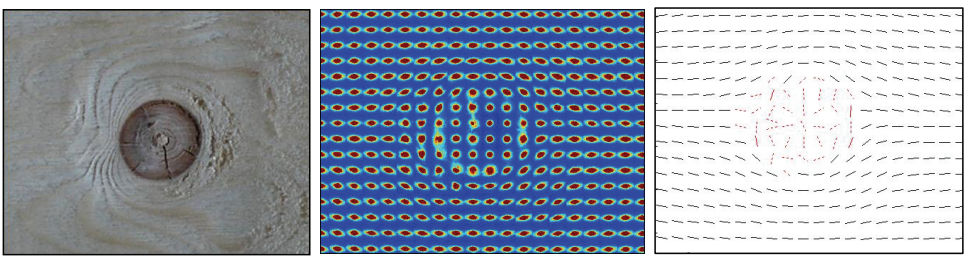

Figure 2 A piece of wood including a knot (left), an image showing how the light from dot lasers spread on the wood surface (middle) and the fibre orientation on the wood surface (right) calculated by identifying the major principal axis of each light spot using image analysis. [Images originate from Petersson (2010).]

The resolution employed for the scanning of the boards, i.e. the distance between laser dots on the surfaces, was 0.8 mm in the longitudinal direction of the board and 3.6 mm in the lateral board direction. It should be noted that the grain angle detected actually represents the fibre orientation projected on the surface. Consequently, the so called diving angle is not assessed here.

Determination of dynamic stiffness

The determination of the lowest longitudinal resonance frequency of each board, which in combination with the board density is used for calculating an average board MOE, was performed using an MTG hand-held timber grader. The MTG grader is a wireless measuring instrument for strength grading of structural timber (Brookhuis Micro-Electronics BV 2009). It is approved as a machine grading system with settings listed in EN 14081-4 (CEN 2009). The frequency measurement is carried out simultaneously as the board is supported by a balance from which the weight is determined. The resonance frequencies of the boards included in this study

were also assessed using a more advanced laboratory setup in which free-free boundary conditions were resembled by suspending the boards in rubber bands. In this test setup the board was hit with an impulse hammer at the one end of the boards and the vibration content was measured using an accelerometer fastened at the other end. The coefficient of determination between the lowest longitudinal resonance frequencies measured using the two different sets of equipment was as high as R^2=0.999.

Static four-point bending test

The local and global static bending stiffness and the bending strength of the boards were determined using a four point bending test according to the European standard EN 408 (CEN 2010b). The total span was 2610 mm long (corresponding to eighteen times the depth of the board) and the two point loads were applied 870 mm apart, each of them 870 mm from the nearest support. For such a load case, the mid-span is subjected to a constant bending moment and no shear force. The predicted weakest part of each board, selected by means of visual inspection, was located within the zone with constant bending moment, i.e. between the two point loads, and was randomly located with respect to the position of the tension side of the board.

Calculation of stiffness on basis of fibre angles

It is well known that wood is a strongly orthotropic material having a very high stiffness and strength in the fibre direction but low stiffness and strength in other directions. In a stem or wooden board, most fibres are close to parallel with the longitudinal stem or board direction, but also small deviations in fibre direction have a significant effect on the board properties. Locally, in particular within and in the close surrounding of knots, the fibre direction may deviate strongly from the longitudinal direction of the stem or board, see Figure 2 (right), and this is crucial for the structural properties of timber.

Figure 3 shows a drawing of a part of a stem and a drawing of a board that could have been cut out from it. Two different coordinate systems are displayed, one global with axes parallel to the sides of the board and one local relating to the main directions of the wood material in a position in the stem. From an engineering point of view one needs to describe the structural properties in relation to a coordinate system where one axis (x) is parallel to the longitudinal direction of the board and the other two axes (y and z) are oriented parallel to the thickness direction and depth direction, respectively. Knowing the fibre orientation locally in relation to the board direction, material transformations can be carried out giving the local material properties corresponding to the principal directions of the board, i.e. the global coordinate system. Assuming that (**l**,**r**,**t**) and (**i**,**j**,**k**) are the unit vectors along the l-r-t system and the x-y-z system, respectively, one can write

$$\begin{bmatrix} \mathbf{l} \\ \mathbf{r} \\ \mathbf{t} \end{bmatrix} = \mathbf{A}^{\mathrm{T}} \begin{bmatrix} \mathbf{i} \\ \mathbf{j} \\ \mathbf{k} \end{bmatrix} \tag{1}$$

where

$$\mathbf{A} = \begin{bmatrix} a_l^x & a_r^x & a_t^x \\ a_l^y & a_r^y & a_t^y \\ a_l^z & a_r^z & a_t^z \end{bmatrix} \tag{2}$$

in which a_l^x , for instance, denotes cosine for the angle between the l- and x-axes.

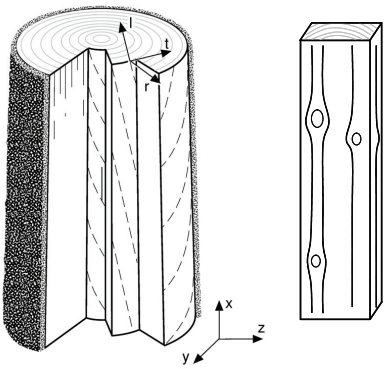

Figure 3 Drawing of a part of a stem and drawing of a board that could have been cut out from it. Two different coordinate systems are displayed, one global with axes parallel to the sides of the board and one local relating to the main directions of the wood material in a position in the stem. [The left drawing originates from Ormarsson (1999).]

The wood material properties relating to local directions can be stored in the compliance matrix $\overline{\mathbf{C}}$ as

$$\overline{\mathbf{C}} = \begin{bmatrix} \frac{1}{E_l} & -\frac{\nu_{rl}}{E_r} & -\frac{\nu_{tl}}{E_t} & 0 & 0 & 0 \\ -\frac{\nu_{lr}}{E_l} & \frac{1}{E_r} & -\frac{\nu_{tr}}{E_t} & 0 & 0 & 0 \\ -\frac{\nu_{lt}}{E_l} & -\frac{\nu_{rt}}{E_r} & \frac{1}{E_t} & 0 & 0 & 0 \\ 0 & 0 & 0 & \frac{1}{G_{lr}} & 0 & 0 \\ 0 & 0 & 0 & 0 & \frac{1}{G_{lt}} & 0 \\ 0 & 0 & 0 & 0 & 0 & \frac{1}{G_{rt}} \end{bmatrix} \tag{3}$$

in which E_l, E_r, E_t are the moduli of elasticity in the orthotropic directions, G_{lr}, G_{lt}, G_{rt} are the shear moduli in the respective orthotropic planes, and the parameters ν_{lr}, ν_{rl}, ν_{lt}, ν_{tl}, ν_{rt} and ν_{tr} are

Poisson's ratios. Note that the relations $v_{rl} = E_r/E_l \times v_{lr}$, $v_{tl} = E_t/E_l \times v_{lt}$ and $v_{tr} = E_t/E_r \times v_{rt}$ hold which means that $\overline{\mathbf{C}}$ only contains nine independent material parameters.

The material matrix $\overline{\mathbf{D}} = \overline{\mathbf{C}}^{-1}$ (relating to the l-r-t system) may be used to expresses a linear elastic constitutive relation between stresses and strains as

$$\overline{\boldsymbol{\sigma}} = \overline{\mathbf{D}}\overline{\boldsymbol{\varepsilon}} \tag{4}$$

where strain and stress components are stored in $\overline{\boldsymbol{\varepsilon}}$ and $\overline{\boldsymbol{\sigma}}$, respectively, as $\overline{\boldsymbol{\varepsilon}} = \begin{bmatrix} \varepsilon_l & \varepsilon_r & \varepsilon_t & \gamma_{lr} & \gamma_{lt} & \gamma_{rt} \end{bmatrix}^{\mathrm{T}}$ and $\overline{\boldsymbol{\sigma}} = \begin{bmatrix} \sigma_l & \sigma_r & \sigma_t & \tau_{lr} & \tau_{lt} & \tau_{rt} \end{bmatrix}^{\mathrm{T}}$. Strains and stresses may be transformed between the l-r-t system and the x-y-z system using a transformation matrix $\mathbf{G}$ as

$$\overline{\boldsymbol{\varepsilon}} = \mathbf{G}\boldsymbol{\varepsilon} \tag{5}$$

and

$$\boldsymbol{\sigma} = \mathbf{G}^{\mathbf{T}}\overline{\boldsymbol{\sigma}} \tag{6}$$

respectively, where the transformation matrix

$$\mathbf{G} = \begin{bmatrix} a_l^x a_l^x & a_l^y a_l^y & a_l^z a_l^z & a_l^x a_l^y & a_l^z a_l^x & a_l^y a_l^z \\ a_r^x a_r^x & a_r^y a_r^y & a_r^z a_r^z & a_r^x a_r^y & a_r^z a_r^x & a_r^y a_r^z \\ a_t^x a_t^x & a_t^y a_t^y & a_t^z a_t^z & a_t^x a_t^y & a_t^z a_t^x & a_t^y a_t^z \\ 2a_l^x a_r^x & 2a_l^y a_r^y & 2a_l^z a_r^z & a_l^x a_r^y + a_l^y a_r^x & a_l^z a_r^x + a_l^x a_r^z & a_l^y a_r^z + a_l^z a_r^y \\ 2a_t^x a_l^x & 2a_t^y a_l^y & 2a_t^z a_l^z & a_t^x a_l^y + a_t^y a_l^x & a_t^z a_l^x + a_t^x a_l^z & a_t^y a_l^z + a_t^z a_l^y \\ 2a_r^x a_t^x & 2a_r^y a_t^y & 2a_r^z a_t^z & a_r^x a_t^y + a_r^y a_t^x & a_r^z a_t^x + a_r^x a_t^z & a_r^y a_t^z + a_r^z a_t^y \end{bmatrix} \tag{7}$$

is based on the components of $\mathbf{A}$ defined in Eq. (2) (Ormarsson 1999). By premultiplication of Eq. (4) by $\mathbf{G}^{\mathbf{T}}$ and by considering Eqs. (5-6) it follows that the material matrix relating to the x-y-z system can be expressed as

$$\mathbf{D} = \mathbf{G}^{\mathbf{T}}\overline{\mathbf{D}}\mathbf{G} \tag{8}$$

Of particular interest for the following is that $c_{1,1}^{-1}$, i.e. the inverse of the component stored in the first row and first column of the globally oriented compliance matrix $\mathbf{C} = \mathbf{D}^{-1}$, now is equal to $E_x(x,y,z)$, i.e. the local MOE valid in the longitudinal direction of the board.

Modulus of elasticity calculated on board surfaces

The description above concerning how to calculate local MOE in the longitudinal board direction is presented in general terms. In practice, however, certain assumptions have to be made as the knowledge regarding true fibre angle orientation is not complete. We now assume that the

projected fibre angles on the lateral board surfaces[7] detected by means of scanning represent the true, three dimensional fibre orientation on these surfaces. We also assume that the normal direction of each lateral board surface is parallel with the radial direction of the wood material, i.e. that each lateral surface is oriented in the longitudinal-tangential plane. If the basic wood material parameters, i.e. the parameters involved in the locally oriented compliance matrix $\overline{\mathbf{C}}$ (Eq. 3 above), are known the MOE on the lateral board surfaces in the longitudinal board direction can now be calculated. The issue of how to determine the basic wood material parameters valid for an individual board is addressed in a separate section below, but it is suitable for our purposes to show, already at this stage, an example of calculation results, with high spatial resolution, regarding MOE on lateral board surfaces. Figure 4 (left) shows photographs of all four sides of one board (denoted board number 74) and MOE in longitudinal board direction over the board surfaces (right) calculated on basis of the local fibre angles (or rather on their projections on the wood surface). The x-axis starts at the root end of the board. Red colour indicates a high MOE, found in areas where the orientation of the wood fibres coincide with the longitudinal direction of the board, and blue colour indicates a particularly low MOE corresponding to a local fibre direction diverging substantially from the longitudinal board direction. Note that areas occupied by knots typically have a fibre orientation substantially diverging from the longitudinal board direction. The absolute level of the MOE in the individual board depends on the basic material parameters, of which the MOE in the fibre direction is the most important one. The centre parts of Figure 4 shows photographs, projected fibre angle field and calculated MOE in the longitudinal board direction of a small part of the board. The topmost centre part of Figure 4 shows an enlargement of the fibre angle field at a single large knot in the board.

[7] A lateral board surface is a surface with a normal direction perpendicular to the longitudinal direction of the board.

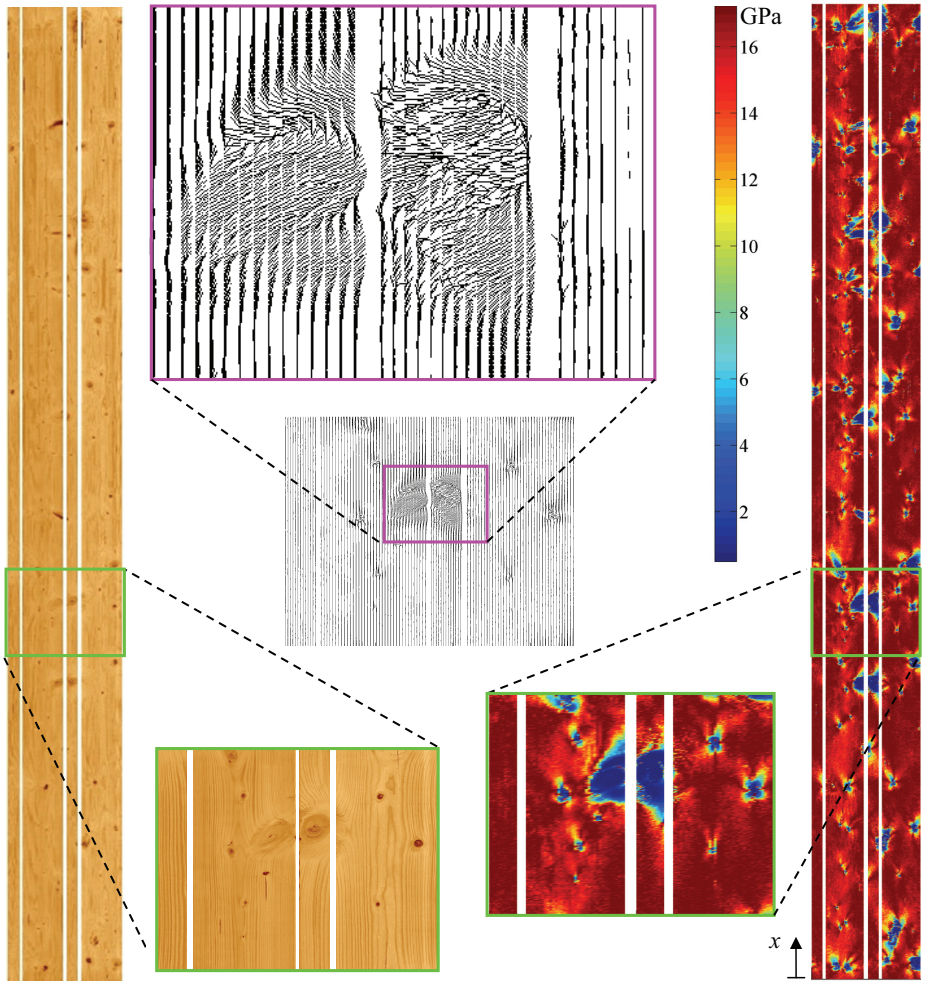

Figure 4 Photographs of all four sides of one board (left) and calculated MOE in longitudinal board direction over the entire board surface (right). The x-axis starts at the root end of the board. Red colour indicates a high MOE, found in areas where the orientation of the wood fibres coincide with the longitudinal direction of the board, and blue colour indicates a particularly low MOE corresponding to a local fibre direction diverging substantially from the longitudinal board direction. The centre parts show photographs, projected fibre angle field and calculated MOE in a small part of the board. The topmost centre part shows an enlargement of the projected fibre angle field at a single large knot in the board.

Integration of cross-sectional stiffness properties

We now return to a more general description and assume that the MOE valid in the longitudinal direction of the board is known in every position within it, i.e. that $E_x = E_x(x,y,z)$ is known for $0 \leq x \leq L$, $-t/2 \leq y \leq t/2$ and $-d/2 \leq z \leq d/2$, where L, t and d is the length, thickness and depth of the board, respectively. Furthermore, we introduce a coordinate system with its origin at the one end of the board and in the geometrical centre of the cross-section. Considering the wooden board as a beam, the position of the neutral axis (i.e. the position (y,z) within the board cross-section where, according to traditional beam theory, we get zero normal stress when the beam is exposed to pure bending around the y-axis and the z-axis, respectively) can be calculated as

$$\bar{y}(x) = \iint E_x \cdot y \, dydz \tag{9}$$

and

$$\bar{z}(x) = \iint E_x \cdot z \, dydz \tag{10}$$

respectively. The bending stiffness along the beam with respect to bending around the y- and z-axis can then be calculated as

$$EI_y(x) = \iint E_x \cdot (z - \bar{z})^2 \, dydz \tag{11}$$

and

$$EI_z(x) = \iint E_x \cdot (y - \bar{y})^2 \, dydz \tag{12}$$

respectively. (One may note that these axes are not actually principal axes.) The longitudinal board stiffness can be calculated as

$$EA(x) = \iint E_x dydz \tag{13}$$

Calculation of cross-sectional stiffness properties under certain assumptions

Knowing the spatial distribution of the material orientation and the stiffness properties of the material everywhere within the board it is thus possible to calculate the stiffness in the longitudinal direction of the board and, by integration, to calculate the stiffness properties on the cross-sectional level. However, with limited information regarding the material orientation within the boards, certain assumptions have to be made before the cross-sectional stiffness properties can actually be calculated. In addition to the assumptions declared above when calculating the MOE in the longitudinal board direction on the lateral board surfaces we now also assume that the detected fibre directions are representative for the material to a certain depth in the board in direction perpendicular to the surfaces. Figure 5 illustrates a suggested way to represent the fibre angle field and MOE within the board. The drawing to the left shows the cross-section divided into small strips, each with one side coinciding with one side of the board. One such strip is highlighted in grey. The drawing to the right shows a small segment of length dx in the longitudinal direction of the board and projected fibre angles, φ, on one surface of this segment.

Fibre angles are detected with a certain resolution which is illustrated by the size of the strips drawn. The MOE in the longitudinal direction of the board is calculated for each fibre angle sampling point and this MOE is considered as being representative for a certain wood volume, i.e. the volume given by the area *dA* times the distance *dx*, cf. Figure 5. A numerical integration is then executed in accordance with Eqs. (9-13) giving, as functions of *x*, the position of the neutral axis, the cross-sectional bending stiffness in the strong and weak direction of the board, respectively, and the longitudinal board stiffness. The distance *a* shown in Figure 5 is set to 35 mm when performing the integration herein. More advanced integration schemes, possibly taking pith location and the general pattern for three dimensional grain flows around knots into account would be an interesting subject for further research.

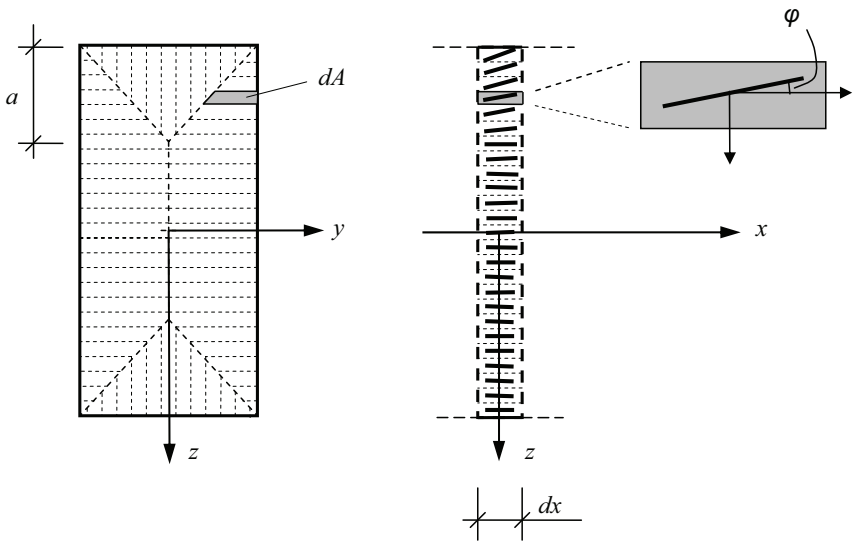

Figure 5 A suggested way to represent the fibre angle field and MOE within the board. The drawing to the left shows the cross-section divided into small strips, each with one side coinciding with one side of the board. One strip is highlighted in grey. The drawing to the right shows a small segment of length *dx* in the longitudinal direction of the board and detected fibre angles on one surface of this segment.

Examples of graphs showing the position of the neutral axis in the *xy*-plane (in relation to the geometric centre axis) and the edgewise bending stiffness profile, respectively, are shown in Figure 6 for one board, here denoted board number 74 (the same board is shown in Figure 4). The calculations are performed using the assumptions and integration scheme described above and results are shown for two different resolutions in the board direction. The two diagrams at the top in Figure 6 show graphs corresponding to the maximum resolution achieved from the scanning, i.e. with values determined at a distance of 0.8 mm apart along the board. The two diagrams at the bottom show graphs where the value at each position (i.e. at each x coordinate) is the average value of the surrounding 80 mm along the board, i.e. along 40 mm on each side of the *x*-coordinate in question. The root end of the board has *x*-coordinate equal to zero.

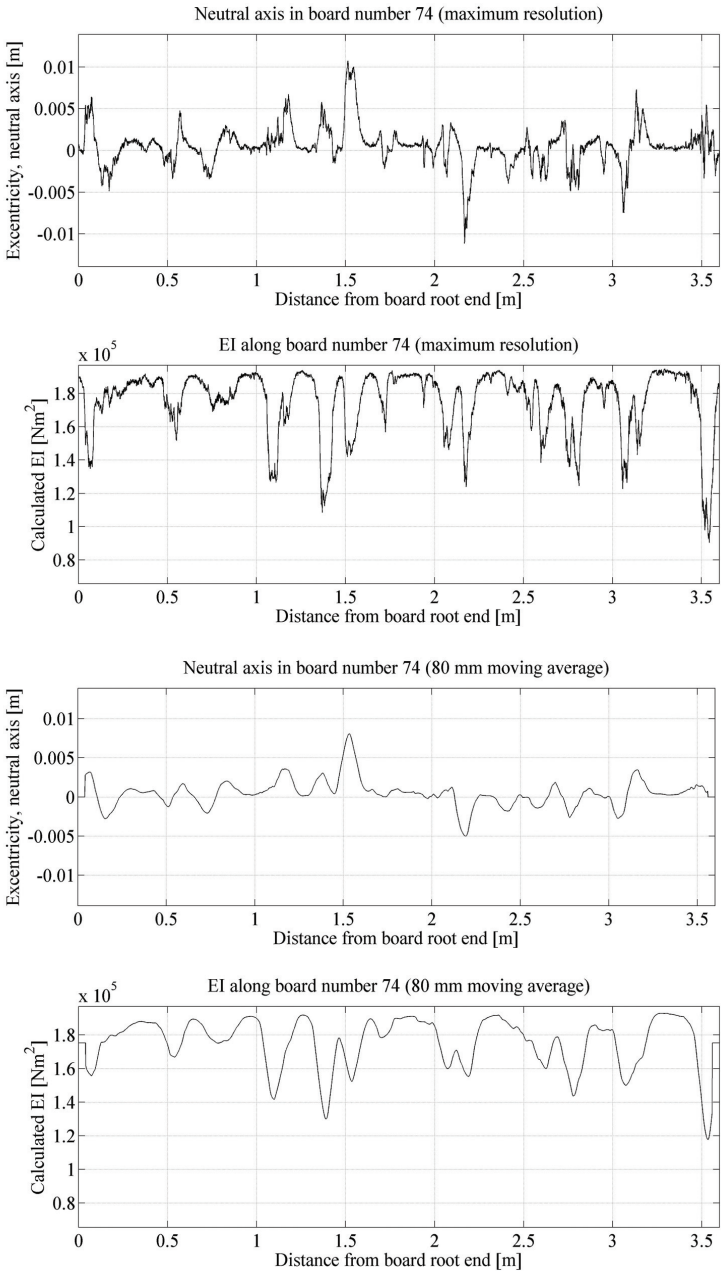

Figure 6 Calculated position of neutral axis and local bending stiffness of board number 74. The two diagrams at the top show graphs corresponding to maximum resolution in the board direction, i.e. with values determined at a distance of 0.8 mm apart along the board. The two diagrams at the bottom show graphs where the value at each position is the average value of the surrounding 80 mm along the board.

Material parameters and calibration of cross-sectional stiffness properties

The procedure described above for calculating cross-sectional stiffness properties along boards requires that the wood material properties are known, i.e. that they are known in relation to a local coordinate system with axes coinciding with the longitudinal, radial and tangential directions, respectively. Though average values for material properties valid for different species can be found in literature, the properties may differ substantially between boards originating from different trees and stands. Even *within* a tree, some properties may vary considerably, particularly in the direction from pith to bark (e.g. Wormuth 1993). The modulus of elasticity in the fibre direction, E_l, is by far the material parameter with the highest influence on the MOE in the board direction. Therefore it is important to assess a value for this parameter valid for each single board. Table 1 shows nominal values, $E_{l,0}$, $E_{r,0}$, $E_{t,0}$, $G_{lr,0}$, $G_{lt,0}$, $G_{rt,0}$, ν_{lr}, ν_{lt}, and ν_{rt}, originating from Dinwoodie (2000), for the wood material parameters used in this study. The material parameters are then adjusted for each individual board by considering an experimentally determined resonance frequency as described below. The parameters are adjusted in such a way that the relations between the different calibrated parameters, E_l, E_r, E_t, G_{lr}, G_{lt}, G_{rt}, are preserved, i.e. they are identical with the corresponding relations for the nominal parameters. The Poisson's ratios, ν_{lr}, ν_{lt} and ν_{rt} are kept constant. This means that a locally oriented compliance matrix, Eq. (3), determined for a particular board only differs compared to the nominal compliance matrices (i.e. a compliance matrix having nominal values for all material parameters involved) by a constant factor. Variations of material parameters within boards are ignored herein, i.e. the locally oriented compliance matrix valid for a particular board is not a function of position within the board.

Table 1 Nominal material parameters employed (Norway spruce).

$E_{l,0}$	10700 MPa
$E_{r,0}$	710 MPa
$E_{t,0}$	430 MPa
$G_{lr,0}$	500 MPa
$G_{lt,0}$	620 MPa
$G_{rt,0}$	24 MPa
ν_{lr}	0.38
ν_{lt}	0.51
ν_{rt}	0.51

As described in a previous section the resonance frequency corresponding to the first longitudinal mode of vibration can be determined experimentally. On basis of such an experiment, an average MOE valid for the longitudinal direction of the board can be calculated as

$$E_{a1} = 4 \cdot \rho \cdot f_{a1}^2 \cdot L^2 \tag{14}$$

where ρ is the average board density, f_{a1} is the measured resonance frequency and L is the board length.

The material parameters representing a particular board should be such that an eigenfrequency analysis on a computational model based on these material parameters should give the same resonance frequency as the one determined experimentally. Therefore a simple one dimensional finite element model of each board is established which resembles the longitudinal stiffness

profile calculated using Eq. (13) on basis of nominal values for material parameters. The stiffness of each finite element in the model represents a short distance, Δx (approximately one centimetre), of the total board length and the axial stiffness of the p:th element is calculated by averaging the axial stiffness obtained from Eq. (13) over the element length

$$k_p = \frac{\int_{(p-1)\Delta x}^{p\Delta x} EA(x)dx}{\Delta x^2} \tag{15}$$

In the FE model the mass of the board is assumed to be uniformly distributed in the longitudinal direction and a resonance frequency denoted $\hat{f}_{a1}$ is calculated by performing eigenvalue analysis on this FE model. The reason for calculating $\hat{f}_{a1}$ is thus to compare it with f_{a1} and to adjust the value employed for material parameters accordingly. Starting with the nominal values for all the material parameters the final values are adjusted in relation to the quota of the two resonance frequencies in square, e.g.

$$E_l = E_{l,0} \frac{f_{a1}^2}{\hat{f}_{a1}^2} \tag{16}$$

The final board stiffness profiles, $EA(x,)$ $EI_y(x)$ and $EI_z(x)$ that may be utilized for strength grading purposes are thus based on material parameters assessed individually for each board after calibration to an experimentally determined resonance frequency. This means, of course, that the calculation results displayed in Figures 4 and 6 are not actually achieved until this part of the calculation process is performed.

Definition and assessment of indicating properties

Below, novel IPs are defined on basis of the cross sectional stiffness profiles calculated as described above. However, in order to evaluate the competitiveness of these IPs, comparisons must be made with IPs that are commonly employed in grading methods of today or within research. Thus also IPs to be employed for comparisons are defined below.

Common IPs to be used for comparison

In EN 408 it is defined how to determine a *local* MOE and a *global* MOE, denoted E_m and $E_{m,g}$, respectively, using four point bending tests. The local MOE is calculated on basis of the local deflection measured within the constant moment zone and over a distance of five times the depth of the board, here 725 mm containing what is supposed to be the weakest part of the board. The global MOE is based on the mid-span deflection of the board. A thorough definition of E_m and $E_{m,g}$ is also given by Olsson et al (2011).

In addition to E_m and $E_{m,g}$, the dynamic MOE calculated on basis of the resonance frequency corresponding to the first longitudinal mode of vibration, i.e. E_{a1} according to Eq. (14), and the average board density, ρ, are used as comparative IPs in the result section below.

Novel IPs based on board stiffness profiles on cross-sectional level

The MOE defined by the lowest edgewise bending stiffness along the board, calculated using Eq. (11) and with calibration according to Eq. (16), can be expressed (if edgewise bending is bending around the *y*-axis) as

$$E_{b,min} = \min_{0 \le x \le L} \left(EI_y(x) \right) / I_{y0} \tag{17}$$

where $I_{y0} = td^3/12$. The bending stiffness $E_{b,min}$ is here evaluated as a possible IP to bending strength. It should be noted that the employed spatial resolution when calculating $EI_y(x)$ is very high, the bending stiffness being assessed every 0.8 mm along the board, and it is likely that an average stiffness value over a certain distance, δ, along the board, would give a better IP to bending strength. Therefore a more general expression for possible IPs is defined as

$$E_{b,min,\delta} = \min_{\delta/2 \le \bar{x} \le L-\delta/2} \left(\frac{1}{\delta} \int_{x=\bar{x}-\delta/2}^{\bar{x}+\delta/2} EI_y(x)\, dx \right) / I_{y0} \tag{18}$$

Considering the fact that large knots or groups of knots in spruce have an extension of typically 60-100 mm it is reasonable to assume that the average bending stiffness over such a distance can give a suitable IP to bending strength. Therefore $E_{b,min,60}$, $E_{b,min,80}$ and $E_{b,min,100}$, i.e. IPs defined according to Eq. (18) with δ = 60 mm, 80 mm and 100 mm, respectively, have been assessed.

The stiffness profile gives information not only about the lowest stiffness value and the extension of the weak zones in the longitudinal direction of the board but also about their position, see the graphs shown in Figure 6. Furthermore, structural timber is rarely exposed to large bending moments close to the ends and in a four point bending test, carried out in accordance with EN 408, only a distance of six times the depth of the board is exposed to the maximum bending moment. In any case, the parts of the boards closer to the ends than about 7*d* can not be exposed to maximum bending moment when assessed according to the standard. Therefore it is reasonable to evaluate an IP defined as

$$E_{b,min,\delta,w} = \min_{d+\delta/2 \le \bar{x} \le L-d-\delta/2} \left(\frac{1}{\delta} \int_{x=\bar{x}-\delta/2}^{\bar{x}+\delta/2} EI_y(x) \cdot w(x)\, dx \right) / I_{y0} \tag{19}$$

where the weight function $w(x)$ is defined as

$$w(x) = \begin{cases} 6d/(x-d) & , \quad d < x < 7d \\ 1 & , \quad 7d \le x \le L-7d \\ 6d/(L-d-x) & , \quad L-7d < x < L-d \end{cases} \tag{20}$$

This gives a weighting of the stiffness profile in correspondence with a load case were the bending moment distribution is such that no bending occurs on a distance *d* from each end of the beam, a linear increase in bending moment then occurs from *d* to 7*d* from each end and a constant, maximum bending moment occurs in the middle part of the beam.

Though it can be expected that the calculated cross sectional stiffness profile $EA(x)$ is less useful for defining efficient IPs to bending strength than what $EI_y(x)$ is, it may be interesting for comparison to evaluate how well the bending strength may be predicted using an IP defined as

$$E_{a,min} = \min_{0 \le x \le L}\left(EA(x)\right)/(t \times d) \quad (21)$$

Results and discussion

The results and discussion presented below is divided into two parts. In the first, statistical results for the measured and calculated properties defined above, which are of general interest for strength grading purposes, are presented and discussed. In the second part additional results and observations regarding the particular test series comprising 105 boards are presented and discussed. These results give indications regarding the potential for further development of the method.

Statistical relations for common board properties and novel IPs to bending strength

Table 2 shows mean values and standard deviations for the bending strength, the local and global MOE, respectively, the dynamic longitudinal MOE, the board density and the novel IPs defined above. It is observed that the novel IP candidates $E_{b,min}$, $E_{b,min,80}$, $E_{b,min,80,w}$ and $E_{a,min}$ are considerably lower than the mean values for E_m, $E_{m,g}$, and E_{a1}. For the lowest MOE calculated for a section along a beam, $E_{b,min}$, the mean value is as low as 7.1 GPa, i.e only 57% of the mean value of E_{a1}. The mean value of $E_{b,min,80}$ is 9.4 MPa, i.e 76% of the mean value of E_{a1}. This gives an indication of how much lower the bending stiffness is on a local level compared to the average board stiffness.

Table 2 Mean values and standard deviations for different properties of the 105 boards.

	Mean value		Standard dev.	
σ_m	38.4	MPa	12.9	MPa
E_m	11.0	GPa	2.8	GPa
$E_{m,g}$	10.6	GPa	2.3	GPa
E_{a1}	12.4	GPa	2.6	GPa
ρ	472	kg/m^3	52	kg/m^3
$E_{b,min}$	7.1	GPa	2.7	GPa
$E_{b,min,80}$	9.4	GPa	2.9	GPa
$E_{b,min,80,w}$	9.7	GPa	2.9	GPa
$E_{a,min}$	8.4	GPa	2.5	GPa

Table 3 shows coefficients of determination between the same properties as those included in Table 2. Of particular interest are the coefficients of determination between IPs and bending strength (printed in bold face in Table 3). The axial dynamic stiffness E_{a1} is often used as an IP in commercial grading and for the boards assessed here it gives a coefficient of determination to the bending strength of 0.59. The IP $E_{b,min}$ gives a better result, R^2=0.64, but an additional improvement was reached using the minimum bending stiffness over a distance of 80 mm, rather than using the lowest value in a single section of the beam. For $E_{b,min,80}$ the coefficient of determination to bending strength was 0.68. Attempts were made for shorter and longer distances, i.e. with other values of δ in $E_{b,min,\delta,w}$, but 80 mm gave the highest coefficient of determination. By considering that the outer parts of the boards, closer to the ends than 7d cannot be subjected to maximum bending moment in a test according to EN 408, the correlation between the IP and the bending strength was improved even further. $E_{b,min,80,w}$ gave a coefficient of

determination as high as 0.71. In practical grading, $E_{b,min,80,w}$ should not be used as an IP as parts from different boards may be joined together by a finger joint and a weak part close to the end of one original graded board may end up in a critical position of an assembled board, but it is presented herein in order to illustrate the ability of the suggested method. In practise, $E_{b,min,80}$ is a more suitable IP. Figure 7 shows scatter plots, coefficients of determination and equations for regression lines between $E_{a1,}$ and σ_m and between $E_{b,min,80,w}$ and σ_m, respectively.

Table 3 Coefficients of determination, R^2, between different properties of the 105 boards.

R^2	σ_m	E_{a1}	ρ	$E_{b,min}$	$E_{b,min,80}$	$E_{b,min,80,w}$	$E_{a,min}$
σ_m	1	**0.59**	**0.27**	**0.64**	**0.68**	**0.71**	**0.61**
E_{a1}	**0.59**	1	0.65	0.80	0.89	0.88	0.88
ρ	**0.27**	0.65	1	0.41	0.47	0.43	0.49
$E_{b,min}$	**0.64**	0.80	0.41	1	0.95	0.92	0.90
$E_{b,min,80}$	**0.68**	0.89	0.47	0.95	1	0.97	0.92
$E_{b,min,80,w}$	**0.71**	0.88	0.43	0.92	0.97	1	0.90
$E_{a,min}$	**0.61**	0.88	0.49	0.90	0.92	0.90	1

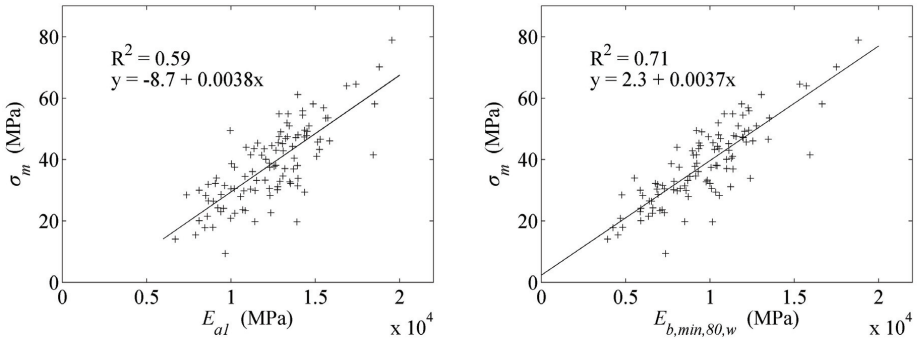

Figure 7 Scatter plots, coefficients of determination and equations for the regression lines between (left) E_{a1} and σ_m and (right) $E_{b,min,80,w}$ and σ_m.

Additional results and observations

For the 105 boards investigated the part of each board including the worst defect, i.e. the knot or group of knots that was supposed to cause failure, was if possible positioned in the maximum bending moment zone when bending strength was determined according to EN 408. If this part was so close to the end that it could not be positioned within this zone the second worst defect was placed in the maximum bending moment zone and so on. For all the boards it was documented where the supports and point loads were positioned and thereby it is known what part of each board that was subjected to maximum bending moment. Furthermore, for each board the location of the failure initialization was documented, although in some cases it was difficult to identify this position accurately in the broken board.

With knowledge regarding how each board was positioned in the testing machine and with a calculated bending stiffness profile for each individual board, it was possible to establish a finite

element (FE) model for the part of each board that was actually subjected to bending and to simulate the load case of four point bending. The FE model employed here consists of a series of beam elements, each approximately 2 cm long. On basis of the displacements obtained in the FE-calculation, MOEs, here denoted $E_{m,c}$ and $E_{m,g,c}$, respectively, were then calculated in analogy with E_m and $E_{m,g}$ obtained from the measured deflections during testing. Table 4 shows coefficients of determination between these different MOEs, based on measurements during testing and based on FE-calculations, respectively, but representing the same timber, i.e. the same $18d = 2610$ mm long parts of the boards in four point bending. The coefficients of determination between these MOEs and the bending strength are also shown in Table 4. The MOEs based on measured deflections, E_m and $E_{m,g}$, correlate considerably better with the bending strength (R^2 = 0.74 and 0.72 respectively) than what the MOEs based on calculated deflections, $E_{m,c}$ and $E_{m,g,c}$, do ($R^2 = 0.61$ for both cases). There is, however, a rather strong correlation between MOEs based on measured and calculated deflections, the coefficients of determination being 0.85 both between E_m and $E_{m,c}$ and between $E_{m,g}$ and $E_{m,g,c}$.

Table 4 Coefficients of determination, R^2, between bending strength and MOEs based on measurements and calculations, respectively.

R^2	σ_m	E_m	$E_{m,g}$	$E_{m,c}$	$E_{m,g,c}$
σ_m	1	**0.74**	**0.72**	**0.61**	**0.61**
E_m	**0.74**	1	0.92	0.85	0.85
$E_{m,g}$	**0.72**	0.92	1	0.89	0.91
$E_{m,c}$	**0.61**	0.85	0.89	1	0.99
$E_{m,g,c}$	**0.61**	0.85	0.91	0.99	1

As both MOEs based on measured and calculated deflections represent the same physical parts of the timber, any differences between E_m and $E_{m,c}$, or between $E_{m,g}$ and $E_{m,g,c}$, reveals a certain lack of precision when trying to calculate the true bending stiffness profile on basis of projected fibre angles, employed integration scheme and longitudinal dynamic excitation. The suggested approach seems to be accurate enough to give a very good correlation between suggested IPs and bending strength, but the results presented in Table 4 indicate that there is a considerable potential to improve the correlation further. If the high resolution of the bending stiffness profiles (which can be calculated rapidly on basis of results from scanning) can reach the accuracy of the measured edgewise bending stiffness (i.e. measured on a more or less global level during four-point bending) it is likely that a coefficient of determination between a single IP and the bending strength may approach or even exceed $R^2 = 0.80$. To what degree the present differences between E_m and $E_{m,c}$, and between $E_{m,g}$ and $E_{m,g,c}$ depend (1) on the fact that projected fibre angles on surfaces are utilized rather than the true, three dimensional fibre angle field within the wooden member, (2) on the simplifying assumption that the wood material parameters relating to the l-r-t system are constant within a wooden member, (3) on the assumption that the stiffness can be captured accurately enough using a beam model, or on some other conditions should be investigated through further research.

A final observation concerns the position along each beam where failure actually was initialized in relation to where it was expected to occur, i.e. where the calculated bending stiffness was at its lowest in relation to the applied bending moment. In 70% of the boards the distance between the actual position of failure and the predicted position was less than 5 cm and for 78% of the boards the distance was less than 10 cm. This indicates a high probability for failure to take place within a close surrounding of the section with the lowest bending stiffness. It

may be noted, however, that many boards have a second weak section, and maybe even a third, with calculated bending stiffness almost as low as the weakest one.

Conclusions

High resolution information regarding local fibre orientation on face and edge surfaces of wooden boards can nowadays be sampled in a speed corresponding to the production speed at a sawmill. By utilizing such information in order to calculate the variation in bending stiffness along an individual board very accurate indicating properties with respect to bending strength can be defined. However, information regarding basic wood material properties, in particular the MOE in the fibre direction, needs to be available for each individual board. One way to obtain such information is to measure the first longitudinal resonance frequency and the board density which in combination with fibre orientation information can be used to calculate an average MOE in the fibre direction.

For a sample consisting of 105 spruce boards of dimension 45 × 145 × 3600 mm it is shown that an IP defined as the edgewise bending stiffness of the weakest (least stiff) 80 mm part along each board gave a coefficient of determination to bending strength of 0.68. If it is considered that sections close to the ends of the boards cannot be subjected to large bending moments when tested the coefficient of determination increases to 0.71. For the same boards the coefficient of determination between global MOE based on the first resonance frequency and the board density is only 0.59.

The theory of how the local stiffness in the direction of a board can be calculated on basis of basic wood parameters and three dimensional fibre directions is presented independently of the simplifying assumptions that need to be introduced when actually calculating the stiffness profiles, indicating properties and coefficients of determination. It is also shown that higher accuracy when determining these properties, i.e. if errors originating from simplifying assumptions can be avoided, an even stronger correlation would be achieved between a local bending stiffness and bending strength. Thus, along with the development of commercial grading procedures on basis of the research results already presented herein, further development towards even more accurate calculations of bending stiffness profiles of boards is encouraged.

To obtain optimum IPs, the distance δ over which the average bending stiffness is calculated may depend on the dimensions of the wooden boards assessed. Some tests and calculations performed on batches of timber of other dimensions than 45 × 145 mm suggest that a distance of about half the depth of the timber member (rather than a constant distance of 80 mm) would give a suitable IP, but further tests and calculations on different dimensions of wooden boards need to be carried out in order to confirm this.

Finally, it should be noted that the calculated stiffness profiles could also be of use in a material efficient production of engineered wood products where the significance of weak sections may depend on their location or when it is suitable to eliminate weak sections before assembling.

References

F. K. Bechtel and J. R. Allen (1987) Methods of Implementing Grain Angle Measurements in the Machine Stress Rating Process. 6th Nondestructive Testing of Wood Symposium, Sept 1987, Washington State University, Pullman.

Brookhuis Micro-Electronics BV (2009) Timber Grader MTG – Operating Instructions. MTG Manual GB 12062009-C.

CEN (2009) EN 14081-4 Timber structures – Strength graded structural timber with rectangular cross section – Part 4: Machine grading – Grading machine settings for machine controlled systems.

CEN (2010a) EN 384 Structural timber – Determination of characteristic values of mechanical properties and density. European Committee for Standardization, CEN/TC124.

CEN (2010b) EN 408 Timber structures – Structural timber and glued laminated timber – Determination of some physical and mechanical properties. European Committee for Standardization, CEN/TC124.

J. M. Dinwoodie (2000) Timber: Its nature and behaviour. E & FN Spon, New Fetter Lane, London.

A. Jehl, L. Bléron, F. Meriaudeau, and R. Collet (2011) Contribution of Slope of Grain Information in Lumber Strength Grading. 17th International Nondestructive Testing and Evaluation of Wood Symposium, Sept 2011, University of West Hungary, Sopron.

C.-J. Johansson (2003) Grading of Timber with Respect to Mechanical Properties. In S. Thelandersson and H. J. Larsen, editors, *Timber Engineering*, pages 23–43. Wiley, Chichester, UK.

D. Larsson (1997) Mechanical Characterization of Engineering Materials by Modal Testing. Doctoral thesis, Chalmers University of Technology, Gothenburg.

H. E. Moore and R. D. Baldwin (2011) Structural Grading of Lumber using Grain Angle in a Production Environment. 17th International Nondestructive Testing and Evaluation of Wood Symposium, Sept 2011, University of West Hungary, Sopron.

Nyström J. (2003) Automatic measurement of fiber orientation in softwoods by using the tracheid effect. Computers and Electronics in Agriculture, 41(1):91-99.

A. Olsson, J Oscarsson, M. Johansson and B. Källsner (2011) Prediction of timber bending strength on basis of bending stiffness and material homogeneity assessed from dynamic excitation. Wood Sci Technol DOI 10.1007/s00226-011-0427-x.

S. Ormarsson (1999) Numerical Analysis of Moisture-Related Distorsions in Sawn Timber. Doctoral thesis, Chalmers University of Technology, Gothenburg.

H. Petersson (2010) Use of Optical and Laser Scanning Techniques as Tools for Obtaining Improved FE-input Data for Strength and Shape Stability Analysis of Wood and Timber. IV European Conference on Computational Mechanics, May 2010, Paris.

G. S. Schajer (2001) Lumber strength grading using x-ray scanning, Forest Products Journal 51(1), 43-50.

E.-W. Wormuth (1993) Study of the relation between flatwise and edgewise modulus of elasticity of sawn timber for the purpose of improving mechanical stress methods. Diploma work, University of Hamburg, Hamburg.

Licentiate thesis Jan Oscarsson

Strength grading of structural timber and EWP laminations of Norway spruce – Development potentials

2012

Available from
School of engineering
Linnæus University

Lnu.se